Spring 2022 – Systems Biology of Reproduction
Discussion Outline – Assisted Reproduction/Contraception
Michael K. Skinner – Biol 475/575
CUE 418, 10:35-11:50 am, Tuesday & Thursday
April 28, 2022
Week 16

Assisted Reproduction/Contraception

Primary Papers:

1. Oritz-Rodriguez, et al. (2019) Plos One 0213420, 1-24.
2. Shetty, et al. (2021) Andrology 9:1603
3. Chang, et al. (2021) Nature Communications 12:1253

Discussion

Student 12: Reference 1 above

- What is the assisted reproductive technology (ART) investigated?
- What is the experimental design and technology used?
- What is the conclusion on the use of this ART technology?

Student 18: Reference 2 above

- What is spermatogonial transplantation?
- What was the experimental design?
- What applications does the technology have?

Student 20: Reference 3 above

- What is the compound and where is it from?
- What was the experimental design?
- Is this a contraceptive and what clinical issues should be investigated?

PLOS ONE

RESEARCH ARTICLE

Transcriptome analysis reveals that fertilization with cryopreserved sperm downregulates genes relevant for early embryo development in the horse

José M. Ortiz-Rodriguez[1], Cristina Ortega-Ferrusola[1], María C. Gil[1], Francisco E. Martín-Cano[1], Gemma Gaitskell-Phillips[1], Heriberto Rodríguez-Martínez[2], Katrin Hinrichs[3], Alberto Álvarez-Barrientos[4], Ángel Román[5], Fernando J. Peña[1]*

1 Laboratory of Equine Reproduction and Equine Spermatology, Veterinary Teaching Hospital, University of Extremadura, Cáceres, Spain, **2** Department of Clinical and Experimental Medicine, Faculty of Medicine and Health Sciences, Linköping University, Linköping, Sweden, **3** Department of Veterinary Physiology and Pharmacology, College of Veterinary Medicine & Biomedical Sciences, Texas A&M University, College Station, Texas, **4** STAB, University of Extremadura, Badajoz, Spain, **5** Department of Biochemistry and Molecular Biology, University of Extremadura, Badajoz, Spain

* fjuanpvega@unex.es

Citation: Ortiz-Rodriguez JM, Ortega-Ferrusola C, Gil MC, Martín-Cano FE, Gaitskell-Phillips G, Rodríguez-Martínez H, et al. (2019) Transcriptome analysis reveals that fertilization with cryopreserved sperm downregulates genes relevant for early embryo development in the horse. PLoS ONE 14 (6): e0213420. https://doi.org/10.1371/journal.pone.0213420

Editor: Christine Wrenzycki, Justus Liebig Universitat Giessen, GERMANY

Received: February 14, 2019

Accepted: June 11, 2019

Published: June 25, 2019

Data Availability Statement: All relevant data are within the manuscript and its Supporting Information files.

Funding: FJP received financial support for this study from the Ministerio de Economía y Competitividad-FEDER, Madrid, Spain, grant AGL2017-83149-R. FJP also received support from the Junta de Extremadura-FEDER (IB16030 and GR18008). HRM received support from the

Abstract

Artificial insemination with cryopreserved spermatozoa is a major assisted reproductive technology in many species. In horses, as in humans, insemination with cryopreserved sperm is associated with lower pregnancy rates than those for fresh sperm, however, direct effects of sperm cryopreservation on the development of resulting embryos are largely unexplored. The aim of this study was to investigate differences in gene expression between embryos resulting from fertilization with fresh or cryopreserved sperm. Embryos were obtained at 8, 10 or 12 days after ovulation from mares inseminated post-ovulation on successive cycles with either fresh sperm or frozen-thawed sperm from the same stallion, providing matched embryo pairs at each day. RNA was isolated from two matched pairs (4 embryos) for each day, and cDNA libraries were built and sequenced. Significant differences in transcripts per kilobase million (TPM) were determined using (i) genes for which the expression difference between treatments was higher than 99% of that in the random case ($P < 0.01$), and (ii) genes for which the fold change was ≥ 2, to avoid expression bias in selection of the candidate genes. Molecular pathways were explored using the DAVID webserver, followed by network analyses using STRING, with a threshold of 0.700 for positive interactions. The transcriptional profile of embryos obtained with frozen-thawed sperm differed significantly from that for embryos derived from fresh sperm on all days, showing significant down-regulation of genes involved in biological pathways related to oxidative phosphorylation, DNA binding, DNA replication, and immune response. Many genes with reduced expression were orthologs of genes known to be embryonic lethal in mice. This study, for the first time, provides evidence of altered transcription in embryos resulting from fertilization with cryopreserved spermatozoa in any species. As sperm cryopreservation is

Swedish Research councils VR, (Grant 521-2011-6553) and FORMAS (Grant 2017-00946), Stockholm. JMOR holds a Predoctoral grant from the Valhondo Calaaf Foundation, Cáceres, Spain. The funders had no role in study design, data collection and analysis, decision to publish, or preparation of the manuscript.

Competing interests: The authors have declared that no competing interests exist.

commonly used in many species, including human, the effect of this intervention on expression of developmentally important genes in resulting embryos warrants attention.

Introduction

Cryopreservation is a common procedure in assisted reproductive technology, in both humans and the animal breeding industry [1–3]. Cryopreserved sperm are routinely used for artificial insemination (AI), in vitro fertilization (IVF) and intracytoplasmic sperm injection (ICSI). However, it is clear that sperm cryopreservation methods are currently sub-optimal, as pregnancy rates with cryopreserved sperm are lower than those with fresh sperm in humans and horses [4–6], among other species. Cryopreservation leads to extensive damage of sperm cell membranes and causes metabolic and functional alteration of sperm [7, 8], particularly of their mitochondria [9–11]. Cryopreservation may alter sperm DNA [12]; recently, specific cryodamage to sperm genes and transcripts have been reported [13, 14], even in samples with good sperm motility post thaw and in the absence of detectable DNA fragmentation. The sperm DNA is epigenetically programmed to regulate embryonic gene expression, and changes to this epigenome cause developmental disregulation [15]. Cryopreservation has been found to significantly change the sperm DNA methylome, as well as to alter expression of epigenetic-related genes such as methyltransferases [12, 16]. Cryopreservation of sperm imposes oxidative stress and redox deregulation in spermatozoa, leading to the presence of toxic adduct-forming compounds such as 4- hydroxynonenal (4-HNE) in sperm membranes [17]. Moreover, mitochondria of spermatozoa surviving cryopreservation show increased production of reactive oxygen species [9, 10, 18]. Signaling pathways crucial to normal embryo development are sensitive to perturbations of endogenous redox state, and are also susceptible to modulation by reactive oxygen species [19]. Thus, fertilization by damaged spermatozoa may impact early embryo development and even have effects that appear later in the life of the offspring [20].

Moreover, appreciation of the contribution of sperm to embryo development has evolved from the concept that the only role of sperm at fertilization is to introduce the male genome into the egg. Sperm carry a myriad of small noncoding RNAs with potential roles in early embryo development [21, 22]. Notably, sperm carry the activating factor PLCζ, which triggers calcium oscillations that induce oocyte activation [23, 24], and it has been shown in mouse and rabbit that alterations in frequency and amplitude of post-fertilization calcium oscillations can affect the phenotype of the resulting embryo into post-implantation development and adulthood [25, 26]. Thus, there are extensive pathways by which cryopreservation of sperm could alter the development of the fertilized oocyte and embryo.

Despite the widespread use of cryopreserved sperm, and the known decrease in pregnancy rates with its use, little direct information is available on the effect of sperm cryopreservation on development of the resulting embryo. Recent advances in transcriptome amplification and next-generation sequencing provide the ability to obtain the full transcriptome of individual embryos [27], thus offering a basis for studies on differences in gene expression associated with fertilization with cryopreserved sperm. In the present study, we analyzed the transcriptome of equine embryos produced with fresh or frozen-thawed sperm, to determine the impact of sperm cryopreservation on gene expression during early equine embryo development.

Material and methods

Animals and experimental design

Animals belonging to and housed in our institution were maintained according to European laws and regulations, and all experimental procedures were reviewed and approved by the Ethical committee of the University of Extremadura, Cáceres, Spain. Six mares were used for this study; they were inseminated with the same stallion of known fertility to reduce genetic variability [28]. Each mare was assigned a day of embryo recovery (8, 10 or 12 days post ovulation) and on successive cycles was assigned to be inseminated with fresh or frozen-thawed sperm from the same stallion, to provide a matched embryo pair for that day of embryo development. The mares were treated with a prostaglandin analogue to shorten the luteal phase and were monitored daily by transrectal ultrasonography. When a follicle of at least 35 mm diameter was detected in the absence of luteal tissue, with marked uterine edema and low cervical tone, mares received 2,500 IU of hCG i.v.. The follicle was monitored by transrectal ultrasonography every 6 h thereafter to detect the time of ovulation. Mares were inseminated immediately once ovulation was detected, with a minimum of 100 million either fresh sperm or frozen-thawed sperm, from the same stallion and ejaculate. For this, semen was collected, and half of the ejaculate was processed as fresh semen for the immediate insemination of the mare. The other half was frozen following the standard protocol in our center [17, 29, 30], and stored in LN for the next insemination of the same mare. Following this protocol, each mare was inseminated with the same ejaculate, first with the fresh extended aliquot and on a second cycle with the frozen-thawed aliquot.

Embryos were obtained by uterine lavage on the designated day after ovulation. For each embryo day, 2 embryos produced with fresh sperm, designated FRSH embryos, and 2 embryos produced with frozen-thawed sperm, designated CRYO embryos were obtained. Embryos were snap-frozen in liquid N_2 and stored at -80˚C until analysis. Previous clinical reports indicated that there is no a significant effect in the rate of embryonic vesicle growth between mares inseminated with fresh or frozen-thawed sperm if both are inseminated post-ovulation [31].

Isolation of RNA

Total RNA was isolated from the embryos using the PicoPure RNA Isolation Kit (Catalog number KIT0204, Thermofisher) following the manufacturer's instructions. RNA concentration and quality were assessed by automatic electrophoresis using 2100 Bioanalyzer (Agilent Technologies, Santa Clara, CA, USA).

RNA-seq analysis

cDNA libraries were built using an IonTorrent S5/XL sequencer (Thermo Fisher Scientific, Waltham, MA USA). The raw reads were aligned to a horse transcriptome generated using ENSEMBL (Equ Cab 2 version) in the Torrent server with proprietary ThermoFisher algorithms. Then, custom scripts were used to transform reads into transcript counts, and transcripts per kilobase million (TPM) scores for each gene were retrieved. A gene was considered expressed if the reads per kilobase or transcript model per million mapped reads was > 0.4. In order to evaluate gene expression differences between treatments (FRSH or CRYO embryos), we calculated two thresholds: first, we calculated the random TPM differences between FRSH and CRYO embryos by permutation of the TPM gene scores. Then we chose the genes whose expression difference between the two conditions was higher than in 95% ($P<0.05$) or in 99% ($P<0.01$) of the random cases. As a second score, we used a fold change ≥ 2 as a threshold in order to avoid expression biases in the selection of the candidate genes.

Gene ontology and pathway analysis

The annotations of the candidate genes selected after the RNA-seq analyses were explored to detect significant differences in molecular pathways between treatments. Specifically, the DAVID webserver [32] was used to retrieve the terms (gene ontology, up-expressed tissues, KEGG and reactome pathways, protein-protein interactions, etc.) with significant over-presence of the candidate genes, using a false discovery rate (FDR) < 0.05. We used the human genome as reference for the analysis because of its increased depth in terms of annotation.

Network analysis

STRING [33] was used to analyze the internal structure of the functional network obtained using the candidate genes. Data included co-expression, genetic fusion, co-occurrence or protein-protein interactions, among others. A high threshold (0.700) was selected for positive interaction between a pair of genes.

Results

A total of 12 conceptuses were analysed (2 FRSH and 2 CRYO at each day). An average of 29,196 transcripts per embryo were obtained.

Day-8 embryos

In Day-8 CRYO embryos, 100 transcripts showed increased abundance and 157 transcripts showed decreased abundance in respect to FRSH embryos of the same age from the same stallion and mare (Fig 1).

Of the 100 transcripts showing increased abundance in CRYO embryos, 23 could be aligned to the genome build (S1 Table). These included the progesterone receptor membrane component (8PGRMC1). Enriched biological processes (Fig 2A) included extracellular region genes, defensing beta 119, insulin like 3, prostaglandin D2 synthase and uteroglobin; genes associated with negative regulation of cysteine type endopeptidase activity involved in apoptotic processes including nuclear receptor subfamily 4 group A member and paired box 2; and genes involved in skeletal muscle cell differentiation including activating transcription factor 3 and nuclear receptor subfamily 4 group 4 A member. STRING analysis revealed no significant enrichments in functional networks for transcripts with increased abundance.

Transcripts showing decreased abundance in CRYO embryos provided more information, with 129 transcripts annotated in the equine database. The complete list of transcripts is presented in S2 Table. Due to the large number of genes retrieved, the threshold was reset at $P< 0.001$ and 62 transcripts were then retrieved (Table 1). Related gene ontology terms are shown in Fig 2B. Enriched terms in KEGG (Kyoto encyclopedia of gene and genomes) pathways included ribosome, Parkinson disease and oxidative phosphorylation (Fig 3). STRING analysis, performed using a threshold of 0.700, obtained a protein-protein interaction (PPI) enrichment P value of $< 1.0 \times 10^{-16}$ (Fig 4). The complete list of genes in this network with their clustering is presented in S3 Table. Enriched biological processes included cellular process, iron ion transport, cellular iron ion homeostasis, metabolic process, response to inorganic substance, biological regulation, single-organism process, cellular macromolecule metabolic process, single organism cellular process, cellular metabolic process, response to stimulus, cellular response to zinc ion, transport, regulation of biological process, oxidation-reduction process, cellular component disassembly, cellular nitrogen compound metabolic process, translation, single organism transport, gene expression, positive regulation of nitrogen compound

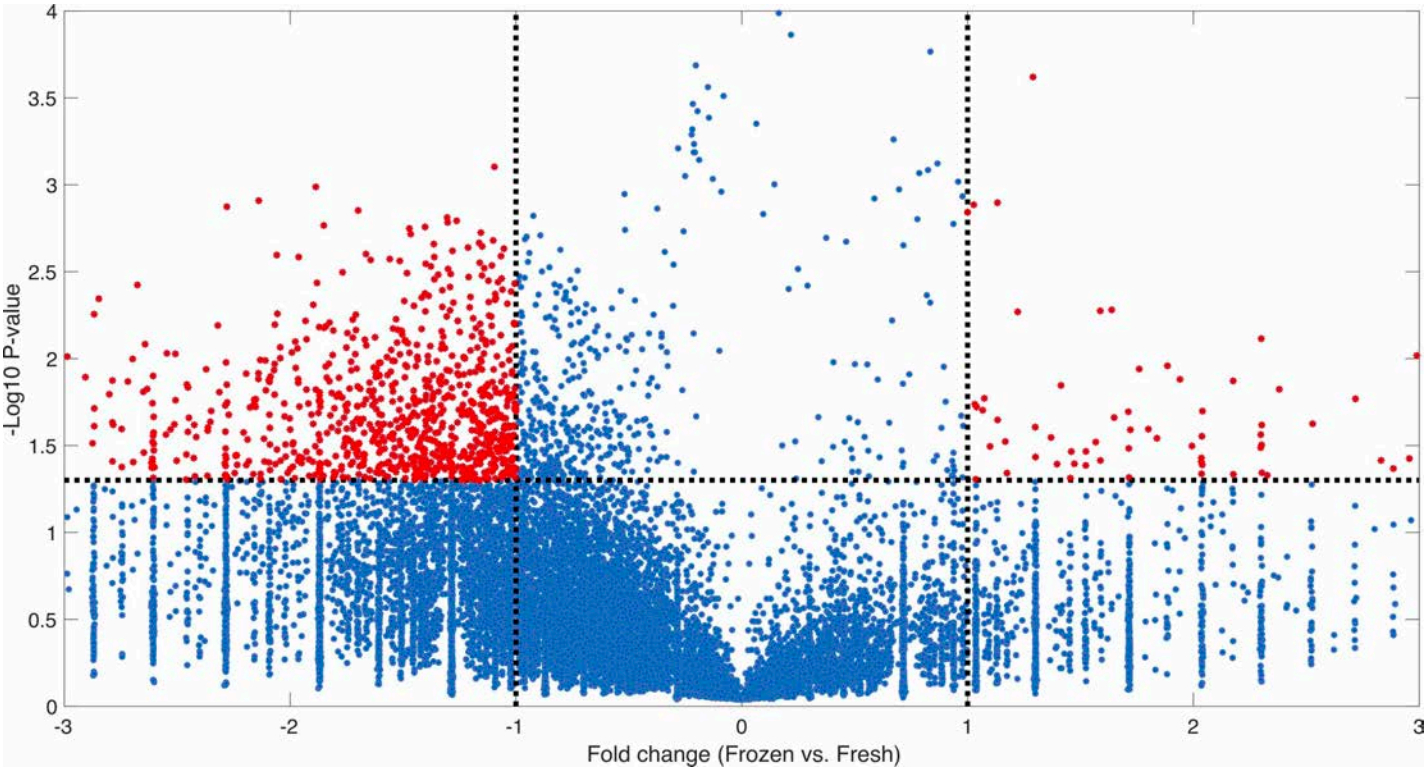

Fig 1. Volcano plot representing the RNA-seq results for Day-8 equine embryos conceived using fresh sperm (FRSH) or frozen-thawed sperm (CRYO). Each point represents a gene. On the X-axis, the fold change was calculated as the log2-ratio between the average gene expression in CRYO embryos and the average gene expression in FRSH embryos. Therefore, positive values indicate genes in which expression is higher in CRYO embryos, while negative values indicate genes whose expression is higher in FRSH embryos. On the Y-axis, the statistical significance for the difference in gene expression (see Methods) is represented as the (-log10) of the P-value. Dashed lines indicate the thresholds for significance on the two axes (-1 and +1 in the case of the X-axis for up-regulated and down-regulated genes, respectively, in CRYO embryos; and 1.30 (equal to a P-value = 0.05) in the case of the Y-axis). Red points mark differentially expressed genes.

https://doi.org/10.1371/journal.pone.0213420.g001

metabolic process, biological process, protein folding, cellular component organization, regulation of cell proliferation, and primary metabolic process.

Day-10 embryos

In Day-10 embryos 239 transcripts showed increased abundance ($P < 0.01$), and 206 showed decreased abundance, in CRYO embryos in comparison with FRSH embryos.

Of the 239 transcripts showing increased abundance in CRYO embryos, 53 aligned to the genome build (S4 Table). Functional annotation revealed these genes to be related to the GO terms and KEGG pathways nucleosome, systemic lupus erythematatosus, DNA replication-dependent nucleosome assembly, protein heterodemerization, alcoholism, nuclear chromosome, telomeric region, regulation of gene silencing, nucleosomal DNA binding, membrane, translation, poly (A) RNA binding, viral carcinogenesis, negative regulation of megakaryocyte differentiation, DNA replication independent nucleosome assembly, extracellular exosome, DNA-templated transcription, xenophagy, ribosome, positive regulation of defense to virus by host, DNA binding, mitochondrion, cytosolic large ribosomal subunit, extracellular space, transcriptional misregulation in cancer, innate immune response in mucosa, U1 snRNP, antibacterial humoral response, telomerase RNA binding and mitochondrial small ribosomal subunit (Fig 5A). STRING analysis revealed a PPI enrichment P value of $< 1.0 \times 10^{-16}$. Functional enrichment included the PFAM protein domain Core histone H2A/H2B/H3/HA and the

A

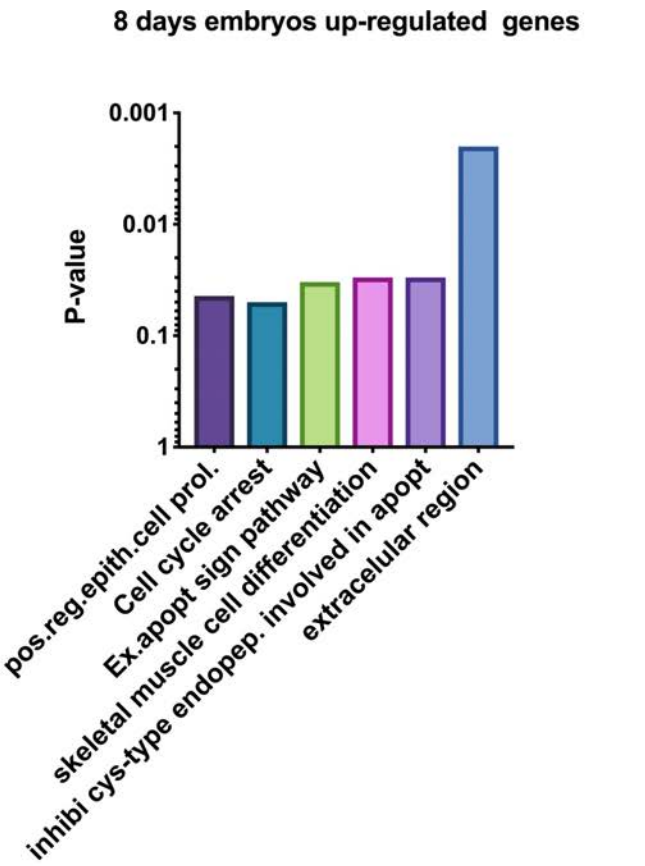
8 days embryos up-regulated genes
P-value
0.001
0.01
0.1
1
pos.reg.epith.cell prol.
Cell cycle arrest
Ex.apopt sign pathway
skeletal muscle cell differentiation
inhibi cys-type endopep. involved in apopt
extracelular region

B

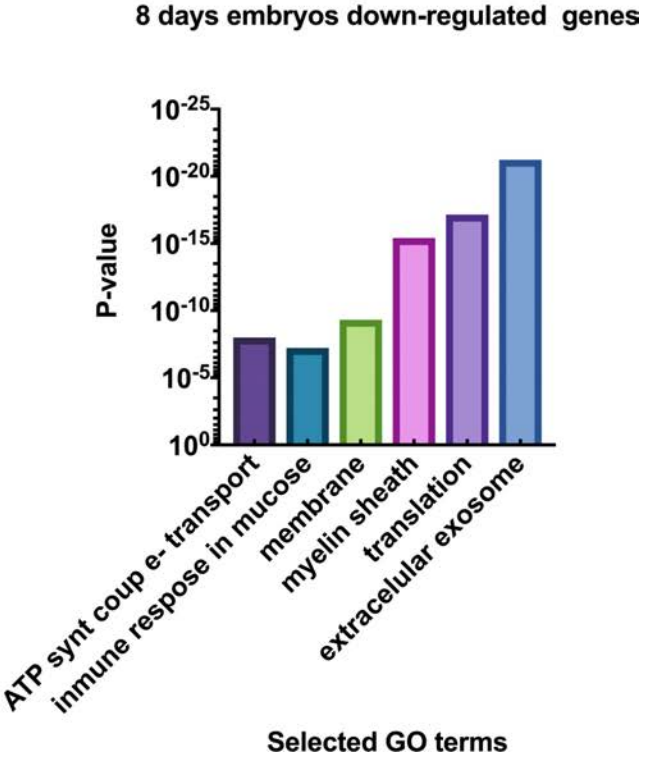
8 days embryos down-regulated genes
P-value
10-25
10-20
10-15
10-10
10-5
100
ATP synt coup e- transport
inmune respose in mucose
membrane
myelin sheath
translation
extracelular exosome
Selected GO terms

Fig 2. Selected enriched GO terms differentially regulated in Day-8 equine embryos obtained using fresh sperm (FRSH) and frozen-thawed sperm (CRYO), (A) transcripts down regulated in 8-Day CRYO embryos, (B) transcripts up regulated in 8-Day CRYO embryos.

https://doi.org/10.1371/journal.pone.0213420.g002

INTERPRO protein domains, including Histone fold, Histone H3/CNEP-A, Histone H2A/H2B/H3, Histone H4, Histone H4 conserved site, TATA box binding protein associated factor (TAF) and ribosomal protein L23/L15e core domain.

Of the 206 transcripts showing decreased abundance in CRYO embryos at Day 10, 115 were aligned. Enriched KEGG pathways that were also detected in Day-8 embryos (Table 2) included oxidative phosphorylation, Parkinson disease, Alzheimer disease, Hungtington disease, Metabolic pathways, Ribosome, cardiac muscle contraction, and non-alcoholic fatty liver disease. Three new KEGG enriched pathways, protein processing in endoplasmic reticulum, systemic lupus erythematosus and phagosome, were detected (Fig 6). More significantly represented GO terms were ATP synthesis coupled proton transport, translation, nucleosome assembly, cell redox homeostasis, extracellular exosome, myelin sheath, respiratory chain, mitochondrion, extracellular space, NADH dehydrogenase (ubiquinone) activity, structural constituent of ribosome, and proton transporting ATP synthase activity rotational mechanism (Fig 5B). A complete list of enriched GO terms retrieved are given in Table 3. STRING analysis revealed functional networks with a PPI enrichment P value of $< 1.0 \times 10^{-16}$ (Fig 7). Functional enrichment included the PAFM domains core histone H2A/H2B/H3/H4, thiorredoxin, NADH deshidrogenase, NADH-Ubiquinone and plastoquinone (Complex I), various chains.

Day-12 embryos

In Day-12 embryos, 149 transcripts showed increased abundance and 157 showed decreased abundance in CRYO embryos. Of the 149 transcripts with increased abundance, 61 were annotated (S5 Table). Enriched KEGG pathways included ribosome and Parkinson disease and the GOterms extracellular exosome, translation, structural constituent of ribosome, nuclear nucleosome, mitochondrial respiratory chain complex I, cytosolic large ribosomal subunit, nucleosome assembly, methylosome, and catalytic step 2 spliceosome (Fig 8A). On STRING analysis, the KEGG pathways Ribosome (Pathway ID 03010) and Parkinson disease (Pathway ID 05012) showed a PPI enrichment P value of $< 8 \times 10^{-10}$.

Of the 157 transcripts showing decreased abundance in Day-12 CRYO embryos, 60 transcripts aligned to the genome build (S6 Table). Enriched KEGG pathways, also detected in 8- and 10-day embryos, included oxidative phosphorylation, Parkinson disease, metabolic pathways, Alzheimer disease, Huntington disease, non-alcoholic fatty acid liver disease and cardiac muscle contraction. In addition a new pathway, folate biosynthesis, was enriched (Fig 9). GO terms enriched annotations (Fig 8B) were NADH dehydrogenase (ubiquinone) activity, mitochondrial respiratory chain complex I, nucleosome, DNA replication dependent nucleosome assembly, protein heterotetramerization, mitochondrion, respiratory chain, negative regulation of megakaryocyte differentiation, DNA template transcription initiation, ATP synthesis coupled electron transport, nuclear chromosome telomeric region, DNA binding, oxireductase activity, mitochondrial inner membrane, integral component of membrane, mitochondrial electron transport NADH to ubiquinone, and extracellular exosome. The complete list is given in Table 4

STRING analysis revealed functional networks with a PPI enrichment P value of $< 1.0 \times 10^{-16}$ (Fig 10). Functional enrichment included the PFAM protein domains core histone H2A/H2B/H3/H4, NADH dehydrogenase, and NADH-ubiquinone/plastoquinone (complex I various chains).

Table 1. Enriched biological processes from DEGs (downregulated) in 8 days embryos obtained after AI with frozen thawed sperm, as identified by DAVID functional annotation analysis.

Functional terms of overrepresented biological processes [a]	P value [b]
Chromosome (21, 35.78)	7.1×10^{-26}
Nucleosome core (19, 42.08)	9.2×10^{-25}
Extracellular exosome (62, 3.56)	5.7×10^{-22}
Histone fold (19, 30.02)	7.5×10^{-22}
Structural constituent of ribosome (24, 13.82)	5.8×10^{-20}
Ribosome (24, 12.89)	1.21×10^{-19}
Histone core (15, 36.91)	1.69×10^{-18}
Translation (21, 14.65)	7.15×10^{-18}
Mylein sheath (18, 16.63)	3.87×10^{-16}
Nucleosome (13, 31.72)	4.20×10^{-15}
Ribonucleoprotein (14, 24.48)	1.15×10^{-14}
Ribosomal protein (13, 29.28)	1.39×10^{-14}
Nucleosome assembly (13, 23.18)	2.14×10^{-13}
Poly (A) RNA binding (34, 4.29)	4.69×10^{-13}
Nuclear nucleosome (10, 40.67)	1.37×10^{-12}
Parkinson's disease (18, 9.52)	2.60×10^{-12}
Cytosolic small ribosomal subunit (10, 33.98)	8.65×10^{-12}
Cytosolic large ribosomal subunit (11, 24.85)	1.46×10^{-11}
Systemic lupus erythematosus (16, 10.14)	2.51×10^{-11}
Hungtinton's disease (19, 7.38)	4.19×10^{-11}
H2B (8, 52.06)	7.18×10^{-11}
Nucleus (26, 4.79)	8.79×10^{-11}
Oxidative phosphorylation (16, 9.01)	$1{,}43 \times 10^{-10}$
Histone H2B (8, 48.75)	1.48×10^{-10}
DNA binding (21, 6.06)	1.81×10^{-10}
Membrane (27, 4.21)	4.82×10^{-10}
Alzheimer disease (17, 7.38)	6.32×10^{-10}
Alcoholism (16, 7.17)	3.64×10^{-9}
ATP synthesis coupled proton transport (7, 41.39)	1.0×10^{-8}
Innate immune response in mucose (6, 51.80)	5.89×10^{-8}
Antibacterial humoral response (6, 48.15)	9.1×10^{-8}
Focal adhesion (15, 6.10)	1.38×10^{-7}
DNA binding (18, 4.18)	1.02×10^{-6}
DNA replication dependent nucleosome assembly (6, 30.64)	1.13×10^{-6}
Hydrogen ion transport (5, 55.38)	1.38×10^{-6}
Protein heterotetramerizacion (6, 29.31)	1.44×10^{-6}
Proton transporting ATP synthase activity, rotational mechanism (5, 51.26)	1.66×10^{-6}
Cytoplasm (11, 5.91)	1.60×10^{-5}
Cytoplasmatic translation (5, 29.56)	2.00×10^{-5}
H4 (4, 60.63)	2.86×10^{-5}
Viral carcinogenesis (13, 4.39)	3.09×10^{-5}
Cardiac muscle contraction (8, 8.53)	3.57×10^{-5}
Histone H4 (4, 56.81)	3.68×10^{-5}
Histone H4 conserved site (4, 56.81)	3.68×10^{-5}
TAF (4, 56.88)	5.56×10^{-5}
Defense response to gram positive bacterium (6, 49.69)	6.14×10^{-5}

(*Continued*)

Table 1. (Continued)

Functional terms of overrepresented biological processes [a]	P value [b]
Tata Box binding protein associated factor (TAF) (4, 14.04)	7.14×10^{-5}
Negative regulation of megakaryocite differentiation (4, 46.53)	1.04×10^{-4}
ATP hydrolysis coupled ion transport (5, 40.85)	1.14×10^{-4}
Acetylation (6, 19.37)	1.32×10^{-4}
H2A (4, 12.08)	3.67×10^{-4}
Mitochondrial electron transport, cytochrome c to oxygen (3, 27.33)	4.57×10^{-4}
Ribosomal large subunit assembly (4, 84.27)	4.94×10^{-4}
DNA replication independent nucleosome assembly (4, 24.96)	4.94×10^{-4}
Histone H2A (4, 24.37)	5.44×10^{-4}
V-ATPase proteolipid subunit C-like domain (3, 76.78)	5.86×10^{-4}
DNA templated transcription, initiation (4, 22.47)	6.81×10^{-4}
Nuclear chromosome, telomeric region (6, 8.22)	7.79×10^{-4}
Non alcoholic fatty liver disease (NAFLD) (9, 4.40)	8.75×10^{-4}
Lactate/malate dehydrogenase (3, 63.99)	8.74×10^{-4}
Lactate malate dehydrogenase, N–terminal (3, 63.99)	8.74×10^{-4}
Mitochondrial proton transporting ATP synthase complex (3, 61.00)	9.60×10^{-4}

[a] Values in parenthesis represent the number of genes involved in and the fold enrichment of the corresponding functional terms

[b] EASE score examine the significance of gene term enrichment with a modified Fisher's exact test

https://doi.org/10.1371/journal.pone.0213420.t001

Comparison of downregulated genes with the mouse genome database

In order to explore mechanisms that may relate to reduced viability in embryos obtained using cryopreserved semen, the Mouse Genome Database [34, 35] was queried to determine whether genes downregulated in CRYO equine embryos were orthologs to mouse genes with known associations with embryo lethality.

Day-8 embryos

In Day-8 CRYO embryos, transcripts of genes associated with the following terms were found to be of low abundance: failure of zygotic division, decreased embryo size, abnormal embryo size, embryonic growth arrest, embryonic growth retardation, embryonic lethality before implantation-complete penetrance, embryonic lethality between implantation and somite formation-complete penetrance, embryonic lethality between somite formation and embryo turning-complete penetrance, embryonic lethality prior to tooth bud stage, abnormal embryonic tissue morphology, abnormal extraembryonic tissue morphology, delayed allantois development, perinatal lethality incomplete penetrance, prenatal lethality-complete penetrance, preweaning lethality-complete penetrance, abnormal male germ cell apoptosis, abnormal spermatogenesis, azoospermia, male infertility, and female infertility.

Day 10 embryos

In Day-10 CRYO embryos, the following gene associations cited above for Day-8 embryos were found: decreased embryo size, abnormal embryo size, failure of zygotic cell division, embryonic lethality between implantation and somite formation, embryonic lethality between implantation and somite formation-complete penetrance, embryonic lethality prior to tooth bud stage, prenatal lethality-complete penetrance, perinatal lethality-incomplete penetrance,

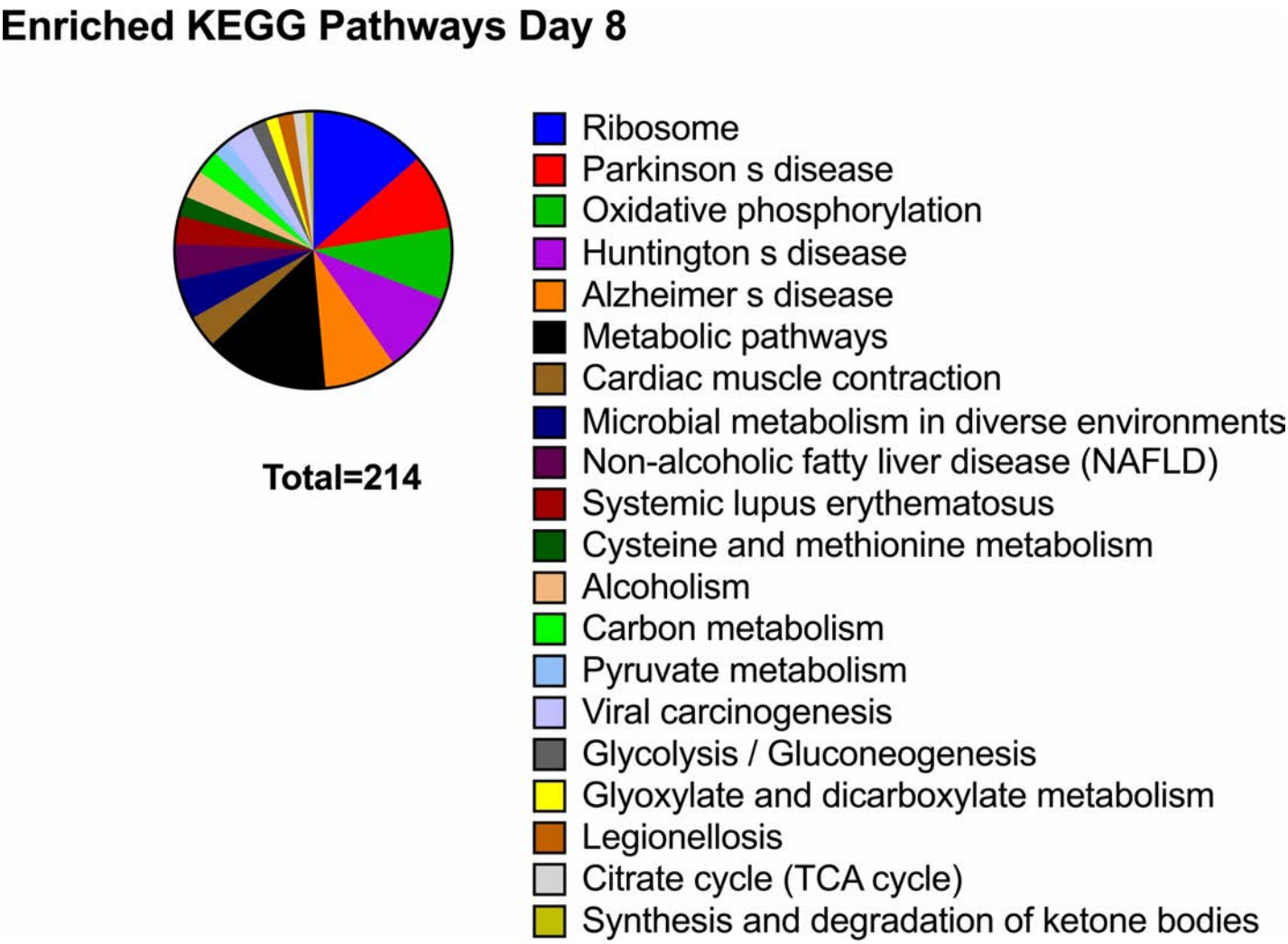

Fig 3. Enriched Kyoto Encyclopedia of Genes and Genomes (KEGG) pathways in transcripts downregulated in 8-Day embryos obtained with frozen-thawed spermatozoa.

https://doi.org/10.1371/journal.pone.0213420.g003

preweaning lethality, preweaning lethality-complete penetrance, and abnormal spermatogenesis.

In addition, the following associations were found: abnormal blastocyst morphology, absent blastocele, abnormal inner cell mass morphology, absent inner cell mass proliferation, empty decidua capsularis, embryonic growth retardation, failure of blastocyst to hatch from the zona pellucida, abnormal preimplantation embryo development, failure to gastrulate, embryonic lethality prior to embryogenesis, failure of embryo implantation, abnormal decidua basalis morphology, abnormal extraembryonic endoderm formation, prenatal lethality prior to heart atrial septation, decreased fetal size, preweaning lethality incomplete penetrance, abnormal gametogenesis, abnormal spermatid morphology, abnormal vas deferens morphology, decreased mature ovarian follicle number, reduced female fertility and small ovary.

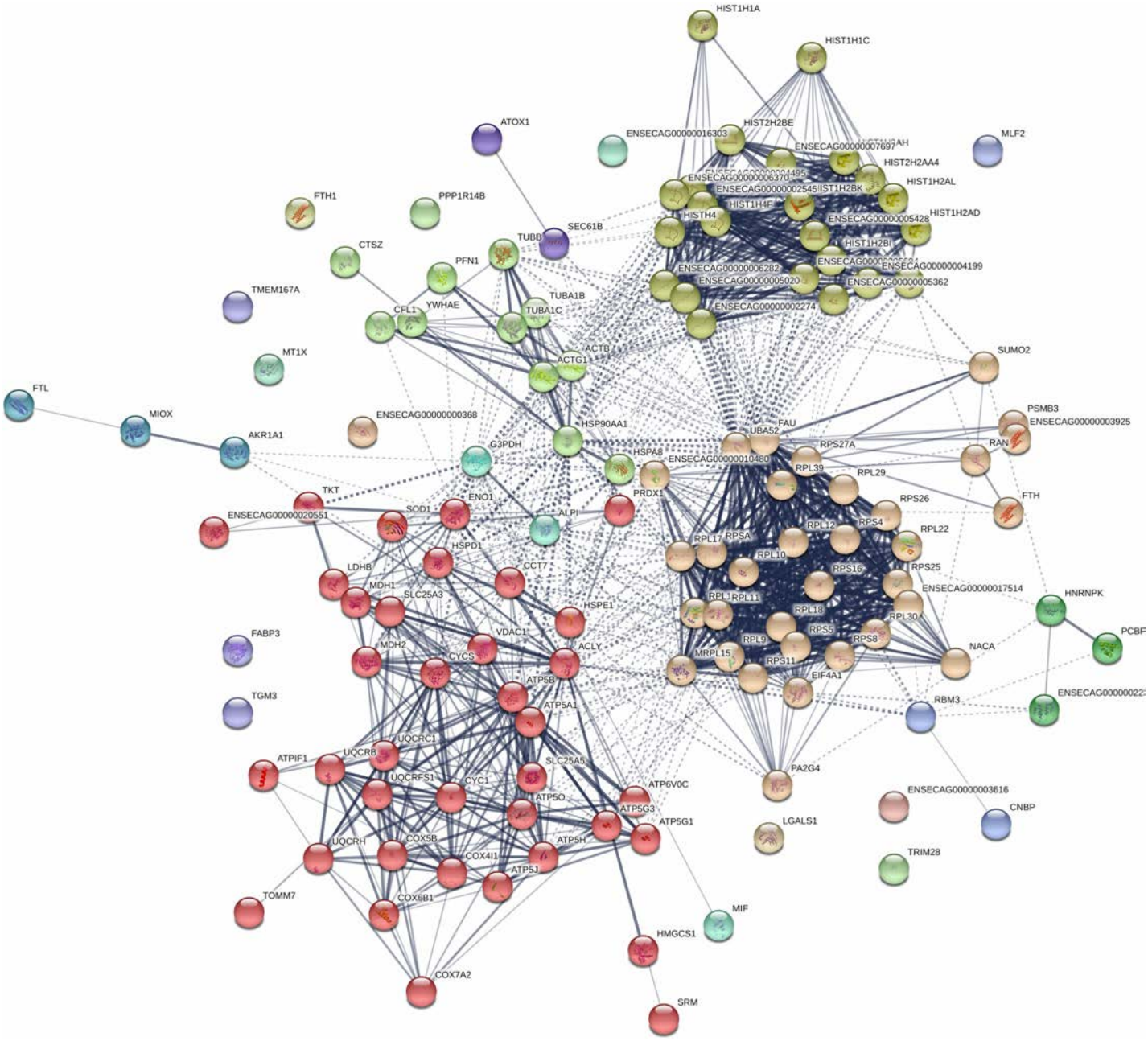

Fig 4. Functional networks (STRING) of transcripts downregulated in 8-Day equine embryos obtained with frozen-thawed sperm (CRYO embryos). Functional networks apply to histones and mitochondrial proteins. Controls are 8-Day embryos from the same mare, obtained with fresh semen from the same ejaculate that was frozen and used to produce the CRYO embryos. A list of the transcripts in each cluster obtained after STRING analysis are presented. Colors for each cluster are given in S3 Table.

https://doi.org/10.1371/journal.pone.0213420.g004

Day 12 embryos

In 12-day CRYO embryos the following gene associations cited above were found: abnormal embryo size, decreased embryo size, prenatal lethality prior to heart atrial septation, embryonic lethality prior to tooth bud stage, preweaning lethality-complete penetrance, male infertility, female infertility, and small ovary.

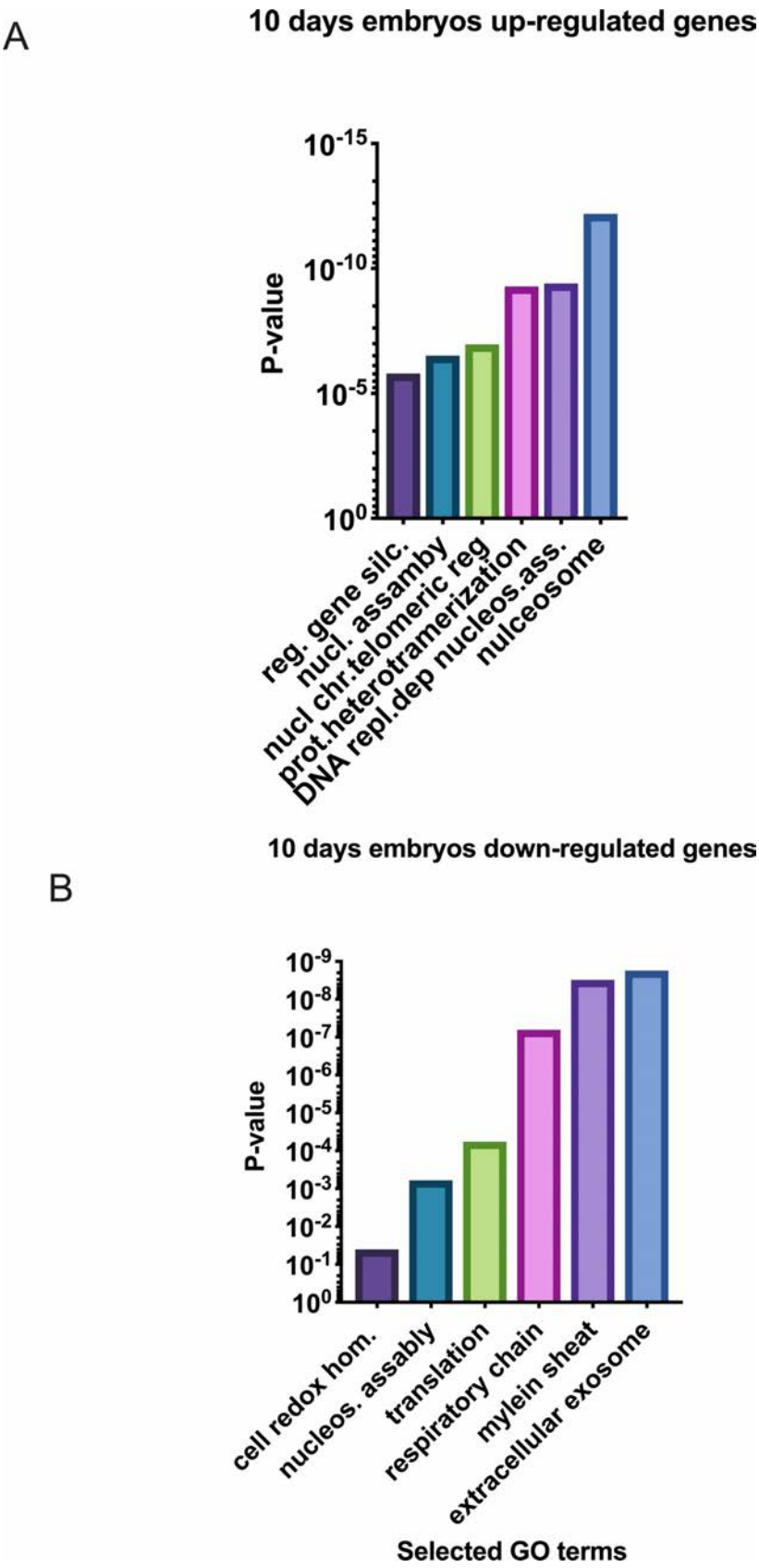
A
10 days embryos up-regulated genes
P-value
10-15
10-10
10-5
100
reg. gene silc.
nucl. assamby
nucl chr.telomeric reg
prot.heterotramerization
DNA repl.dep nucleos.ass.
nulceosome
B
10 days embryos down-regulated genes
P-value
10-9
10-8
10-7
10-6
10-5
10-4
10-3
10-2
10-1
100
cell redox hom.
nucleos. assably
translation
respiratory chain
mylein sheat
extracellular exosome
Selected GO terms

Fig 5. Selected enriched GO terms differentially regulated in 10-Day equine embryos obtained with fresh sperm (FRSH) and frozen-thawed sperm (CRYO), (A) transcripts down regulated transcripts 10-Day CRYO embryos, (B) transcripts up regulated in 10-Day CRYO embryos.

https://doi.org/10.1371/journal.pone.0213420.g005

In addition, the following associations were found: incomplete embryo turning, embryonic lethality prior to organogenesis, embryonic lethality during organogenesis-complete penetrance, decreased FSH level, small seminal vesicle, small seminiferous tubules, small testis, absent mature ovarian follicles, abnormal ovulation, abnormal corpus luteum morphology, uterus hypoplasia, and vaginal atresia.

Discussion

Here we report, for the first time, evidence that procedures performed during handling of sperm, such as freezing and thawing, have a significant impact on critical aspects of the early embryo transcriptome. The equine model used in our study has a number of advantages, including a long pre-attachment embryonic period in which the embryo remains spherical, which facilitates embryo collection, and the possibility of repeated embryo collections from the same animals over successive estrus cycles. Additionally, the stallion serves as an excellent model for the human male, as stallions are typically not selected for sperm quality nor the ability of semen to be cryopreserved, in contrast to males in production species, such as the bull. Moreover, since many stallions reach advanced age, the horse can be used as a model to study the impact of paternal age on embryo quality.

Our study, focused on three embryo ages (8, 10 and 12 days post ovulation), revealed a significant impact of sperm cryopreservation on the transcriptome of the resulting embryo. Importantly, transcripts with decreased abundance reflected genes related to DNA replication and assembly, and oxidative phosphorylation. Exploration of differentially-expressed genes at the molecular and cellular level revealed alterations in important functions including ATP synthesis, regulation of transcription, nucleosome assembly, chromatin silencing, protein synthesis, and redox regulation. Alterations in these genes help to explain the reduced fertility observed with cryopreserved sperm attributable to increased early embryo mortality [11, 12].

The pre-implantation period is a period of rapid embryo growth, requiring a ready supply of ATP. The equine embryo appears to have a significant capacity for glycolysis, but also uses oxidative phosphorylation [36]. The KEGG pathways analysis of downregulated genes revealed enriched annotations for oxidative phosphorylation, pyruvate metabolism, glycolysis, and the TCA cycle, suggesting compromised energy metabolism in CRYO embryos. A similar picture was observed in Day-10 and Day-12 embryos, with the pathways for oxidative

Table 2. Selected enriched Kyoto Encyclopedia of Genes and Genomes (KEGG) pathways enriched in downregulated transcripts of in 10 days embryos obtained after AI with frozen thawed sperm.

KEGG pathway	Pathway description	observed gene count	false discovery rate
190	Oxidative phosphorylation	21	2,45E-23
5012	Parkinson s disease	20	4,64E-21
5010	Alzheimer s disease	15	1,05E-12
5016	Huntington s disease	15	3,42E-12
1100	Metabolic pathways	28	4,29E-09
3010	Ribosome	11	8,96E-09
4260	Cardiac muscle contraction	7	2,56E-06
4932	Non-alcoholic fatty liver disease (NAFLD)	9	3,96E-06
4141	Protein processing in endoplasmic reticulum	9	1,61E-05

https://doi.org/10.1371/journal.pone.0213420.t002

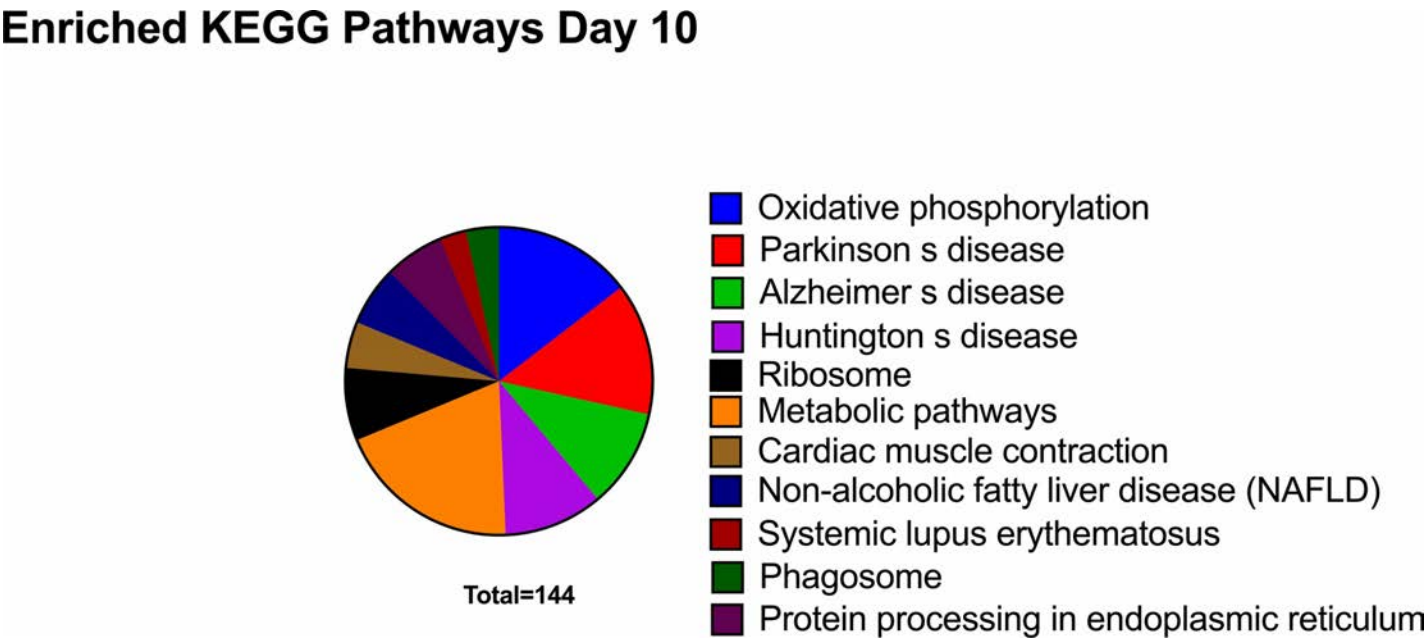

Fig 6. Enriched Kyoto Encyclopedia of Genes and Genomes (KEGG) pathways in transcripts downregulated in 10-Day embryos obtained with frozen-thawed spermatozoa.

https://doi.org/10.1371/journal.pone.0213420.g006

phosphorylation, metabolic pathways, and non alcoholic fatty liver disease significantly over-represented in transcripts with reduced abundance of all CRYO embryos obtained.

When we evaluated low-abundance equine transcripts for their mouse orthologs, we found that many of the genes downregulated in CRYO embryos have knockout database annotation terms related to reduced embryonic viability. This finding opens the possibility that not only genes related to the metabolism and thus growth of embryos, but also genes directly related to embryo organogenesis, embryo survival, and offspring health are affected by the use of cryopreserved sperm, and thus these genes warrant further investigation.

While the mechanisms behind the effects reported here are as yet unclear, a major factor may be the well-documented oxidative damage that the genome and epigenome experiences during cryopreservation and thawing [11–14]. Cryopreservation is a major cause of oxidative stress [37] and lipid peroxidation in stallion spermatozoa [10, 17, 38, 39]. Lipid peroxidation in spermatozoa surviving cryopreservation [37] is associated with increased levels of 4-hydroxinonenal (4-HNE) [17]. This compound is able to interact with DNA to form adducts that have been related directly to increased rates of mutation in important cell-cycle regulators [40, 41]. The production of 4-HNE during cryopreservation of stallion spermatozoa is well documented [10, 17, 39], and it is possible that significant amounts of 4-HNE and other toxic lipid aldehydes are incorporated to the oocyte, potentially causing alterations in embryo development. In addition to DNA damage, 4-HNE can alkylate the sperm centrioles, and in horses, as in humans, paternal centrioles are inherited by the embryos. Damaged centrioles may cause disrupted cytoskeletal protein organization during early cleavage [42].

Supporting this line of reasoning, recent reports have linked abnormal early cleavage events and changes in embryo transcript abundance to fertilization with spermatozoa showing oxidative stress. Macaque embryos obtained after fertilization with ROS-treated sperm showed significantly lower rates of development to the four- and eight-cell stages, and changes in transcript abundance for genes related to actin cytoskeleton organization, cell junction

Table 3. Gene ontology annotations enriched in downregulated transcripts of 10 days embryos obtained after AI with frozen thawed sperm.

Term	P Value
GO:0070062~extracellular exosome	1,72E-09
GO:0043209~myelin sheath	3,03E-09
GO:0070469~respiratory chain	6,30E-08
GO:0022625~cytosolic large ribosomal subunit	5,33E-07
GO:0008137~NADH dehydrogenase (ubiquinone) activity	8,07E-07
GO:0005747~mitochondrial respiratory chain complex I	3,12E-06
GO:0015986~ATP synthesis coupled proton transport	4,78E-06
GO:0003735~structural constituent of ribosome	1,66E-05
GO:0000788~nuclear nucleosome	2,25E-05
GO:0046933~proton-transporting ATP synthase activity, rotational mechanism	2,90E-05
GO:0005925~focal adhesion	4,41E-05
GO:0006412~translation	5,75E-05
GO:0046961~proton-transporting ATPase activity, rotational mechanism	1,59E-04
GO:0000786~nucleosome	1,73E-04
GO:0042773~ATP synthesis coupled electron transport	2,22E-04
GO:0006334~nucleosome assembly	5,99E-04
GO:0005743~mitochondrial inner membrane	0,001576512
GO:0004129~cytochrome-c oxidase activity	0,002995144
GO:0005739~mitochondrion	0,00444262
GO:0006336~DNA replication-independent nucleosome assembly	0,005364717
GO:0045261~proton-transporting ATP synthase complex, catalytic core F(1)	0,011191606
GO:0015991~ATP hydrolysis coupled proton transport	0,013628447
GO:0006457~protein folding	0,017943471
GO:0051603~proteolysis involved in cellular protein catabolic process	0,019505148
GO:0003677~DNA binding	0,022056606
GO:0006123~mitochondrial electron transport, cytochrome c to oxygen	0,024396132
GO:0044822~poly(A) RNA binding	0,032707627
GO:0005753~mitochondrial proton-transporting ATP synthase complex	0,0332053
GO:0005615~extracellular space	0,040768468
GO:0005687~U4 snRNP	0,044030068
GO:0045454~cell redox homeostasis	0,047994139
GO:0006122~mitochondrial electron transport, ubiquinol to cytochrome c	0,048204941
GO:1902166~negative regulation of intrinsic apoptotic signaling pathway in response to DNA damage by p53 class mediator	0,054067016
GO:0006120~mitochondrial electron transport, NADH to ubiquinone	0,059893472
GO:0045653~negative regulation of megakaryocyte differentiation	0,065684522
GO:0030330~DNA damage response, signal transduction by p53 class mediator	0,065684522
GO:0016020~membrane	0,071097195
GO:0004185~serine-type carboxypeptidase activity	0,07400431
GO:0034719~SMN-Sm protein complex	0,075791838
GO:0005685~U1 snRNP	0,075791838
GO:0002227~innate immune response in mucosa	0,077161252
GO:0007569~cell aging	0,077161252
GO:0005682~U5 snRNP	0,080983251
GO:0071157~negative regulation of cell cycle arrest	0,082847353
GO:0019731~antibacterial humoral response	0,082847353
GO:0005975~carbohydrate metabolic process	0,083234703

(*Continued*)

Table 3. (Continued)

Term	P Value
GO:0005686~U2 snRNP	0,086145885
GO:0030970~retrograde protein transport, ER to cytosol	0,088498889
GO:0000784~nuclear chromosome, telomeric region	0,089088094
GO:0045787~positive regulation of cell cycle	0,094116067

https://doi.org/10.1371/journal.pone.0213420.t003

assembly and cell adhesion [43]. Although seen at a much later stage of development, in our study we also found that genes for cytoskeleton components tubulin alpha 1 a, tubulin beta 2

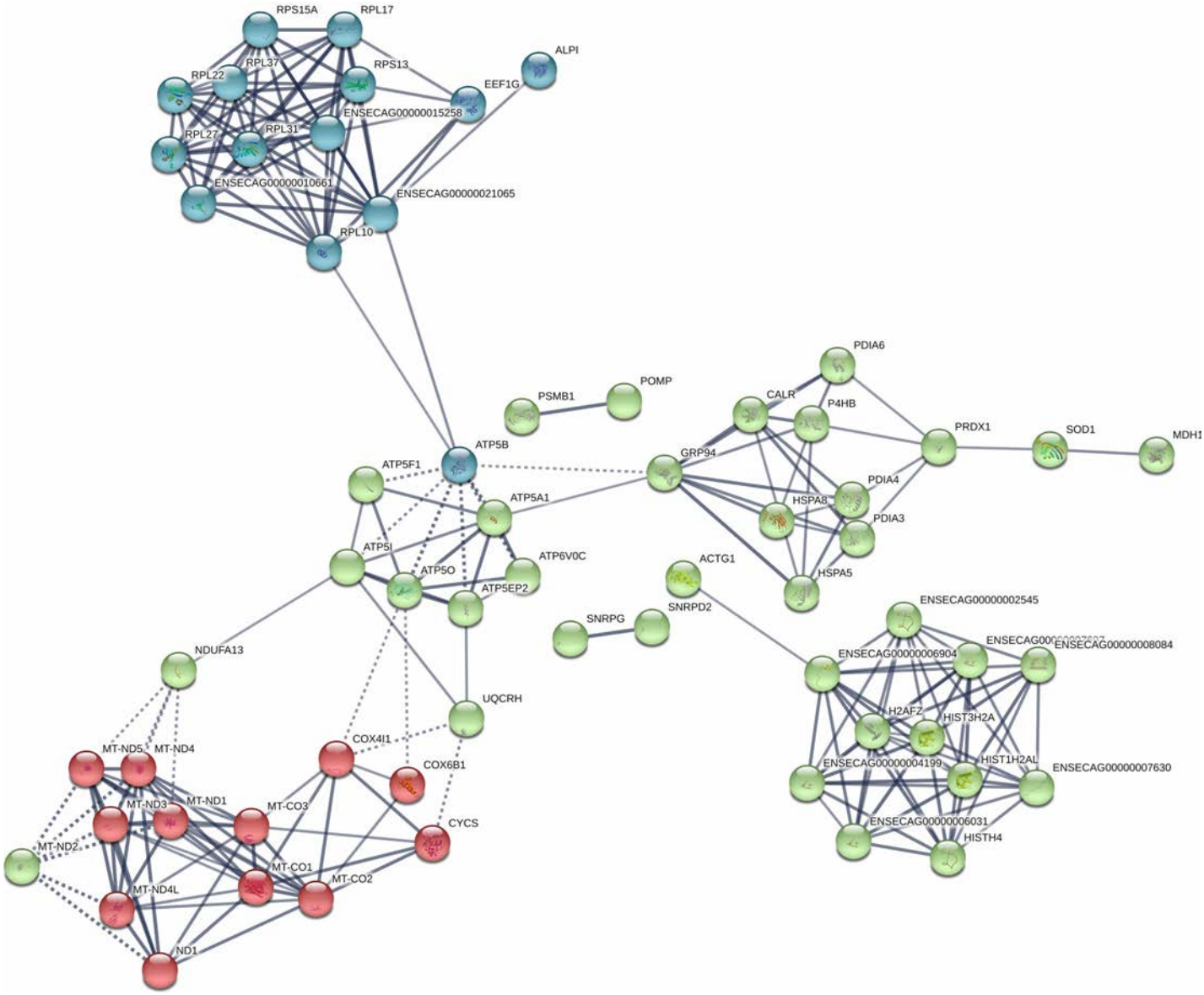

Fig 7. Functional networks (STRING) of transcripts downregulated in 10-Day equine embryos obtained with frozen-thawed sperm (CRYO embryos). Functional networks apply to histones and mitochondrial proteins. Controls are same-age embryos from the same mare, obtained with fresh semen from the same ejaculate that was frozen and used to produce the CRYO embryos.

https://doi.org/10.1371/journal.pone.0213420.g007

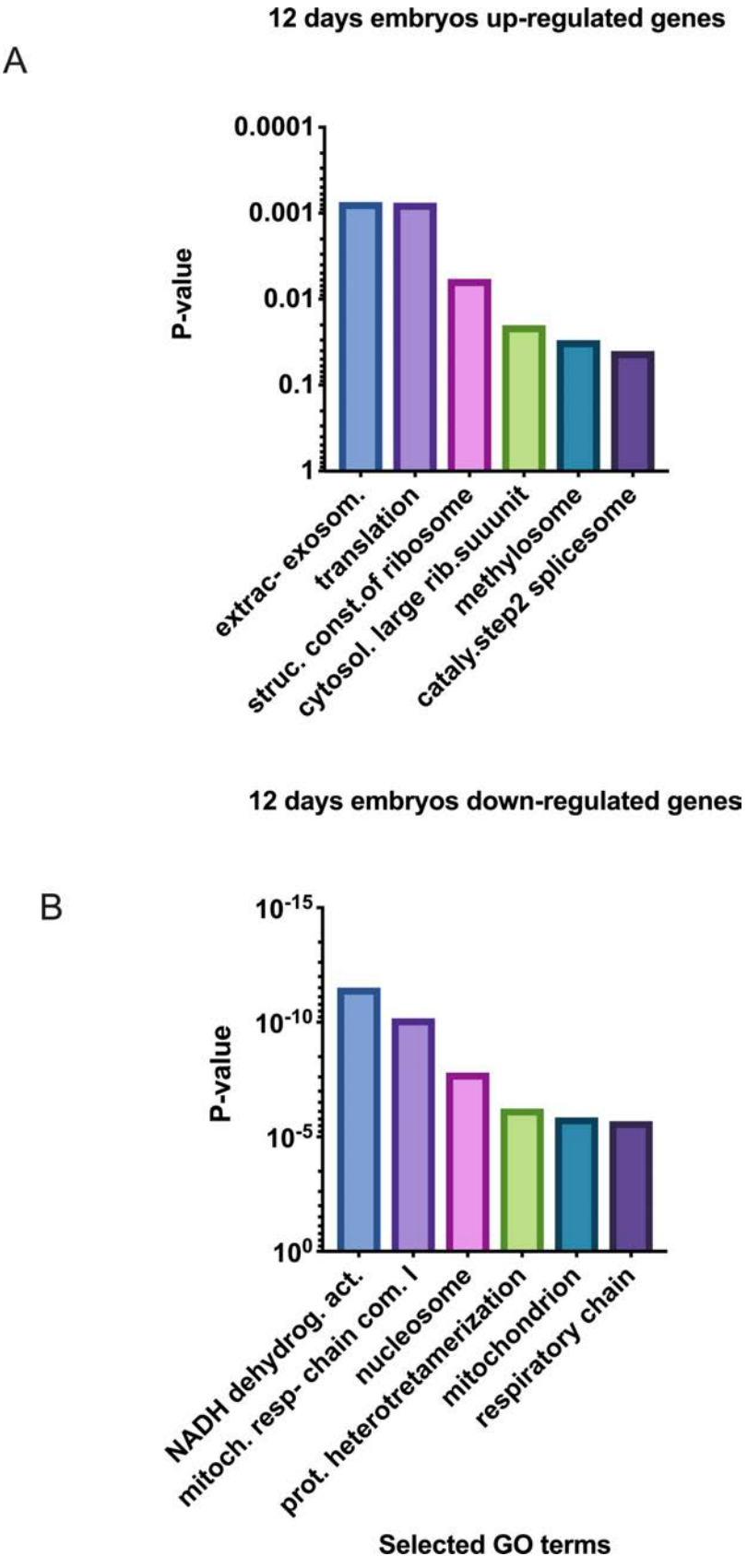
12 days embryos up-regulated genes
A
P-value
0.0001
0.001
0.01
0.1
1
extrac- exosom.
translation
struc. const.of ribosome
cytosol. large rib.suuunit
methylosome
cataly.step2 splicesome
12 days embryos down-regulated genes
B
P-value
10-15
10-10
10-5
100
NADH dehydrog. act.
mitoch. resp- chain com. I
nucleosome
prot. heterotretamerization
mitochondrion
respiratory chain
Selected GO terms

Fig 8. Selected enriched GO terms differentially regulated in 12-Day equine embryos obtained with fresh sperm (FRSH) and frozen-thawed sperm (CRYO), (A) transcripts down regulated in 12-Day CRYO embryos, (B) transcripts up regulated in 12-Day CRYO embryos.

https://doi.org/10.1371/journal.pone.0213420.g008

class II a and actin, cytoplasmic 1, N-terminally processed were downregulated in 8-day CRYO embryos.

Cryopreservation may also directly affect the epigenome of the paternal DNA; recent studies have shown that cryopreservation increases the level of DNA methylation in equine sperm [12] and the expression of genes important to intracellular regulation of epigenetic status [16]. Notably, we also found significant reduction in abundance of transcripts for histones in CRYO embryos.

The finding that many differentially regulated genes in CRYO embryos are orthologs of mouse genes that have knockout database annotation terms related to reduced embryonic viability provides further evidence linking cryopreserved sperm to reduced embryonic viability. These annotations consistently appeared on analysis of low-abundance transcripts in all CRYO embryos, and included genes related to embryonic growth retardation and embryo lethality. Interestingly, annotations related to male and female infertility were also present; this warrants further investigation on the effect of sperm origin on the fertility of resulting offspring.

In summary, the present study provides for the first time transcriptomic analysis of equine embryos in relation to the handling of semen used for their production, however we acknowledge the preliminary and descriptive nature of this report but our data provide strong evidence that cryopreservation of sperm exerts a profound impact on the transcriptome of early

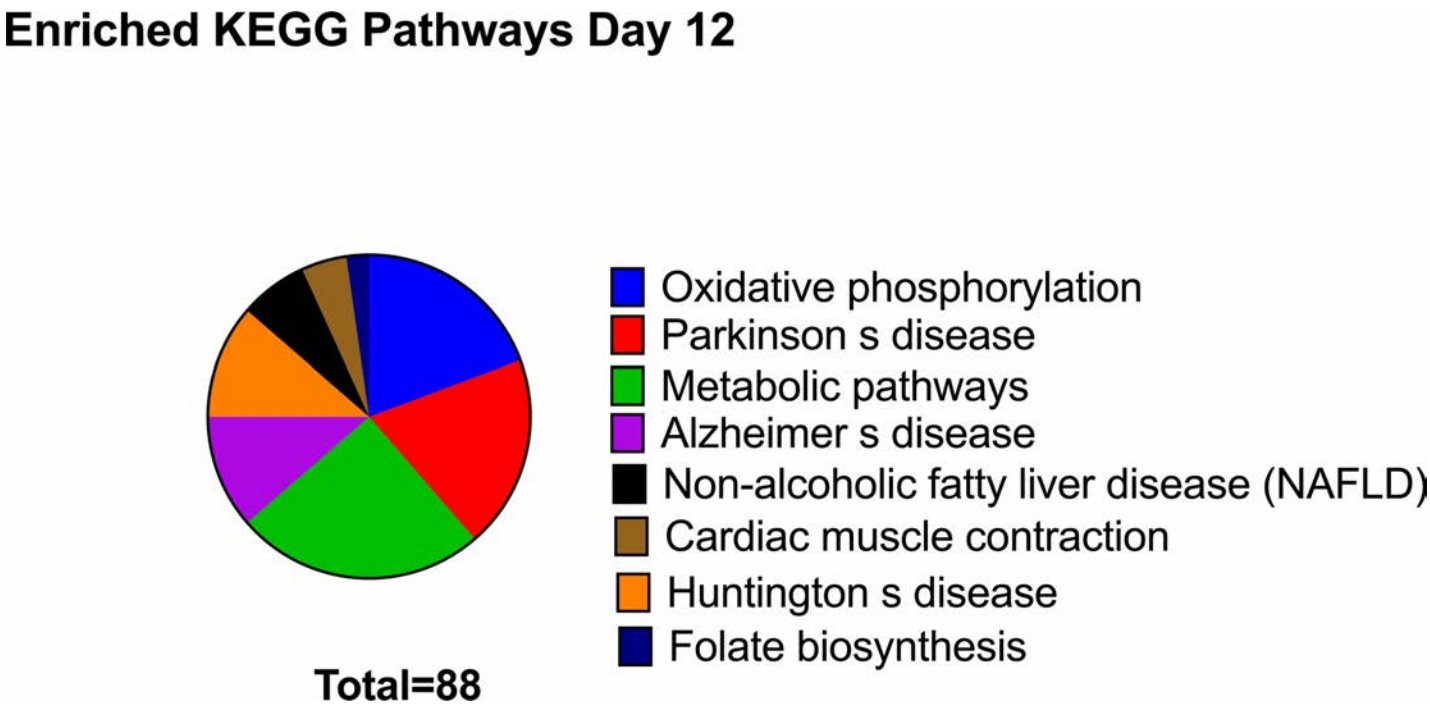

Fig 9. Enriched Kyoto Encyclopedia of Genes and Genomes (KEGG) pathways in transcripts downregulated in 12-Day embryos obtained with frozen thawed spermatozoa.

https://doi.org/10.1371/journal.pone.0213420.g009

Table 4. Functional annotation chart of differentially expressed genes (downregulated) in Day-12 equine embryos obtained after AI with frozen-thawed sperm.

Category	Term	Count	PValue
UP_KEYWORDS	Membrane	22	0,035165176
GOTERM_CC_DIRECT	GO:0016021~Integral component of membrane	19	0,023827798
KEGG_PATHWAY	ecb01100:Metabolic pathways	18	8,33E-05
GOTERM_CC_DIRECT	GO:0005739~Mitochondrion	14	1,40E-06
KEGG_PATHWAY	ecb00190:Oxidative phosphorylation	13	1,69E-12
KEGG_PATHWAY	ecb05012:Parkinson's disease	13	3,57E-12
GOTERM_CC_DIRECT	GO:0070062~Extracellular exosome	13	0,047249394
UP_KEYWORDS	Chromosome	10	4,30E-12
UP_KEYWORDS	Mitochondrion	10	1,63E-10
UP_KEYWORDS	DNA-binding	10	2,09E-05
UP_KEYWORDS	Transport	10	3,60E-05
UP_KEYWORDS	Nucleus	10	6,21E-04
UP_KEYWORDS	Respiratory chain	9	7,16E-16
UP_KEYWORDS	Electron transport	9	3,97E-14
UP_KEYWORDS	Nucleosome core	9	2,19E-11
INTERPRO	IPR009072:Histone-fold	9	2,07E-10
UP_KEYWORDS	Ubiquinone	8	3,96E-16
GOTERM_MF_DIRECT	GO:0008137~NADH dehydrogenase (ubiquinone) activity	8	3,09E-12
GOTERM_CC_DIRECT	GO:0005747~Mitochondrial respiratory chain complex I	8	6,67E-11
GOTERM_MF_DIRECT	GO:0003677~DNA binding	8	5,87E-04
UP_SEQ_FEATURE	Transmembrane region	8	9,18E-04
GOTERM_CC_DIRECT	GO:0000786~Nucleosome	7	1,55E-08
UP_KEYWORDS	NAD	7	5,92E-08
KEGG_PATHWAY	ecb05322:Systemic lupus erythematosus	7	3,03E-05
UP_KEYWORDS	Oxidoreductase	7	4,97E-05
KEGG_PATHWAY	ecb05034:Alcoholism	7	2,10E-04
GOTERM_CC_DIRECT	GO:0016020~Membrane	7	0,047593153
UP_KEYWORDS	Mitochondrion inner membrane	6	2,81E-07
KEGG_PATHWAY	ecb05010:Alzheimer's disease	6	0,001939005
KEGG_PATHWAY	ecb05016:Huntington's disease	6	0,003145256
GOTERM_BP_DIRECT	GO:0006335~DNA replication-dependent nucleosome assembly	5	4,77E-07
GOTERM_BP_DIRECT	GO:0051290~Protein heterotetramerization	5	5,76E-07
INTERPRO	IPR007125:Histone core	5	2,52E-05
GOTERM_CC_DIRECT	GO:0000784~Nuclear chromosome, telomeric region	5	2,30E-04
GOTERM_CC_DIRECT	GO:0005743~Mitochondrial inner membrane	5	0,001683893
SMART	SM00417:H4	4	6,25E-07
SMART	SM00803:TAF	4	1,22E-06
GOTERM_CC_DIRECT	GO:0070469~Respiratory chain	4	2,03E-06
INTERPRO	IPR019809:Histone H4, conserved site	4	2,80E-06
INTERPRO	IPR001951:Histone H4	4	2,80E-06
GOTERM_BP_DIRECT	GO:0045653~Negative regulation of megakaryocyte differentiation	4	4,00E-06
INTERPRO	IPR004823:TATA box binding protein associated factor (TAF)	4	5,47E-06
GOTERM_BP_DIRECT	GO:0006336~DNA replication-independent nucleosome assembly	4	1,95E-05
GOTERM_BP_DIRECT	GO:0006352~DNA-templated transcription, initiation	4	2,71E-05
INTERPRO	IPR020904:Short-chain dehydrogenase/reductase, conserved site	4	1,57E-04
INTERPRO	IPR002347:Glucose/ribitol dehydrogenase	4	6,29E-04
GOTERM_BP_DIRECT	GO:0006334~Nucleosome assembly	4	8,65E-04
GOTERM_MF_DIRECT	GO:0016491~Oxidoreductase activity	4	0,001585835

(*Continued*)

Table 4. (Continued)

Category	Term	Count	PValue
INTERPRO	IPR016040:NAD(P)-binding domain	4	0,016019866
KEGG_PATHWAY	ecb04932:Non-alcoholic fatty liver disease (NAFLD)	4	0,045179763
INTERPRO	IPR001750:NADH:ubiquinone/plastoquinone oxidoreductase	3	3,19E-05
GOTERM_BP_DIRECT	GO:0042773~ATP synthesis coupled electron transport	3	5,21E-05
GOTERM_CC_DIRECT	GO:0000788~Nuclear nucleosome	3	0,004620686
KEGG_PATHWAY	ecb04978:Mineral absorption	3	0,022822957
GOTERM_CC_DIRECT	GO:0000790~Nuclear chromatin	3	0,073903618

https://doi.org/10.1371/journal.pone.0213420.t004

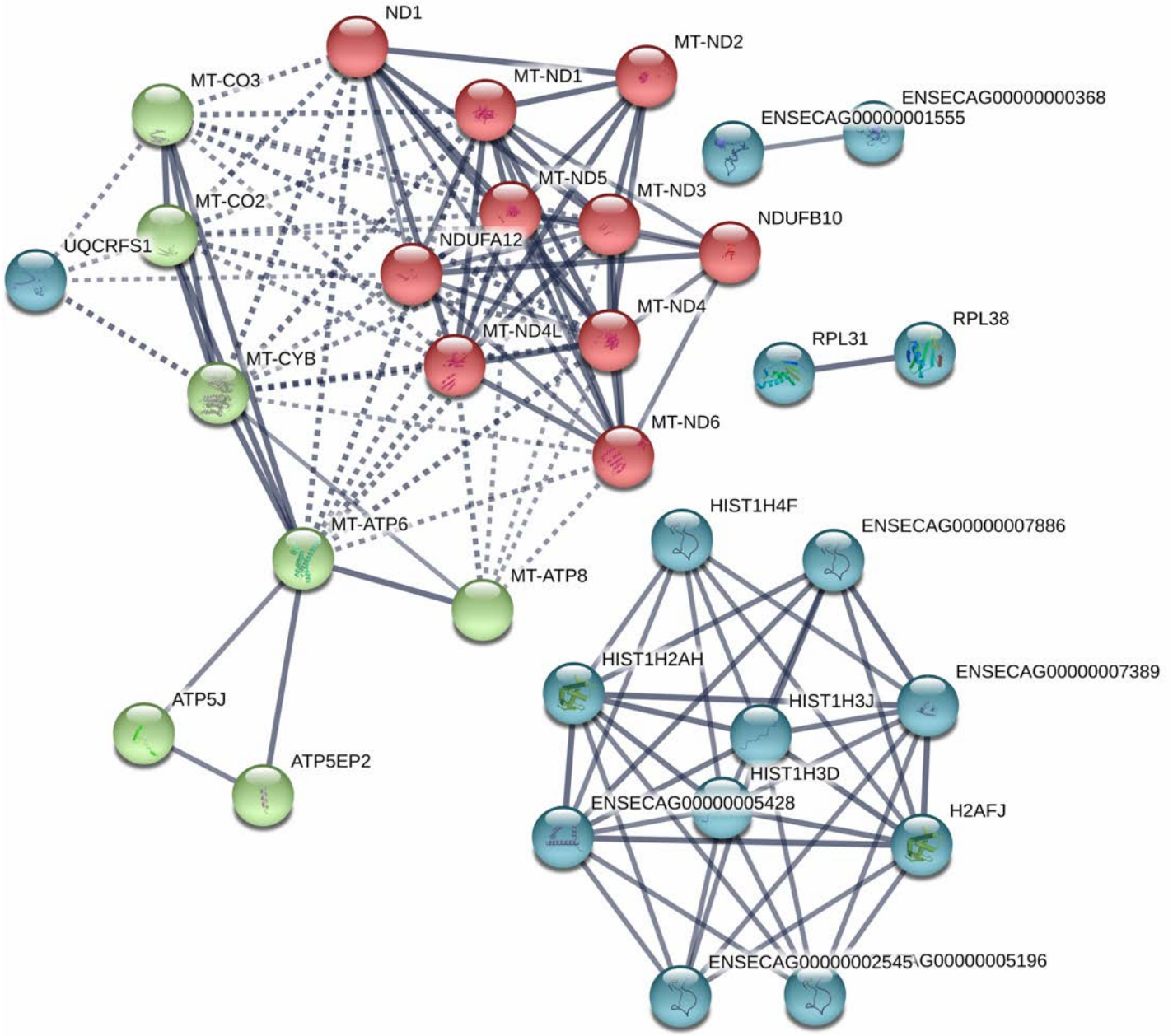

Fig 10. Functional networks (STRING) of transcripts downregulated in 12-Day equine embryos obtained with frozen thawed sperm (CRYO). Functional networks apply to histones and mitochondrial proteins. Controls are same-age embryos from the same mare obtained with fresh semen from the same ejaculate that was frozen and used to produce the CRYO embryos.

https://doi.org/10.1371/journal.pone.0213420.g010

embryos. Our findings may stimulate new lines of research to improve this biotechnology in humans and animals.

Supporting information

S1 Table. Transcripts upregulated in 8-Day embryos obtained with frozen-thawed spermatozoa with respect to controls obtained with fresh semen.
(XLSX)

S2 Table. Transcripts downregulated in 8-Day embryos obtained with frozen-thawed spermatozoa.
(XLSX)

S3 Table. Network analysis of transcripts downregulated in 8-Day embryos obtained with frozen-thawed spermatozoa. List of transcripts in each cluster obtained after STRING analysis; genes in each cluster are presented and colors for each cluster are given. Network is presented in Fig 4.
(XLSX)

S4 Table. Transcripts upregulated in 10-Day embryos obtained with frozen-thawed spermatozoa.
(XLSX)

S5 Table. Transcripts upregulated in 12-day embryos obtained with frozen-thawed spermatozoa.
(XLSX)

S6 Table. Transcripts downregulated in 12-Day embryos obtained with frozen-thawed spermatozoa.
(XLSX)

Author Contributions

Conceptualization: Heriberto Rodríguez-Martínez, Fernando J. Peña.

Data curation: Ángel Román.

Formal analysis: Alberto Álvarez-Barrientos, Ángel Román, Fernando J. Peña.

Funding acquisition: Fernando J. Peña.

Investigation: José M. Ortiz-Rodriguez, Cristina Ortega-Ferrusola, María C. Gil, Francisco E. Martín-Cano, Gemma Gaitskell-Phillips, Fernando J. Peña.

Methodology: Alberto Álvarez-Barrientos, Ángel Román.

Resources: Alberto Álvarez-Barrientos.

Software: Francisco E. Martín-Cano, Ángel Román.

Supervision: Katrin Hinrichs, Fernando J. Peña.

Validation: Ángel Román.

Visualization: Ángel Román.

Writing – original draft: Katrin Hinrichs, Fernando J. Peña.

Writing – review & editing: Heriberto Rodríguez-Martínez, Katrin Hinrichs, Fernando J. Peña.

References

1. Pena FJ, Garcia BM, Samper JC, Aparicio IM, Tapia JA, Ferrusola CO. Dissecting the molecular damage to stallion spermatozoa: the way to improve current cryopreservation protocols? Theriogenology. 2011; 76(7):1177–86. https://doi.org/10.1016/j.theriogenology.2011.06.023 PMID: 21835453.
2. Dearing CG, Jayasena CN, Lindsay KS. Human sperm cryopreservation in cancer patients: Links with deprivation and mortality. Cryobiology. 2017; 79:9–13. https://doi.org/10.1016/j.cryobiol.2017.10.003 PMID: 29031884.
3. Jiang XP, Zhou WM, Wang SQ, Wang W, Tang JY, Xu Z, et al. Multivariate model for predicting semen cryopreservation outcomes in a human sperm bank. Asian J Androl. 2017; 19(4):404–8. https://doi.org/10.4103/1008-682X.178488 PMID: 27080478; PubMed Central PMCID: PMC5507083.
4. Camillo F, Vannozzi I, Tesi M, Sabatini C, Rota A, Paciolla E, et al. Induction of ovulation with buserelin in jennies: in search of the minimum effective dose. Anim Reprod Sci. 2014; 151(1–2):56–60. Epub 2014/10/09. https://doi.org/10.1016/j.anireprosci.2014.09.011 PMID: 25293536.
5. Thomson LK, Fleming SD, Aitken RJ, De Iuliis GN, Zieschang JA, Clark AM. Cryopreservation-induced human sperm DNA damage is predominantly mediated by oxidative stress rather than apoptosis. Hum Reprod. 2009; 24(9):2061–70. https://doi.org/10.1093/humrep/dep214 PMID: 19525298.
6. Panzani D, Rota A, Marmorini P, Vannozzi I, Camillo F. Retrospective study of factors affecting multiple ovulations, embryo recovery, quality, and diameter in a commercial equine embryo transfer program. Theriogenology. 2014; 82(6):807–14. Epub 2014/08/03. https://doi.org/10.1016/j.theriogenology.2014.06.020 PMID: 25085596.
7. Jodar M, Selvaraju S, Sendler E, Diamond MP, Krawetz SA, Reproductive Medicine N. The presence, role and clinical use of spermatozoal RNAs. Hum Reprod Update. 2013; 19(6):604–24. https://doi.org/10.1093/humupd/dmt031 PMID: 23856356; PubMed Central PMCID: PMC3796946.
8. Sendler E, Johnson GD, Mao S, Goodrich RJ, Diamond MP, Hauser R, et al. Stability, delivery and functions of human sperm RNAs at fertilization. Nucleic Acids Res. 2013; 41(7):4104–17. https://doi.org/10.1093/nar/gkt132 PMID: 23471003; PubMed Central PMCID: PMC3627604.
9. Davila MP, Munoz PM, Bolanos JM, Stout TA, Gadella BM, Tapia JA, et al. Mitochondrial ATP is required for the maintenance of membrane integrity in stallion spermatozoa, whereas motility requires both glycolysis and oxidative phosphorylation. Reproduction. 2016; 152(6):683–94. https://doi.org/10.1530/REP-16-0409 PMID: 27798283.
10. Pena FJ, Plaza Davila M, Ball BA, Squires EL, Martin Munoz P, Ortega Ferrusola C, et al. The Impact of Reproductive Technologies on Stallion Mitochondrial Function. Reprod Domest Anim. 2015; 50(4):529–37. https://doi.org/10.1111/rda.12551 PMID: 26031351.
11. Kopeika J, Thornhill A, Khalaf Y. The effect of cryopreservation on the genome of gametes and embryos: principles of cryobiology and critical appraisal of the evidence. Hum Reprod Update. 2015; 21(2):209–27. https://doi.org/10.1093/humupd/dmu063 PMID: 25519143.
12. Aurich C, Schreiner B, Ille N, Alvarenga M, Scarlet D. Cytosine methylation of sperm DNA in horse semen after cryopreservation. Theriogenology. 2016; 86(5):1347–52. https://doi.org/10.1016/j.theriogenology.2016.04.077 PMID: 27242182.
13. Valcarce DG, Carton-Garcia F, Riesco MF, Herraez MP, Robles V. Analysis of DNA damage after human sperm cryopreservation in genes crucial for fertilization and early embryo development. Andrology. 2013; 1(5):723–30. https://doi.org/10.1111/j.2047-2927.2013.00116.x PMID: 23970451.
14. Valcarce DG, Carton-Garcia F, Herraez MP, Robles V. Effect of cryopreservation on human sperm messenger RNAs crucial for fertilization and early embryo development. Cryobiology. 2013; 67(1):84–90. https://doi.org/10.1016/j.cryobiol.2013.05.007 PMID: 23727067.
15. Teperek M, Simeone A, Gaggioli V, Miyamoto K, Allen GE, Erkek S, et al. Sperm is epigenetically programmed to regulate gene transcription in embryos. Genome Res. 2016; 26(8):1034–46. https://doi.org/10.1101/gr.201541.115 PMID: 27034506; PubMed Central PMCID: PMC4971762.
16. Zeng C, Peng W, Ding L, He L, Zhang Y, Fang D, et al. A preliminary study on epigenetic changes during boar spermatozoa cryopreservation. Cryobiology. 2014; 69(1):119–27. https://doi.org/10.1016/j.cryobiol.2014.06.003 PMID: 24974820.
17. Martin Munoz P, Ortega Ferrusola C, Vizuete G, Plaza Davila M, Rodriguez Martinez H, Pena FJ. Depletion of Intracellular Thiols and Increased Production of 4-Hydroxynonenal that Occur During Cryopreservation of Stallion Spermatozoa Lead to Caspase Activation, Loss of Motility, and Cell Death. Biol Reprod. 2015; 93(6):143. https://doi.org/10.1095/biolreprod.115.132878 PMID: 26536905.
18. Plaza Davila M, Martin Munoz P, Tapia JA, Ortega Ferrusola C, Balao da Silva CC, Pena FJ. Inhibition of Mitochondrial Complex I Leads to Decreased Motility and Membrane Integrity Related to Increased

Hydrogen Peroxide and Reduced ATP Production, while the Inhibition of Glycolysis Has Less Impact on Sperm Motility. PLoS One. 2015; 10(9):e0138777. https://doi.org/10.1371/journal.pone.0138777 PMID: 26407142; PubMed Central PMCID: PMC4583303.

19. Timme-Laragy AR, Hahn ME, Hansen JM, Rastogi A, Roy MA. Redox stress and signaling during vertebrate embryonic development: Regulation and responses. Semin Cell Dev Biol. 2017. https://doi.org/10.1016/j.semcdb.2017.09.019 PMID: 28927759; PubMed Central PMCID: PMC5650060.

20. Fernandez-Gonzalez R, Moreira PN, Perez-Crespo M, Sanchez-Martin M, Ramirez MA, Pericuesta E, et al. Long-term effects of mouse intracytoplasmic sperm injection with DNA-fragmented sperm on health and behavior of adult offspring. Biol Reprod. 2008; 78(4):761–72. https://doi.org/10.1095/biolreprod.107.065623 PMID: 18199884.

21. Bouckenheimer J, Assou S, Riquier S, Hou C, Philippe N, Sansac C, et al. Long non-coding RNAs in human early embryonic development and their potential in ART. Hum Reprod Update. 2016; 23(1):19–40. https://doi.org/10.1093/humupd/dmw035 PMID: 27655590.

22. Chen Q, Yan W, Duan E. Epigenetic inheritance of acquired traits through sperm RNAs and sperm RNA modifications. Nat Rev Genet. 2016; 17(12):733–43. https://doi.org/10.1038/nrg.2016.106 PMID: 27694809; PubMed Central PMCID: PMC5441558.

23. Saunders CM, Larman MG, Parrington J, Cox LJ, Royse J, Blayney LM, et al. PLC zeta: a sperm-specific trigger of Ca(2+) oscillations in eggs and embryo development. Development. 2002; 129 (15):3533–44. PMID: 12117804.

24. Fujimoto S, Yoshida N, Fukui T, Amanai M, Isobe T, Itagaki C, et al. Mammalian phospholipase Czeta induces oocyte activation from the sperm perinuclear matrix. Dev Biol. 2004; 274(2):370–83. https://doi.org/10.1016/j.ydbio.2004.07.025 PMID: 15385165.

25. Banrezes B, Sainte-Beuve T, Canon E, Schultz RM, Cancela J, Ozil JP. Adult body weight is programmed by a redox-regulated and energy-dependent process during the pronuclear stage in mouse. PLoS One. 2011; 6(12):e29388. https://doi.org/10.1371/journal.pone.0029388 PMID: 22216268; PubMed Central PMCID: PMC3247262.

26. Ozil JP, Huneau D. Activation of rabbit oocytes: the impact of the Ca2+ signal regime on development. Development. 2001; 128(6):917–28. Epub 2001/02/27. PMID: 11222146.

27. Iqbal K, Chitwood JL, Meyers-Brown GA, Roser JF, Ross PJ. RNA-seq transcriptome profiling of equine inner cell mass and trophectoderm. Biol Reprod. 2014; 90(3):61. https://doi.org/10.1095/biolreprod.113.113928 PMID: 24478389; PubMed Central PMCID: PMC4435230.

28. Graf A, Krebs S, Zakhartchenko V, Schwalb B, Blum H, Wolf E. Fine mapping of genome activation in bovine embryos by RNA sequencing. Proc Natl Acad Sci U S A. 2014; 111(11):4139–44. Epub 2014/03/05. https://doi.org/10.1073/pnas.1321569111 PMID: 24591639; PubMed Central PMCID: PMC3964062.

29. Ortega Ferrusola C, Anel-Lopez L, Ortiz-Rodriguez JM, Martin Munoz P, Alvarez M, de Paz P, et al. Stallion spermatozoa surviving freezing and thawing experience membrane depolarization and increased intracellular Na(). Andrology. 2017; 5(6):1174–82. https://doi.org/10.1111/andr.12419 PMID: 28973824.

30. Rodriguez AM, Ferrusola CO, Garcia BM, Morrell JM, Martinez HR, Tapia JA, et al. Freezing stallion semen with the new Caceres extender improves post thaw sperm quality and diminishes stallion-to-stallion variability. Anim Reprod Sci. 2011; 127(1–2):78–83. https://doi.org/10.1016/j.anireprosci.2011.07.009 PMID: 21821371.

31. Cuervo-Arango J, Aguilar J, Newcombe JR. Effect of type of semen, time of insemination relative to ovulation and embryo transfer on early equine embryonic vesicle growth as determined by ultrasound. Theriogenology. 2009; 71(8):1267–75. https://doi.org/10.1016/j.theriogenology.2008.12.020 PMID: 19246082.

32. Jiao X, Sherman BT, Huang da W, Stephens R, Baseler MW, Lane HC, et al. DAVID-WS: a stateful web service to facilitate gene/protein list analysis. Bioinformatics. 2012; 28(13):1805–6. https://doi.org/10.1093/bioinformatics/bts251 PMID: 22543366; PubMed Central PMCID: PMC3381967.

33. Szklarczyk D, Franceschini A, Wyder S, Forslund K, Heller D, Huerta-Cepas J, et al. STRING v10: protein-protein interaction networks, integrated over the tree of life. Nucleic Acids Res. 2015; 43(Database issue):D447–52. https://doi.org/10.1093/nar/gku1003 PMID: 25352553; PubMed Central PMCID: PMC4383874.

34. Blake JA, Bult CJ, Eppig JT, Kadin JA, Richardson JE, Mouse Genome Database G. The Mouse Genome Database genotypes::phenotypes. Nucleic Acids Res. 2009; 37(Database issue):D712–9. https://doi.org/10.1093/nar/gkn886 PMID: 18981050; PubMed Central PMCID: PMC2686566.

35. Bult CJ, Eppig JT, Kadin JA, Richardson JE, Blake JA, Mouse Genome Database G. The Mouse Genome Database (MGD): mouse biology and model systems. Nucleic Acids Res. 2008; 36(Database

issue):D724–8. https://doi.org/10.1093/nar/gkm961 PMID: 18158299; PubMed Central PMCID: PMC2238849.

36. Lane M, O'Donovan MK, Squires EL, Seidel GE Jr., Gardner DK. Assessment of metabolism of equine morulae and blastocysts. Mol Reprod Dev. 2001; 59(1):33–7. https://doi.org/10.1002/mrd.1004 PMID: 11335944.

37. Ortega Ferrusola C, Gonzalez Fernandez L, Morrell JM, Salazar Sandoval C, Macias Garcia B, Rodriguez-Martinez H, et al. Lipid peroxidation, assessed with BODIPY-C11, increases after cryopreservation of stallion spermatozoa, is stallion-dependent and is related to apoptotic-like changes. Reproduction. 2009; 138(1):55–63. https://doi.org/10.1530/REP-08-0484 PMID: 19380427.

38. Ortega-Ferrusola C, Anel-Lopez L, Martin-Munoz P, Ortiz-Rodriguez JM, Gil MC, Alvarez M, et al. Computational flow cytometry reveals that cryopreservation induces spermptosis but subpopulations of spermatozoa may experience capacitation-like changes. Reproduction. 2017; 153(3):293–304. https://doi.org/10.1530/REP-16-0539 PMID: 27965398.

39. Munoz PM, Ferrusola CO, Lopez LA, Del Petre C, Garcia MA, de Paz Cabello P, et al. Caspase 3 Activity and Lipoperoxidative Status in Raw Semen Predict the Outcome of Cryopreservation of Stallion Spermatozoa. Biol Reprod. 2016; 95(3):53. https://doi.org/10.1095/biolreprod.116.139444 PMID: 27417910.

40. Feng Z, Hu W, Amin S, Tang MS. Mutational spectrum and genotoxicity of the major lipid peroxidation product, trans-4-hydroxy-2-nonenal, induced DNA adducts in nucleotide excision repair-proficient and -deficient human cells. Biochemistry. 2003; 42(25):7848–54. https://doi.org/10.1021/bi034431g PMID: 12820894.

41. Wei X, Yin H. Covalent modification of DNA by alpha, beta-unsaturated aldehydes derived from lipid peroxidation: Recent progress and challenges. Free Radic Res. 2015; 49(7):905–17. https://doi.org/10.3109/10715762.2015.1040009 PMID: 25968945.

42. Lu Y, Lin M, Aitken RJ. Exposure of spermatozoa to dibutyl phthalate induces abnormal embryonic development in a marine invertebrate Galeolaria caespitosa (Polychaeta: Serpulidae). Aquat Toxicol. 2017; 191:189–200. https://doi.org/10.1016/j.aquatox.2017.08.008 PMID: 28843738.

43. Burruel V, Klooster KL, Chitwood J, Ross PJ, Meyers SA. Oxidative damage to rhesus macaque spermatozoa results in mitotic arrest and transcript abundance changes in early embryos. Biol Reprod. 2013; 89(3):72. https://doi.org/10.1095/biolreprod.113.110981 PMID: 23904511; PubMed Central PMCID: PMC4094196.

Received: 28 September 2020 | Revised: 30 April 2021 | Accepted: 3 May 2021

DOI: 10.1111/andr.13033

ORIGINAL ARTICLE

ANDROLOGY WILEY

Postpubertal spermatogonial stem cell transplantation restores functional sperm production in rhesus monkeys irradiated before and after puberty

Gunapala Shetty[1] | Jennifer M. Mitchell[2] | Truong N. A. Lam[1] | Thien T. Phan[1] | Jie Zhang[1] | Ramesh C. Tailor[3] | Karen A. Peters[4] | Maria Cecilia Penedo[5] | Carol B. Hanna[6] | Amander T. Clark[7] | Kyle E. Orwig[4] | Marvin L. Meistrich[1]

[1]Department of Experimental Radiation Oncology, The University of Texas MD Anderson Cancer Center, Houston, TX, USA

[2]Department of Veterinary Medicine and Surgery, The University of Texas MD Anderson Cancer Center, Houston, TX, USA

[3]Department of Radiation Physics, The University of Texas MD Anderson Cancer Center, Houston, TX, USA

[4]Department of Obstetrics, Gynecology and Reproductive Sciences, Magee-Womens Research Institute, University of Pittsburgh School of Medicine, Pittsburgh, PA, USA

[5]Veterinary Genetics Laboratory, University of California, Davis, CA, USA

[6]Assisted Reproductive Technology Core, Oregon National Primate Research Center, Beaverton, OR, USA

[7]Department of Molecular, Cell and Developmental Biology, Eli and Edythe Broad Center of Regenerative Medicine and Stem Cell Research, University of California Los Angeles, Los Angeles, CA, USA

Correspondence
Gunapala Shetty, Department of Experimental Radiation Oncology, The University of Texas MD Anderson Cancer Center, Houston, Texas 77030, USA.
Email: sgunapal@mdanderson.org

Funding information
Center for Strategic Scientific Initiatives, National Cancer Institute, Grant/Award Number: P30 CA016672; National Institute of Child Health and Human Development, Grant/Award Number: P01 HD075795 and R01 HD100197; National

Abstract

Background: Cancer treatment of prepubertal patients impacts future fertility due to the abolition of spermatogonial stem cells (SSCs). In macaques, spermatogenesis could be regenerated by intratesticular transplantation of SSCs, but no studies have involved cytotoxic treatment before puberty and transplantation after puberty, which would be the most likely clinical scenario.

Objectives: To evaluate donor-derived functional sperm production after SSC transplantation to adult monkeys that had received testicular irradiation during the prepubertal period.

Materials and methods: We obtained prepubertal testis tissue by unilaterally castrating six prepubertal monkeys and 2 weeks later irradiated the remaining testes with 6.9 Gy. However, because spermatogenic recovery was observed, we irradiated them again 14 months later with 7 Gy. Three of the monkeys were treated with GnRH-antagonist (GnRH-ant) for 8 weeks. The cryopreserved testis cells from the castrated testes were then allogeneically transplanted into the intact testes of all monkeys. Tissues were harvested 10 months later for analyses.

Results: In three of the six monkeys, 61%, 38%, and 11% of the epididymal sperm DNA were of the donor genotype. The ability to recover donor-derived sperm production was not enhanced by the GnRH-ant pretreatment. However, the extent of filling seminiferous tubules during the transplantation procedure was correlated with the eventual production of donor spermatozoa. The donor epididymal spermatozoa from the recipient with 61% donor contribution were capable of fertilizing rhesus eggs and forming embryos. Although the transplantation was done into the rete testis, two GnRH-ant-treated monkeys, which did not produce donor-derived epididymal spermatozoa, displayed irregular tubular cords in the interstitium containing testicular spermatozoa derived from the transplanted donor cells.

Discussion and Conclusion: The results further support that sperm production can be restored in non-human primates from tissues cryopreserved prior to prepubertal and

Institutes of Health, Grant/Award Number: P51 OD011092

post-pubertal gonadotoxic treatment by transplantation of these testicular cells after puberty into seminiferous tubules.

KEYWORDS
GnRH-antagonist, intracytoplasmic sperm injection, radiation, spermatogenesis, transplantation

1 | INTRODUCTION

Sustained progress in cancer therapies over the past several decades has led to a rise in pediatric cancer survival rates to approximately 88%.[1] However, the gonadotoxicity and risk of infertility from the treatment remains a major health concern in these survivors as it affects the quality of life. Since prepubertal boys are not producing spermatozoa, there are currently no standard-of-care options to preserve their fertility. We estimate that each year an additional 1,400 young men will become sterile due to cancer therapy and myeloablative conditioning therapy for hematopoietic stem cell transplants for non-malignant conditions.[2] This is a significant human health concern,[3,4] and development of new methods of fertility preservation to prevent these effects or restore normal reproductive function after cytotoxic treatment is of great importance to these young male cancer survivors.

If spermatogonial stem cells (SSCs) are completely lost after gonadotoxic therapy, the only way to preserve future fertility of prepubertal males is by harvesting tissue containing SSCs prior to therapy and cryopreservation. With increased awareness and need for fertility preservation, it is the current clinical practice in various centers in the world to cryopreserve the testicular tissues before gonadotoxic therapies in boys,[5-8] hoping that a satisfactory technique will be developed to produce spermatozoa from the SSCs present in this tissue. Transplantation of a cell suspension containing SSCs into the seminiferous tubules is one of the techniques that have the potential to restore spermatogenesis and sperm production *in vivo*. Spermatozoa can be obtained from the testis, epididymis, or the ejaculate and have been successfully used to produce live offspring in rodents[9-11] and goats,[12] and embryos in non-human primates.[2,13]

Previously, we showed that, in macaques, irradiated during adulthood, autologous[14] or allogeneic[2] transplantation of SSCs to the testis produced donor-derived spermatozoa in the recipient. These spermatozoa were also competent to fertilize the eggs to produce embryos by ICSI.[2] In an attempt to model the prepubertal boys undergoing gonadotoxic therapy and requiring fertility restoration when they reach adulthood, we cryopreserved testis tissue from prepubertal monkeys, irradiated them prepubertally, and planned to transplant the stored cells into the testes after puberty and subsequently test the establishment of donor-derived spermatogenesis and the fertilizing potential of the spermatozoa produced. However, a second dose of irradiation had to be given to these monkeys, since there was spermatogenic recovery at puberty. Furthermore, although autologous transplantation is desired in the clinical scenario, allogeneic transplantation was used in this study so that donor-derived spermatogenesis and the paternity of embryos produced could be reliably quantified using microsatellites that differed between the donor-recipient pairs.

In an attempt to increase the success of the recovery of spermatogenesis from transplanted cells in a non-human primate, we also tested the effect of gonadotropic and gonadal hormone suppression with a GnRH-antagonist, a method that had proved very successful in rodents.[15,16] Although one of our previous studies with macaques[14] had indicated that hormonal suppression just prior transplantation enhanced the recovery of spermatogenesis from the donor, a second study[2] failed to indicate such a beneficial effect.

Furthermore, we previously reported a single case in which transplantation of a suspension of testicular cells from a prepubertal monkey resulted in the development of donor-derived *de novo* tubules containing advanced germ cells in the interstitium.[17] Since this study also involves transplantation of prepubertal monkey cells into the testes, we scrutinized the transplanted testes tissues for such structures.

2 | MATERIALS AND METHODS

2.1 | Animals

Six male rhesus monkeys (*Macaca mulatta*) were purchased from the Michale E. Keeling Center for Comparative Medicine and Research, MD Anderson Cancer Center, Bastrop, Texas, as both donor and recipient monkeys for testicular cell transplantation to the testis. They were prepubertal at the time of purchase and were housed in pairs initially at the M.D. Anderson Cancer Center, Houston, Texas, in steel cages with a sliding panel between two adjacent compartments to allow social interaction with another companion of the same study group. The animals were fed Harlan TEKLAD Primate diet #7195 with daily enrichment foods, such as seeds, peanuts, fruits, and vegetables; the environment was maintained at a constant temperature (24°C–27°C) and humidity (40%–55%) with a 12-h light/12-h dark cycle. During parts of the study when there were minimal interventions for procedures, the monkeys were temporarily housed at the MD Anderson Cancer Center facility in Bastrop, Texas, with the same conditions as described above.

All animal care and treatment protocols were approved by the Institutional Animal Care and Use Committees of MD Anderson Cancer Center and Magee-Womens Research Institute.

2.2 | Experimental design

Prepubertal monkeys, at 40–41 weeks of age, were unilaterally castrated (Figure 1). The castrated testes were weighed and 6–27 mm^3 pieces from the testes were cryopreserved for later allogeneic transplantation. Two weeks later, the remaining testes of the monkeys were given 6.9 Gy of irradiation.

Testis volumes, testosterone levels, and sperm counts in the ejaculates were monitored, generally every four weeks, to observe signs of puberty. At about 50 weeks after the first irradiation, the monkeys showed increased testosterone levels, suggesting their entrance to puberty. However, because the testis volumes and sperm counts indicated significant spermatogenic recovery, they were given one more dose of 7-Gy irradiation at 64 weeks from the first dose to deplete endogenous SSCs and the recovering spermatogenesis. The monkeys were then divided into two groups of three each; one group was treated with GnRH-antagonist (GnRH-ant) for 8 weeks. At the end of 8 weeks, the testis of each monkey was allogeneically transplanted with cells prepared from the cryopreserved testis pieces of another monkey in the group. To prevent rejection of the transplanted cells, the monkeys were immunosuppressed; the testes and epididymis were harvested 44 weeks after transplantation for analyses as in previous studies.[14]

2.3 | General surgical and post-surgical procedures

For all procedures, the monkeys were first sedated with an IM injection of ketamine (10–25 mg/kg) and then anesthetized with 1–3% isoflurane in oxygen. Before castration surgery, 2% lidocaine was instilled into the spermatic cord to provide local anesthesia. All surgical procedures were performed under aseptic conditions. Each animal received an analgesic (buprenorphine, 0.01–0.03 mg/kg body weight) prior to and at the end of the day of surgery, and two times per day for up to 3 days as needed by appearance of the animal under constant monitoring. In addition, at the discretion of the Clinical Veterinarian, daily IM injections of Baytril antibiotic (5 mg/kg) were given for a week post-surgery.

2.4 | Semen and blood collection

Blood (5–10 ml) was drawn by venipuncture of the saphenous vein of sedated animals. Serum was separated and stored at −20°C. In general, blood sampling was done at monthly intervals, but was drawn more frequently during and immediately after GnRH-ant treatment, to assess its effects on hormone levels.

Semen was obtained from anesthetized monkeys by electroejaculation using a rectal probe (Beltron Instruments), as described previously.[14] The sample was allowed to liquefy at 37°C for an hour before spermatozoa were counted in the exudate using a hemocytometer. Sperm counts were expressed per total ejaculate (volume of exudate plus remaining coagulum). Semen collection was done only once before the second irradiation to confirm puberty and assess spermatogenic recovery after the first irradiation. Monthly semen collections were then performed starting at 16 weeks after transplantation.

2.5 | Testicular measurements

Individual testis volumes were determined by measuring the length and width of each testis within the scrotum of anesthetized monkey with calipers and modeling the testis as a prolate ellipsoid, applying the following formula: testis volume $=\pi \times \text{width}^2 \times \text{length}/6$.

2.6 | Hemicastration and tissue cryopreservation

A scalpel incision was made in the scrotum of anesthetized prepubertal monkeys, and the dartos and tunica vaginalis were dissected to expose the left testis. The blood supply to the testis was tied off,

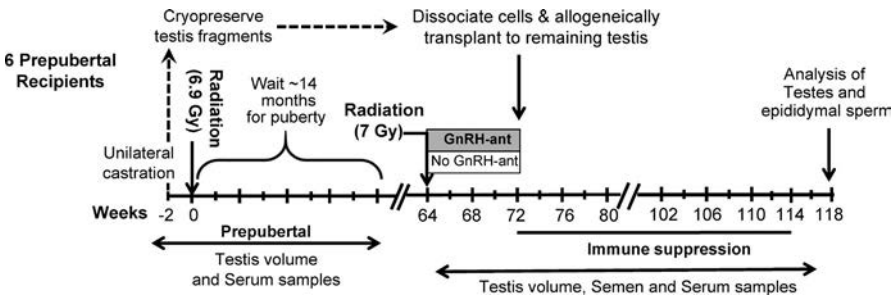

FIGURE 1 Study design. The monkeys were evaluated before unilateral castration and periodically after exposure to two doses of radiation, hormone suppression, and transplantation. Evaluation included sampling of serum and measurements of testis volume. In addition, periodic semen analysis was performed after the animals reached puberty. Starting immediately after second exposure to testicular irradiation, three monkeys underwent GnRH-ant-mediated hormone suppression for 8 weeks; the other three received only sham injections. At the end of the 8-week period, they received allogeneic transplantation of cryopreserved testis tubular cells into one testis, followed by 9 months of immune suppression

the testis along with the epididymis was removed by cutting the spermatic cord, and the incision was closed by suturing.

The removed testis tissues were washed in Petri dishes using Hanks' balanced salt solution (HBSS) and, using a single-edged blade, were cut into small pieces of about 6–27 mm^3 and cryopreserved.[18] About 5–7 pieces of tissue were placed in a 2-ml cryovial containing 5% DMSO and 5% fetal bovine serum (FBS) in minimal essential medium (MEMα). The vials were placed on ice for 30 min, transferred to −1°C/min containers, and placed at −20°C for 90 mins, and then, these containers were placed overnight at −80°C. Next day, the vials were plunged into liquid nitrogen.

2.7 | Irradiation

The testes of anesthetized monkeys were irradiated using a cobalt-60 gamma-irradiator[14,17] with a 5 × 5 cm field size in an antero-posterior direction. Tissue-equivalent bolus material (5-mm thick) was placed over the scrotum to provide a buildup layer. The remaining right testes of prepubertal monkeys were irradiated at a total calculated dose of 6.9 Gy at a rate of 77–91 cGy/min, with a source-to-skin distance of 80 cm measured to the bolus. This dose was chosen because 7 Gy was previously shown to provide prolonged depletion of spermatogenesis in adult macaque testes.[2,14] Although we were aware of reports that this dose might not deplete spermatogenesis in immature macaques,[19] higher doses were not given to the prepubertal testis because our preliminary data (not shown) and studies of others[20] have shown that irradiation of prepubertal testes with 10 Gy produced failure of the development of the somatic elements of the testis. Instead, it was necessary to give the monkeys a second dose of 7-Gy irradiation when they reached adulthood to eliminate most of the surviving endogenous SSC and the recovering endogenous spermatogenesis.

2.8 | GnRH-antagonist treatment

The GnRH-ant, Acyline, was obtained from the Contraceptive Development Program of the NICHD, Rockville, MD, USA. Stock solutions of Acyline (2 mg/ml) in 5% aqueous mannitol were prepared and stored at 4°C for a maximum of 1 week. Based on the pharmacokinetics of Acyline,[21] and our previous data on hormone suppression in macaques, [14] one group of three monkeys was given twice-weekly subcutaneous injections of Acyline on Mondays and Thursdays at doses of 200 μg/kg and 300 μg/kg, respectively[14,17]; the other group of three was sham injected with bacteriostatic water.

2.9 | Allogeneic transplantation

To prepare the cells for transplantation, the cryovials were thawed in a 37°C water bath and washed with HBSS. Tissue pieces were incubated with collagenase IV and DNase I to digest interstitial tissue, and the undigested tissue was then incubated with trypsin-DNase to release tubular cells.[22,23] The recovered cells were washed, counted, and prepared for transplantation as in our previous study.[14] The remaining right testes of the unilaterally castrated monkeys were allogeneically transplanted with these cells, choosing the donor-recipient pairs to maximize the unique microsatellite markers between these monkeys.

Transplantation of cells was done essentially as described previously.[13,14] Briefly, cells were suspended at 49–180 × 10^6 viable cells/ml in MEMα containing 10% FBS, 0.4 mg trypan blue/ml, 20% (v/v) Optison ultrasound contrast agent (GE Healthcare), 1% antibiotic-antimycotic (a combination of penicillin, streptomycin, and amphotericin B; Gibco), and 0.1 mg DNase I/ml. The cells were transplanted in volumes between 350 and 500 μl via ultrasound-guided injections into the rete testis. A 13 MHz linear superficial probe and a MicroMaxx ultrasound machine (Sonosite) were used to visualize the rete testis space and to guide a 25-gauge, 1.5" hypodermic needle into the space. Cells were manually injected under slow constant pressure and chased with saline solution. A transplantation efficiency score was recorded for each transplantation as done previously, based on an ultrasound-visualized estimate of the percentage of the circumference of tubules, going outward from the rete testis, that were filled by donor cell suspension.[2] The scores were as follows: 5 = >80%; 4 = 60–80%; 3 = 40–60%; 2 = 20–40%; and 1 = <20%. For example, the filling of the tubules recorded in a previous study,[13] Movie S1, would be a score of 5. To prevent T cell–mediated rejection of the transplanted allogeneic cells, the recipients were immunosuppressed with human/mouse chimeric anti-CD154 IgG 5C8 (NIH Nonhuman Primate Reagent Resource, University of Massachusetts Medical School) at 20 mg/kg on days (relative to transplant) −1, 0, 3, 10, 18, 28, and monthly thereafter for an additional 8 months. This treatment of rhesus monkeys was shown to functionally protect renal allografts[24] and had been successfully used in allogeneic transplantation of SSCs.[2,13]

2.10 | Hormone assays

Testosterone was assayed using radioimmunoassay (RIA) kit KIR1709 (Immuno-Biological Laboratories America). We used our own testosterone standard for the assay that was diluted in the zero-standard provided in the kit.[18] The detection limit of the assay is 0.05 ng/ml. The intra- and inter-assay coefficients of variation were 5% and 16%, respectively.

Circulating concentrations of FSH and luteinizing hormone (LH) were determined by RIA at the Endocrine Technologies Support Core, Oregon National Primate Research Center, Beaverton. The sensitivities of both the FSH and LH assays were 0.05 ng/ml. The intra-assay coefficients of variation were 12.5% and 8.2%, respectively, for FSH and LH.

2.11 | Histological and immunohistochemical procedures

After harvest, the testes were first weighed and pieces of tissue were fixed in either Bouin solution, 4% PFA, or 70% ethanol.

For histology, Bouin-fixed pieces were embedded in paraffin, and sections were stained with periodic acid–Schiff reagent and hematoxylin. For analysis of spermatogenic recovery at the end of the study, at least three sections chosen from different regions of the testis were assessed by systematic scanning across the entire section and a minimum of 2654 tubules were scored per testis. Sertoli cell–only tubules were categorized into two types: those with normal appearing columnar Sertoli cells with a relatively small empty lumen, and those with flatter Sertoli cells with a large empty lumen. The presence of germ cells was scored by calculating the tubule differentiation index (TDI), which is the percentage of seminiferous tubule cross sections containing at least three differentiated germ cell type (B spermatogonia or later stages). In addition, the extent of the progression of germ cell differentiation was assessed by determining the percentages of tubules with germ cells that contained spermatocytes, round spermatids, or elongating/elongated spermatids as the most advanced germ cell type present.

In some sections, areas packed with irregularly shaped tubular cords containing germ cells, often with incomplete basement membranes, were observed. These were readily distinguished from normal seminiferous tubules and appeared identical to the donor-derived *de novo* tubules we observed in a previous study.[17]

2.12 | Epididymal sperm isolation

The cauda epididymis was minced thoroughly in about 200 µl of pre-warmed modified human tubal fluid (HTF, Cat. No. 90126; Irvine Scientific) in a 60-mm Petri dish and transferred to a 2-ml microfuge tube. The epididymal mince was incubated thrice with 500 µl of HTF, each time suspending the tissue and allowing it to settle at unit gravity and aspirating the supernatant containing the spermatozoa. The supernatant was filtered through a pre-wet 100-µm cell strainer basket (BD 352350) into a 50-ml conical tube, and the total volume of the filtrate was brought to 2 ml by adding pre-warmed HTF. The number of spermatozoa, their motility, and the number of blood cells were counted in the filtrate, which was then divided into two portions: one for genotyping and one for ICSI.

When the level of contaminating somatic cells was <50%, the sperm samples for genotyping were washed in DPBS and pellets were frozen at −80°C. However, when the level of somatic cells was >50%, the spermatozoa were further purified by Percoll gradient separation, reducing the somatic contamination to ~5%, prior to washing and freezing.

The ICSI samples were transferred to 5-ml tubes, and equal volumes of pre-warmed Test Yolk Buffer freezing medium were added drop-wise over a 30-second period, mixing thoroughly after each drop of freezing medium was added to avoid osmotic shock to the spermatozoa. The mixture was allowed to equilibrate for 10 min at room temperature and then transferred into multiple 2-ml vials. The samples were chilled for 1 h in the refrigerator (2–5°C), followed by exposure to liquid nitrogen vapor for 30–60 mins, and then transferred to a liquid nitrogen tank for storage at −196°C.

2.13 | Preparation of DNA from the blood, tissue, and spermatozoa

To genotype the monkeys used as donors and recipients, DNA was prepared from non-coagulated blood using the DNeasy Blood & Tissue Kit from Qiagen (Cat No.: 69504).

To extract DNA from spermatozoa, the pellets were suspended in saline sodium citrate buffer and were treated with 0.2% sodium dodecyl sulfate (SDS) to lyse remaining non-sperm cells. In cases in which spermatozoa were not Percoll purified, the spermatozoa were washed one additional time and treated again with SDS; this further eliminated the somatic contaminants and consequently decreased the percentages of recipient DNA in the sperm samples by 1 to 5%. The sperm samples were lysed and digested using proteinase K and dithiothreitol (DTT) at final concentrations of 2 mg/ml and 10 mM, respectively, for 3 h at 56°C. Then, the proteinase K was heat-inactivated at 95°C for 15 min, and the extract was directly used for PCR.

For genotyping the suspected *de novo* regions, we first identified regions with irregularly shaped tubules in PAS-hematoxylin stained, 70% ethanol-fixed testicular sections. These slides were used as guides to identify suspected regions of interest in adjacent unstained serial sections. The surrounding unwanted tissues were scraped off using a razor blade, under a dissection microscope. The proteinase K/DTT lysis solution was carefully dropped on the slide containing the required section, the tissue was released into the solution using a pipette tip and aspirated into a microfuge tube, and processed as was done for spermatozoa above.

2.14 | DNA microsatellite analysis

Microsatellite repeat fingerprinting was done with a panel of 29 microsatellites as described previously.[17] Microsatellites were amplified, and the PCR products were separated by capillary electrophoresis on ABI 3730 DNA Analyzer (Applied Biosystems). Fragment size analysis and genotyping was done with the computer software STRand.

To determine parental origin and sex of ICSI embryos, genotyping was done as above except that before PCR the cells were put through the whole genome amplification (WGA) process using the REPLI-g kit, which contains reagents and primers that will replicate most of the cell genome, producing sufficient DNA for testing: https://www.qiagen.com/us/service-and-support/learning-hub/technologies-and-research-topics/wga/replig-principal-procedure/. In addition to the panel of 29 microsatellites, the primers 5′-CCCTGGGGCTCTGTAAAGAATAGTG-3′ and 5′-ATCAGAGCTTAAACTGGGAAGCTG-3′ were used to amplify sequences from the amelogenin gene which differs on the X and Y chromosomes, to determine the gender of the embryos.

TABLE 1 Baseline recipient and donor monkey characteristics, treatments, and cells for transplantation

	Parameters of monkeys at time of unilateral orchiectomy and first irradiation (6.9 Gy)				Parameters of monkeys at time of second irradiation (7 Gy)				Donor cells and transplantation				
Treatment groups	Recipient monkey number	Age (months)[e]	Serum T (ng/ml)[a]	Average testis volume (cm^3)[a]	Age (months)	Serum T (ng/ml)[b]	Testis volume (cm^3)	Sperm count/per ejaculate ($x10^6$)[c]	Donor monkey number	Testis weight (g)	Total cells injected (millions)	Viability (%)	Transplant efficiency score
No GnRH-ant control[d]	092	40.0	0.60	1.7	55.2	1.21	5.8	0	120	1.02	40	81%	3
	114	41.0	0.45	1.5	56.1	2.57	14.0	11.24	094	0.93	41	92%	5
	120	40.7	0.46	1.8	55.8	3.89	13.6	1.06	124	1.46	42	84%	3.5
GnRH-ant[d]	094	40.3	0.64	1.4	55.5	2.51	9.9	6.51	122	1.12	62	95%	4
	122	40.9	0.48	1.5	56.0	0.90	6.8	NE	092	0.93	17	89%	4.5
	124	40.4	0.66	1.6	55.5	5.81	15.1	0.08	114	1.21	32	81%	5

[a]Average of last two measurements made on the day of (but just before) unilateral orchiectomy, and a week before. First testicular irradiation of the remaining testis was performed 2 weeks after unilateral orchiectomy.

[b]Average of last 5 measurements.

[c]Collected on 12/7/17; NE indicates no ejaculate was obtained.

[d]No differences were observed between GnRH-ant treatment groups in any parameters (*t* test, $p > 0.05$).

[e]Measured at the time of irradiation.

2.15 | Intracytoplasmic Sperm Injection (ICSI)

Controlled ovarian stimulation was performed on six female rhesus macaques as previously described.[25,26] Oocytes were collected and fertilized with spermatozoa by ICSI, and resulting embryos were cultured as described.[27-29] Additional details are provided in the Supplementary Information. Following ICSI and in vitro development, individual embryos were vitrified and sent from the Oregon National Primate Research Center to the Veterinary Genetics Laboratory, University of California, Davis, for microsatellite analysis.

2.16 | Statistical analysis

The serum FSH levels, testis volume, and testis weights are presented as arithmetic mean ± SEM. The serum testosterone and LH levels were represented as means ± SEM calculated from log-transformed values. Comparison of the group treated with GnRH-ant and the control group was done using a *t* test. When multiple longitudinal measurements were made, the Bonferroni correction for multiple comparisons was applied. Correlations between different endpoints were analyzed using the non-parametric Spearman's rank-order correlation coefficient. Analyses were performed with the IBM SPSS (version 23) statistical package.

3 | RESULTS

3.1 | Observations during course of the study

We used the experimental design shown in Figure 1. The monkeys were 40–41 months of age with an average testis volume of 1.5 cm^3 and serum testosterone levels of 0.6 ng/ml (Table 1), when the unilateral castration was performed. Histology showed that the castrated testes of all the monkeys were indeed prepubertal containing only spermatogonia, mostly A_{dark} and A_{pale} (Figure S1). The recipient monkeys were monitored to determine when they reached puberty, as indicated by the serum testosterone levels consistently at or above 0.9 ng/ml (Figure 2B, Figure S2; and Table 1) which began at about 40 weeks after the hemicastration and irradiation. The achievement of puberty was confirmed by increases in testis volume resulting from increases in somatic elements and/or development of spermatogenesis (Figure 2A). In four of the six monkeys, testis volumes increased to at least 10 cm^3 (Figure S3), which is greater than that observed in adult monkeys in which spermatogenesis had been well depleted by irradiation.[2] The volume increase and the presence of spermatozoa in the ejaculates (Table 1) indicated that much of the volume increase was due to regeneration of endogenous spermatogenesis. Because of this, at 64 weeks after the first irradiation, the now post-pubertal monkeys were given another dose of 7-Gy testicular irradiation, which resulted in a decrease in testis volume (Figure 2A) as expected due to the depletion of the germ cells.

The monkeys were assigned to two treatment groups so that the distributions of ages, testes sizes, and testosterone levels were similar in the two groups (Table 1). One group of three monkeys was treated with GnRH-ant for the 8 weeks between the second irradiation and transplantation, and the other three monkeys received only sham injections. All six monkeys received allogenic transplantation of testis cells from other monkeys in the group at 72 weeks after the first irradiation dose.

As anticipated, [2,14] serum LH and testosterone levels were markedly suppressed during GnRH-ant treatment, and when the treatment was stopped, they reverted to normal levels for irradiated monkeys (Figure 2B and Figure S4). The reductions in testis volumes after the second irradiation (Figure 2A) were consistent with the loss of germ cells due to irradiation; the group treated with GnRH-ant

had a tendency toward a greater decrease consistent with the loss of Sertoli and Leydig cell volume seen with hormone suppression in other species.[30,31]

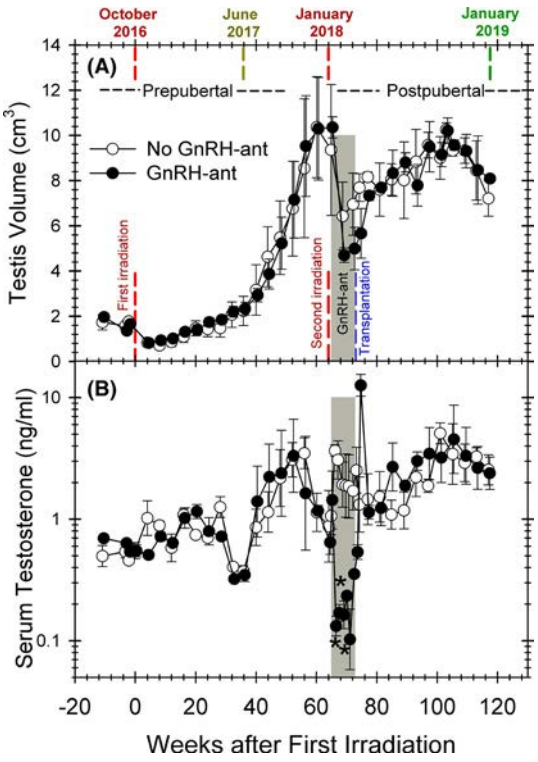

FIGURE 2 Changes in testis volumes (A) and serum testosterone levels (B) in monkeys during the study. The vertical red and blue dashed lines represent the times of the two doses of irradiation and of transplantation, respectively. The average values for the three monkeys receiving GnRH-ant treatment (filled circle) (n = 3) or sham injections (open circle) (n = 3) before transplantation are plotted. The gray shaded area represents the duration of the GnRH-ant treatment. For statistical analysis, the axis was divided into three time segments, after initial irradiation, after the second irradiation during GnRH-ant treatment, and after transplantation, during which there were 15, 6, and 13 comparisons, respectively. The only statistical difference between the two treatment groups (marked with asterisks) was decreased serum testosterone during the GnRH-ant treatment

The ability to obtain ejaculates was not very successful in these monkeys, even during the breeding season of October-February.[32,33] After the second irradiation and transplantation, only one ejaculate greater than 1 ml was recorded (Table S1). The ejaculates that were obtained during this period were azoospermic (<6 × 10^2/ml), with one exception that had only a few spermatozoa.

3.2 | Results from harvested tissues at the end of the study

At the end of the study, 44 weeks after transplantation, the remaining right testis and the cauda epididymis of all the six monkeys were harvested.

The testis weights in these monkeys varied between 3.3 and 7.0 g (Table 2; Figure 3A). Histology, as expected, showed that the majority of the tubule cross sections contained only Sertoli cells with the complete absence of germ cells (Figure 4A). In 5 out of 6 monkeys, Sertoli cells were mostly columnar with a small empty lumen (asterisks in Figure 4B,C,D), which were considered normal for irradiated macaque testes. However, in one of the monkeys (#092), 99% of the Sertoli-only tubules displayed large empty lumens and lower epithelial height of the Sertoli cells (Table 2; Figure 4E,F). This tubule dilation is likely a consequence of damage from the first prepubertal irradiation, as this monkey showed very little increase in testis size after the first irradiation (Figure S3A). Low numbers of such dilated tubules (< 1% of tubules) were also observed in three monkeys: #094, #122, and #124 (Table 2; Figure 4C,D).

Germ cell differentiation, identified by nuclear morphology and location, was observed in the seminiferous tubules of all monkeys (Figure 5). In monkey #092 with the extensive dilated tubules, only one normal tubule showed spermatogenic cell differentiation. In the other five monkeys, germ cell differentiation, quantified by the tubule differentiation index (TDI), was observed in 2% to 33% of the normal tubules (Figure 3B). Spermatogenesis proceeded to the late spermatid stage in 70% of the differentiating tubules (Figure 5C). In

TABLE 2 Parameters of spermatogenic recovery in the recipient testis/epididymis

Treatment groups	Recipient monkey number	Testis volume (cm^3)[b]	Testis weight (g)[a]	TDI (%)[a]	Percent of differentiating tubules with late spermatids[a]	Percentage of dilated tubules[a]	Presence of *de novo* cords in testis	Cauda epididymal spermatozoa ($x10^6$)[a]	Percentage of donor spermatozoa in cauda epididymis[a]	Donor spermatozoa in cauda epididymis ($x10^6$)[a]
No GnRH-ant control	092	5.7	3.6	0.03%	0%	98.7%	No	0	NA	0
	114	7.9	7.0	33.1%	76%	0%	No	26	38%	9.9
	120	8.1	6.2	1.6%	56%	0.0%	No	0.6	11%	0.07
GnRH-ant	094	8.3	5.2	20.1%	82%	0.9%	Yes	4.7	0%	0
	122	7.8	3.3	3.0%	64%	0.4%	Yes	0.9	0%	0
	124	8.1	6.1	27.9%	66%	0.1%	No	13	61%	7.9

[a]No differences were observed between hormone treatment groups (t test, $p > 0.05$).

[b]Measurements include scrotal wall thickness

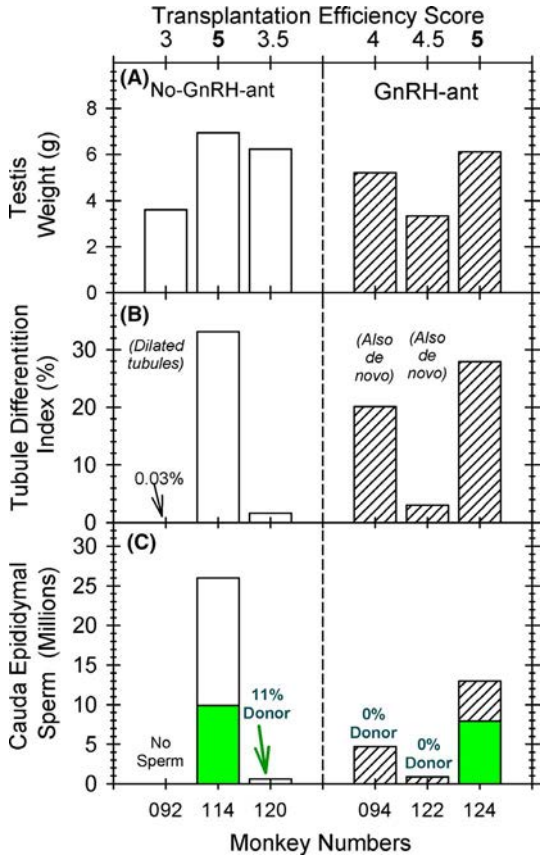

FIGURE 3 Spermatogenic endpoints in individual monkeys. Testis weights (A), tubule differentiation indices (B), and yield of spermatozoa from the cauda epididymis (C) are shown for the monkeys treated with GnRH-ant (hatched bars) and those receiving only sham injections. Testes with abnormal tubules (dilated or *de novo*) are indicated in (B). The portion of the columns filled with green in (C) shows the numbers of spermatozoa that were donor derived

addition, two monkeys (#094 and #122) displayed irregular tubule-like cords, as will be discussed below.

Epididymal sperm counts in five of the monkeys varied between 0.6 and 26 × 10^6; one monkey (#092) had no spermatozoa in the epididymis (Figure 3C; Table 2). As expected, there was a perfect positive correlation between the cauda epididymal sperm count and the TDI (Spearman coefficient 1.0, $p < 0.01$) among the different animals. Microsatellite analysis revealed that, in three of the recipient monkeys, 61%, 38%, and 11% of the epididymal spermatozoa were of the donor genotype, but in the other two of the monkeys with epididymal spermatozoa, there were no donor-derived spermatozoa (Table 3; Figure S5). The monkeys with 61% and 38% donor spermatozoa had high epididymal sperm numbers, with 8 and 10 million donor spermatozoa, respectively, indicating the potential for fertility preservation.

We next assessed the factors that might be responsible for the variability in the success of the transplantation as measured by the numbers of donor spermatozoa in the epididymis (Table 2; Figure 3). The GnRH-ant treatment before transplantation had no significant effect on donor spermatogenic output (*t* test $p > 0.6$). The numbers of donor cells injected and donor cell viability were unrelated to the extent of donor spermatogenesis (Spearman correlation, $p > 0.9$). However, there were trends or significance that the testis volume ($p = 0.02$) and serum T ($p = 0.08$) measured at the time or second irradiation (8 weeks before transplantation) and the transplantation efficiency score ($p = 0.14$) were positively related to the numbers of donor spermatozoa in the epididymis. For instance, the two monkeys with a transplantation score of five had the highest numbers of donor spermatozoa in their epididymis. On the other hand, the presence of dilated tubules ($p = 0.04$) and the irregular tubule-like cords ($p = 0.15$) appeared to be negatively related to the success of the transplantation. Testicular damage from the first irradiation, as evidenced by small testis volumes and low levels of serum T in monkey #092, likely contributed to the dilated tubules and extremely low levels of both endogenous and donor spermatogenic recovery observed in this monkey at tissue harvest.

The irregular tubule-like cords observed in monkeys #094 and #122 appeared to be identical to the *de novo* tubular cords we have described previously (Figure 6A,B).[17] These abnormal cords filled an estimated 1.5–4.2% of the testis volume. They possessed incomplete basal laminae and contained germ cells up to and including round spermatids and, although rarely, mature spermatids (Figure 6B). Immunostaining for Vasa and acrosin confirmed the identification of germ cells and spermatids, respectively, in these cords (data not shown). In both of these cases, these cords were observed in the interstitium adjacent to the rete testis (Figure 6C). Microsatellite analysis of the DNA extracted from the regions containing these abnormal cord structures showed 65% and 80% of donor genotypes in the two monkeys (Table 3), confirming that they indeed originated *de novo* from transplanted donor cells (Figure S6). The remaining percentages were likely contributed mostly by the recipient interstitial cells in addition to any possible minor contaminants from the endogenous tubular area.

3.3 | Intracytoplasmic Sperm Injection (ICSI) Results

To test whether the donor-derived spermatozoa obtained after transplantation were functional, we injected the cryopreserved spermatozoa from the recipients into *in vivo* matured rhesus oocytes. A total of 85 ova were injected with spermatozoa from recipients #124 and #114; 14 developed into zygotes (16% of injected ova) and were maintained for 8 days in culture (Table S2). Six reached the compact morula stage (Figure 7A) and one reached early blastocyst. In the first set of injections using the epididymal spermatozoa from recipient #124, which had 61% donor contribution, four embryos were successfully genotyped by microsatellite analysis and two had the paternal genotype of the transplant donor and two had the genotype of the transplant recipient (Table S2; Figure 7B). These results confirmed that the spermatozoa produced from the transplanted SSCs are fertilization competent and can produce embryos. Three embryos from the second set of injections were transferred into

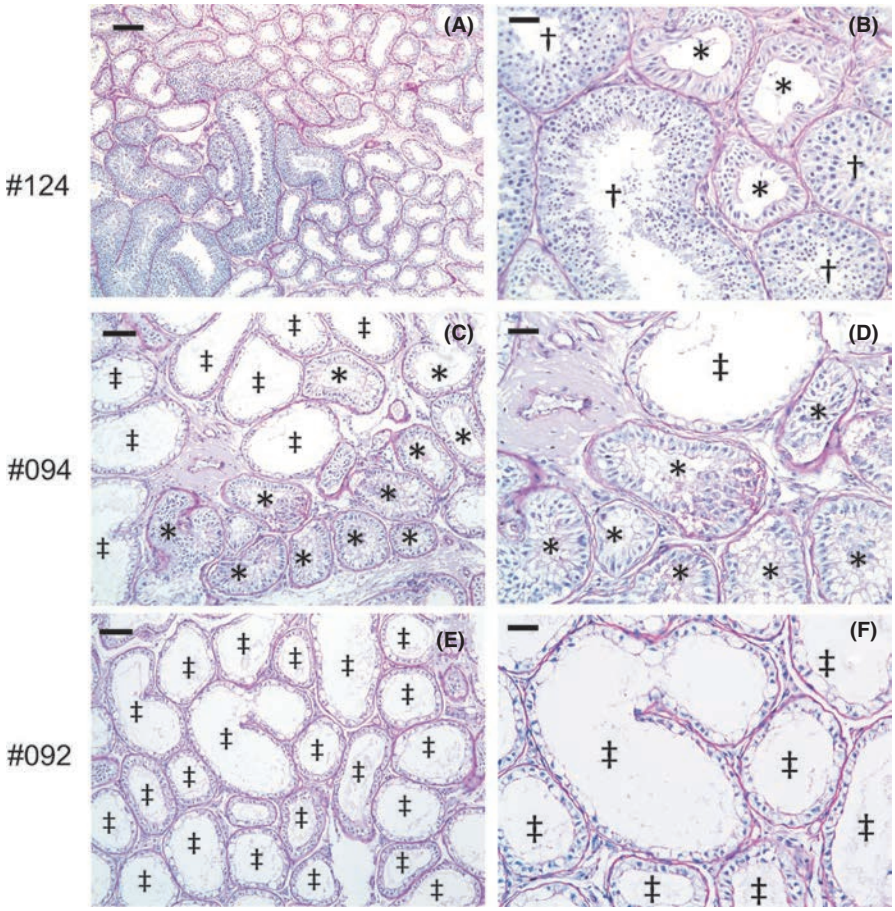

FIGURE 4 Testis histology at tissue harvest, 44 weeks after transplantation. (A) Most tubules only contain Sertoli cells (B) Normal Sertoli-only tubules (*) and tubules showing regeneration of spermatogenesis (†). Note that the Sertoli cells in normal tubules have columnar appearance with a small lumen often with the presence of cytoplasmic processes. (C-F) Abnormal dilated Sertoli-only tubules (‡) with low epithelial heights and large empty lumens and some adjacent normal Sertoli-only tubules (*). Monkey numbers are indicated beside panels. Scale bars: (A): 200 µm; (C, E): 100 µm; (B,D,F): 50 µm

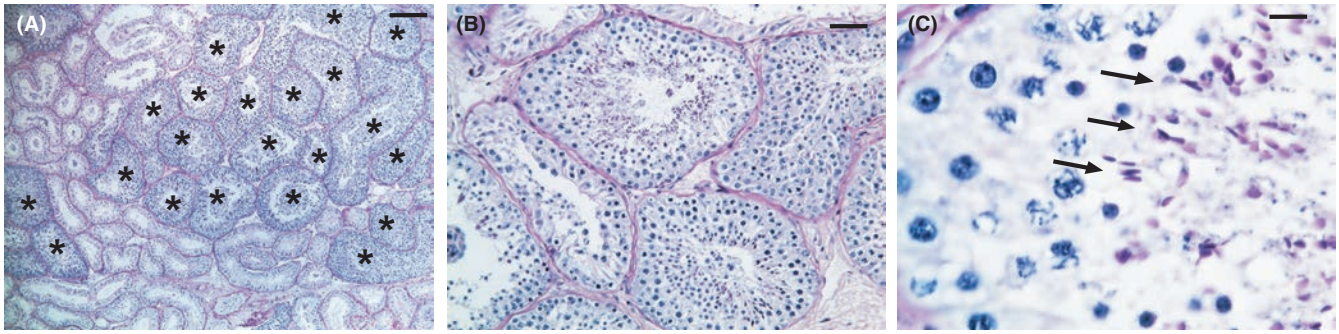

FIGURE 5 Histology of the testis of a monkey that showed donor-derived spermatozoa in the epididymis. Representative PAS-hematoxylin-stained testis sections at the end of the study from monkey #114. Tubules showing differentiating germ cells in (A) are indicated by asterisks. Note the presence mature spermatids (arrows in C) indicating complete spermatogenesis. Scale bars: (A): 200 µm; (B): 50 µm; (C):10 µm

timed recipients (Supporting Methods), but no pregnancies were established. In the third set of injections, when the recipient (#114) with 38% donor spermatozoa was used, embryo genotyping was successful in four embryos; two had developed parthenogenetically, and two were derived from endogenous spermatozoa produced by the recipient male. It was not known why embryo development was suboptimal and no pregnancies were achieved; it was not specific to possible quality problems with the donor-derived spermatozoa, since ICSI with spermatozoa derived from endogenous SSC did not yield any better results.

4 | DISCUSSION

The most important finding in the current study was that, in a model that closely relates to gonadotoxic cancer treatment before puberty and transplantation of prepubertal testis cells back into the testis after puberty, significant donor-derived spermatogenesis was obtained in three out of six monkeys. In two of these monkeys, 13 and 26 million spermatozoa were recovered from the cauda epididymis and 61% and 38% of these spermatozoa, respectively, were donor derived. The high percentages of donor spermatozoa demonstrate

TABLE 3 Microsatellite analysis of the cauda epididymal spermatozoa, or testicular cells (retrieved from regions of the section suspected to contain *de novo* cords), from testicular irradiated monkeys transplanted with testicular cells containing SSCs

Treatment groups	Recipient monkey number	Donor monkey number	Percentage of donor genotype transplanted		Unique microsatellite loci analyzed
			Epididymal spermatozoa	Testicular cells from suspected *de novo* region	
No GnRH-ant control	092	120	No spermatozoa	No *de novo*	NA
	114	094	37.7 s± 1.2	No *de novo*	D2S1333, D3S1768, D4S2365, D6S501
	120	124	10.7 ± 0.3	No *de novo*	D2S1333, D3S1768, D6S501, D11S2002
GnRH-ant	094	122	0	65.1± 0.8%	D2S1333, D3S1768, D6S501, D7S794
	122	092	0	80.4± 1.6%	D2S1333, D3S1768, D6S501, D8S1106
	124	114	61.1 ± 2.0%	No *de novo*	D3S1768, D4S2365, D11S2002, D12S364

Note: Wherever chimerism was observed, the percent donor DNA was calculated from the heights of donor and recipient peaks, and the results are averages and SEM of analyses of at least 4 microsatellite loci.

Abbreviation: NA, Not applicable.

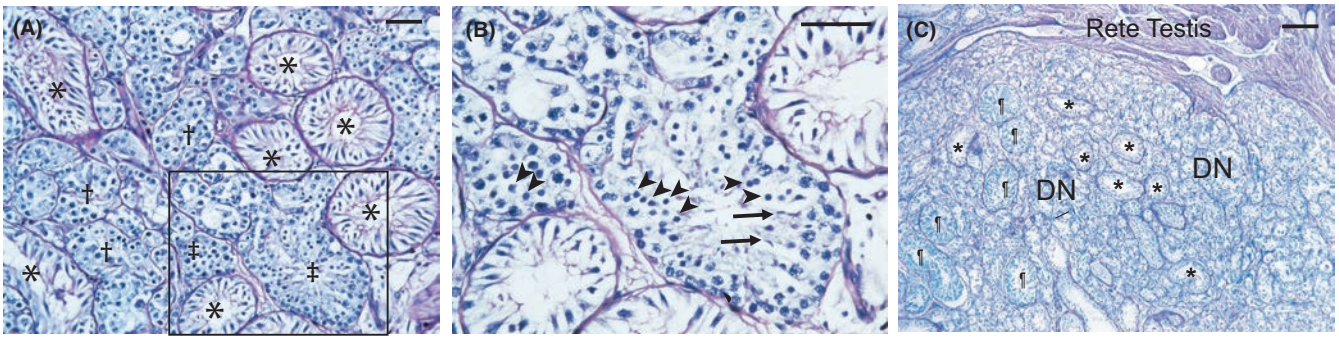

FIGURE 6 (A) Region of irregular *de novo* tubular cords with interspersed endogenous Sertoli cell–only tubules (*). *De novo* cords with spermatogenic development to the spermatocyte (†) and spermatid (‡) stages are indicated. (B) Higher magnification of region from (A) showing round spermatids (arrowheads) and elongated spermatids (arrows). (C) Region of *de novo* cords (DN) showing that it is adjacent to the rete testis area. Interspersed normal tubules that are Sertoli cell–only (*) and with recovery spermatogenesis (¶) are indicated. Scale bars: (A &B): 50 μm; (C): 200 μm

the success of the transplantation. The observation that the tubule differentiation indices in these two monkeys were 28% and 33%, respectively, as compared to 0.03–20% in the remaining four monkeys, supports the conclusion that this was a result of enhanced donor cell colonization. A third monkey had 11% donor representation in the epididymal spermatozoa, but there were only 0.6 million spermatozoa.

Comparison with previous studies (Table 4) emphasizes that this is the only study in which some of the gonadotoxic treatment was delivered prepubertally, and the transplantation was done after puberty, which will most likely be the clinically used strategy in humans. Unfortunately, because the 6.9-Gy radiation dose was insufficient for the desired level of SSC depletion in the prepubertal testis, it was also necessary to give another radiation dose after they reached puberty, which deviates from the usual clinical scenario. Nevertheless, the result that three of six recipient monkeys produced donor spermatozoa is within the range of most of the previous studies.

It is important to determine what specific factors might be associated with good colonization with donor cells. The effect of GnRH-ant treatment on the presence and yield of donor spermatozoa was evaluated. Whereas two of the three control monkeys not treated with GnRH-ant produced donor spermatozoa, only one of the three GnRH-ant-treated monkeys produced donor spermatozoa (Table 2), and we concluded that overall the GnRH-ant treatment showed no correlation with spermatogenic recovery from donor SSCs. This result is similar to that observed recently in a study involving allogeneic transplantation in rhesus monkeys,[2] but differs from the stimulation of recovery of donor spermatogenesis by GnRH-ant treatment observed earlier in a study involving autologous transplantation in cynomolgus macaques (Table 4).[14] The inability to see any favorable effects of GnRH-ant in these allogeneic transplantation studies might be due to a possible enhancement of immune responses when testosterone is suppressed,[34] resulting in the immune suppression being inadequate. This possibly could offset any benefit

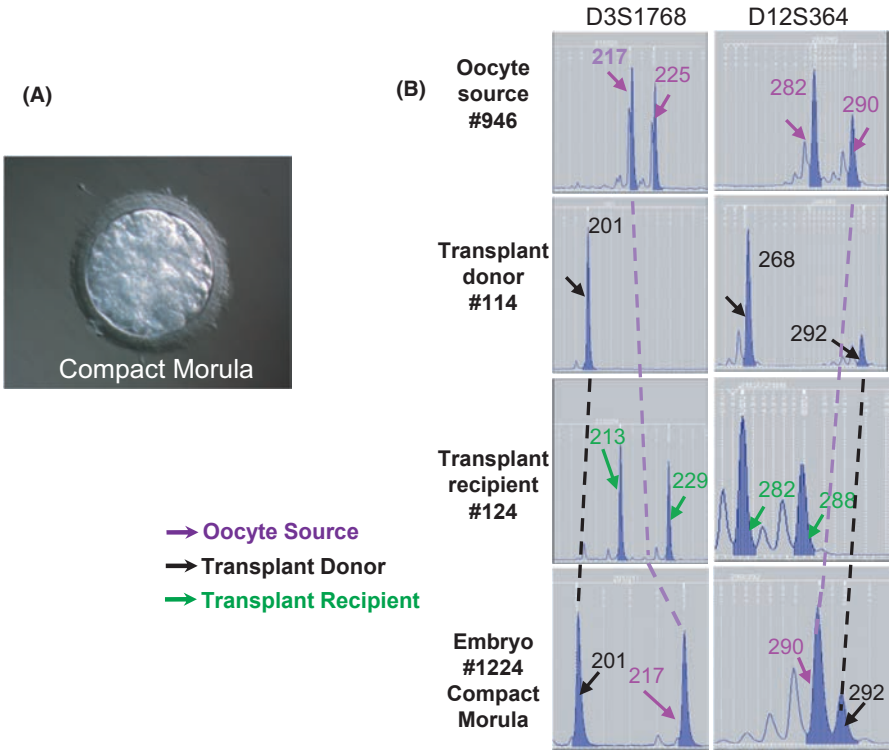

FIGURE 7 Embryo produced by ICSI with epididymal spermatozoa from a monkey (#124) with high percentage of donor-derived spermatozoa. (A) Compact morula resulting from in vitro culture of the fertilized oocyte. (B) Microsatellite DNA analysis of one donor-derived embryo and comparison with the oocyte, SSC donor and recipient male profiles. Alleles specific for the oocyte donor (represented by purple font and arrow), transplant donor (represented by black font and arrow), and transplant recipient (represented by green font and arrow) are indicated on the electropherogram panels. The presence of the alleles at 201 and 292 nucleotide pairs in the embryo demonstrates the paternal origin as being from the donor

the hormone and immune suppression might have on colonization and recovery, but could also be a result of the species difference.

The effect of the efficiency of the filling of seminiferous tubules with the donor cell suspension on the production of donor spermatozoa was assessed. The two cases with a transplantation efficiency score of five resulted in the highest levels of donor spermatozoa in the epididymis. Although these data suggested a trend that transplantation efficiency was important for the success of the transplant, the correlation was not statistically significant (p = 0.14). A similar trend toward higher donor sperm production with better transplantation efficiency was also observed in our previous study,[2] and when we combined the data of both studies, the association was highly statistically significant (Spearman's correlation, ρ = 0.58, p = 0.006). Thus, efficient transfer of the injected cell suspension to the seminiferous tubules is indeed an important factor in successful transplantation.

The characteristics and functional integrity of the recipient testis may be factors in the ability to colonize, especially after the damaging prepubertal cytotoxic treatment.[35] Both the serum T levels and testis volumes, measured at the time of the second irradiation, 8 weeks before transplantation, seemed to be correlated with the donor sperm production. The serum T level is a measure of pubertal development and testis volume is a measure of both pubertal development and recovery of spermatogenesis after the first irradiation. These results indicate that success from transplantation is dependent on the somatic cells of the testis going through relatively normal pubertal development despite the prepubertal irradiation. Further studies of transplantation are needed with a model of more complete spermatogenic cell depletion, because the transplantation is only needed when there is a failure of endogenous spermatogenic recovery.

Also, the presence of dilated tubules, observed in the final histological samples taken 10 months after transplantation, was negatively correlated with the yield of donor spermatozoa and appeared to be a factor limiting the development of donor spermatogenesis. Whereas in previous studies we have never observed such structural damage to the seminiferous tubule from 7 Gy testicular irradiation of adult monkeys,[2,14] four of the six monkeys receiving 6.9 Gy prepubertally had dilated tubules in the final histological sample taken 10 months after transplantation, and in one (#092) of them, nearly all the tubules were dilated. It is likely that this was due to damage incurred from the first dose of 6.9 Gy since this monkey failed to show the increase in testicular volume (Figure S3A) that would be expected from maturation of the somatic elements of the testis during puberty. Dilated tubules in adult rhesus monkeys after prepubertal irradiation had also been observed previously, but no dose-response was reported,[19] and we have also observed such tubule dilation (7%, 24%) in two rhesus monkeys that had received only 1 dose of 6.9 Gy before puberty (data not shown). The immature Sertoli cells in prepubertal testis, which are expected to be still proliferating,[36] are likely one of the targets for such sensitivity of the somatic structure of the testis in these juvenile monkeys. Future studies of molecular markers of Sertoli cell functional status in such cases are important for further development of SSC transplantation.

It has been suggested that it might be possible to restore tubular function and the SSC niche by donor Sertoli cells, as was demonstrated after chemical ablation of Sertoli cells in mice.[37] Our previous studies [38] showed that transplanted donor Sertoli cells colonized

TABLE 4 Comparison with Previous Studies of Spermatogonial Stem Cell Transplantation in Non-human Primates

Species of Macaque	Recipient Prep	Age Cytotoxic Treatment	Age Transplant	Donor SSCs	Donor Marking	Enhanced recovery in transplant testis[a]	Donor Spermatozoa[a]	Percent Donor (%)	Reference
Cynomolgus	Irradiation (2 Gy)	Adult	Adult	Autologous	None	2/5	ND[b]	– –	43
Rhesus	Irradiation (10 Gy)	Prepubertal	Prepubertal	Autologous	None	1/4	ND[b]	– –	20
Rhesus	Irradiation (10 Gy)	Pubertal	Pubertal	Autologous	None	0/2	ND[b]	– –	20
Rhesus	Busulfan (8–12 mg/kg)	Prepubertal	Prepubertal[c]	Autologous	Lentivirus	NA[d]	3/5	– –	13
Rhesus	Busulfan (8–12 mg/kg)	Adult	Adult	Autologous	Lentivirus	NA[d]	9/12	– –	13
Rhesus	Busulfan (8–11 mg/kg)	Adult	Adult	Allogeneic	Microsatellites	NR[e]	2/6	10, 1.1	13
Cynomolgus	Irradiation (7 Gy)	Adult	Adult	Autologous	Lentivirus	2/11[g]	6/12[h]	– –	14
Rhesus	Irradiation (7 Gy)	Adult	Adult	Allogeneic	Microsatellites	2/15[i]	5/15[j]	93, 84, 1.7, 0.4, 1.0	2
Rhesus	Irradiation (6.9+7 Gy)	Prepubertal & Adult[f]	Adult	Allogeneic	Microsatellites	NA	3/6[k]	61, 38, 11	Present Study

[a] Number positive results/number transplanted.

[b] ND: Not detectable because autologous transplantation was done with unmarked cells.

[c] Transplantation was done 9–15 weeks after busulfan treatment. The pubertal status at this time was not reported.

[d] NA: Not applicable because all or nearly all of the recipients were hemicastrated.

[e] NR: Not reported.

[f] 6.9 Gy was given prepubertally and an additional 7 Gy was given after puberty because of recovery of spermatogenesis.

[g] 2/6 for GnRH-ant-treated, 0/5 for no GnRH-ant.

[h] 5/6 for GnRH-ant-treated, 1/6 for no GnRH-ant.

[i] 1/10 for GnRH-ant-treated, 1/5 for no GnRH-ant.

[j] 3/10 for GnRH-ant-treated, 2/5 for no GnRH-ant.

[k] 1/3 for GnRH-ant-treated, 2/3 for no GnRH-ant.

irradiated rat tubules but did not restore the somatic environment to support differentiation of endogenous spermatogonia, which were otherwise blocked from differentiation. Although transplantation of Sertoli cells as a niche replacement strategy may be beneficial to enhance recovery from transplanted cells in prepubertally irradiated monkeys, we as yet have no data as to whether or not the rhesus Sertoli cells in the transplantation suspension colonize the tubules of these irradiated monkeys.

However, in two of the six recipients, we observed the formation of *de novo* tubular cords containing somatic and germ cells, derived from the donor, in the interstitial space (Figure 6). This result extends our previous observation on a single-irradiated adult monkey transplanted with prepubertal testis cells in which we confirmed that both germ and somatic components of the *de novo* tubules were of donor origin.[17] As was the case in the previous study, the ultrasound visualization of the transplantation demonstrated that the cells were indeed injected into the rete testis and entered the tubules (transplant efficiency score ≥4) (Table 1). However, various studies have shown that even when injection is done into the rete, there is significant leakage of the cells to the interstitium.[39,40] The location of *de novo* cords adjacent to the rete testis suggest that the rete itself may be the source of the leakage. Based on the observation that all three monkeys, in which we observed *de novo* cords in the interstitium, were treated with GnRH-ant, we suggest that the hormone suppression might increase the leakage of transplanted cells into the interstitium and/or create an environment favorable to the development of these *de novo* cords. It was noteworthy that none of these three monkeys showed any evidence of donor spermatozoa in the epididymis, indicating that there was no intratubular development of transplanted cells. Although the leakage and formation of *de novo* cords in the interstitium appears negatively correlated with intratubular donor spermatogenesis, the production of donor spermatozoa in these cords potentially can be used for fertilization. Thus, if the seminiferous tubules do not support donor spermatogenesis from the cryopreserved SSCs due to endogenous Sertoli cells rendered defective by gonadotoxic therapies, spermatogenesis from such *de novo* derived cords may be an alternative strategy for fertility preservation.

Since there have been no reports as to whether chemotherapy treatment also results in similar damage to the Sertoli cells, we re-analyzed the testicular tissues from a previous study,[13] in which five prepubertal monkeys were treated with 8–12 mg/kg busulfan when they were prepubertal and then given autologous transplantation of lentivirus-transduced testicular cells. There were no dilated tubules

nor any morphological abnormalities in these testes that were harvested about 3 years after busulfan exposure. Even in the few Sertoli-only tubules, the Sertoli cells had a regular columnar appearance. However, it should be noted that even at these high doses of busulfan, 97% of tubules showed recovering spermatogenesis, 83% of which progressed to the spermatid stage. Most of this recovery must be from endogenous surviving SSC since two of the monkeys were negative for production of lentivirus-marked spermatozoa. This is in contrast to our results with two prepubertal monkeys (not shown) irradiated with 6.9 Gy that showed spermatogenic recovery in only 33% of tubules at 2 years after irradiation. Thus, although busulfan does not produce the damage to the somatic testis tissue that irradiation does, busulfan in not as effective at producing prolonged loss of spermatogenesis in prepubertal animals. Since even 6.9 Gy did not fully eliminate endogenous spermatogenesis, there is a need for a better model that would kill SSCs with minimal somatic testicular tissue damage.

In conclusion, we have demonstrated that SSC transplantation after puberty can restore spermatogenesis and fertilization-competent sperm production after prepubertal and post-pubertal irradiation and have characterized the factors that may be related to the success of the technique. Particularly the precise delivery of cells and filling of tubules at the injection appears to be an important factor. However, complete depletion of germ cells without causing somatic damage was not possible with single doses of radiation during the prepubertal period and improvements in the treatment paradigm are necessary. Since the spermatogenic function of the human testis is more sensitive to fractionated doses of radiation [41] or combining radiation with alkylating agents, such as busulfan,[42] than to single doses of radiation, these may be better models to deplete the germ cells. It is hoped that these procedures will more closely model the cohort of patients treated prepubertally with gonadotoxic cancer therapies, who have normal tubular somatic cells but with spermatogenic depletion, and are in need of fertility preservation procedures.

ACKNOWLEDGEMENTS

This work was supported by research grants P01 HD075795 from NIH/NICHD to KO, R01 HD100197 from NIH/NICHD to KO and MLM, Cancer Center Support Grant P30 CA016672 from NIH/NCI to the University of Texas MD Anderson Cancer Center and P51 OD011092 from NIH to the Oregon National Primate Research Center. We would like to acknowledge the outstanding work of Jennifer M. Meyer who assisted in managing the treatment of the monkeys, sample collections, and animal health issues and also Cathy Ramsey and Fernanda de Carvalho for their valuable assistance in the ovarian stimulation, embryo culture, and ICSI procedures. We sincerely thank Dr. Min S. Lee, National Institute for Child Health and Human Development, for providing the Acyline.

CONFLICT OF INTEREST

The authors have no conflicts of interest to declare.

AUTHORS' CONTRIBUTIONS

G.S. participated in the conceptualization and design of the study, performed the majority of the experiments, analyzed the results, and prepared the manuscript. J.M. Mitchell participated in the study design, treatment of the monkeys, and surgeries. T.N.A.L and T.T.P. prepared the cells for transplantation and performed immunostaining of the tissue sections, testosterone assays and xenotransplantation. J.Z. assisted in the histological preparations of tissues. R.C.T. performed the dosimetry for the testicular radiation of the monkeys. K.A.P. assisted in the transplantation of testicular cells into the monkey testes. C.M.P. performed microsatellite analysis of the samples. C.H. participated in oocyte retrieval, ICSI, and embryo culture. A.T.C. contributed to conceptual input and participated in design of the study. K.E.O. provided important conceptual input, participated in design of the study, and performed transplantation of testicular cells into the monkey testes. M.L.M. participated in the conception of the study, design of the experiments, analysis of results, and preparation of the manuscript.

ORCID

Gunapala Shetty https://orcid.org/0000-0001-5786-0667
Marvin L. Meistrich https://orcid.org/0000-0002-2857-639X

REFERENCES

1. Siegel RL, Miller KD, Jemal A. Cancer statistics, 2020. *CA Cancer J Clin*. 2020;70:7-30.
2. Shetty G, Mitchell JM, Meyer JM, et al. Restoration of functional sperm production in irradiated pubertal rhesus monkeys by spermatogonial stem cell transplantation. *Andrology*. 2020;8:1428-1441.
3. Kenney LB, Antal Z, Ginsberg JP, et al. Improving male reproductive health after childhood, adolescent, and young adult cancer: progress and future directions for survivorship research. *J Clin Oncol*. 2018;36:2160-2168.
4. Green D, Galvin H, Horne B. The psycho-social impact of infertility on young male cancer survivors: a qualitative investigation. *Psychooncology*. 2003;12:141-152.
5. Valli-Pulaski H, Peters KA, Gassei K, et al. Testicular tissue cryopreservation: 8 years of experience from a coordinated network of academic centers. *Hum Reprod*. 2019;34:966-977.
6. Gassei K, Orwig KE. Experimental methods to preserve male fertility and treat male factor infertility. *Fertil Steril*. 2016;105:256-266.
7. Goossens E, Jahnukainen K, Mitchell RT, et al. Fertility preservation in boys: recent developments and new insights (dagger). *Hum Reprod Open*. 2020;2020(3):hoaa016.
8. Giudice MG, de Michele F, Poels J, Vermeulen M, Wyns C. Update on fertility restoration from prepubertal spermatogonial stem cells: how far are we from clinical practice? *Stem Cell Res*. 2017;21:171-177.
9. Brinster RL. Male germline stem cells: from mice to men. *Science*. 2007;316:404-405.
10. Zhang Z, Renfree MB, Short RV. Successful intra- and interspecific male germ cell transplantation in the rat. *Biol Reprod*. 2003;68:961-967.
11. Ryu BY, Orwig KE, Avarbock MR, Brinster RL. Stem cell and niche development in the postnatal rat testis. *Dev Biol*. 2003;263:253-263.
12. Honaramooz A, Behboodi E, Megee SO, et al. Fertility and germline transmission of donor haplotype following germ cell transplantation in immunocompetent goats. *Biol Reprod*. 2003;69:1260-1264.

13. Hermann BP, Sukhwani M, Winkler F, et al. Spermatogonial stem cell transplantation into rhesus testes regenerates spermatogenesis producing functional sperm. *Cell Stem Cell*. 2012;11:715-726.
14. Shetty G, Uthamanthil RK, Zhou W, et al. Hormone suppression with GnRH antagonist promotes spermatogenic recovery from transplanted spermatogonial stem cells in irradiated cynomolgus monkeys. *Andrology*. 2013;1:886-898.
15. Ogawa T, Dobrinski I, Avarbock MR, Brinster RL. Leuprolide, a gonadotropin-releasing hormone agonist, enhances colonization after spermatogonial transplantation into mouse testes. *Tissue Cell*. 1998;30:583-588.
16. Wang G, Shao SH, Weng CC, Wei C, Meistrich ML. Hormonal suppression restores fertility in irradiated mice from both endogenous and donor-derived stem spermatogonia. *Toxicol Sci*. 2010;117:225-237.
17. Shetty G, Mitchell JM, Lam TNA, et al. Donor spermatogenesis in de novo formed seminiferous tubules from transplanted testicular cells in rhesus monkey testis. *Hum Reprod*. 2018;33:2249-2255.
18. Fayomi AP, Peters K, Sukhwani M, et al. Autologous grafting of cryopreserved prepubertal rhesus testis produces sperm and offspring. *Science*. 2019;363:1314-1319.
19. de Rooij DG, van de Kant HJ, Dol R, et al. Long-term effects of irradiation before adulthood on reproductive function in the male rhesus monkey. *Biol Reprod*. 2002;66:486-494.
20. Jahnukainen K, Ehmcke J, Quader MA, et al. Testicular recovery after irradiation differs in prepubertal and pubertal non-human primates, and can be enhanced by autologous germ cell transplantation. *Hum Reprod*. 2011;26:1945-1954.
21. Herbst KL, Coviello AD, Page S, Amory JK, Anawalt BD, Bremner WJ. A single dose of the potent gonadotropin-releasing hormone antagonist acyline suppresses gonadotropins and testosterone for 2 weeks in healthy young men. *J Clin Endocrinol Metab*. 2004;89:5959-5965.
22. Hermann BP, Sukhwani M, Lin CC, et al. Characterization, cryopreservation, and ablation of spermatogonial stem cells in adult rhesus macaques. *Stem Cells*. 2007;25:2330-2338.
23. Hermann BP, Sukhwani M, Simorangkir DR, Chu T, Plant TM, Orwig KE. Molecular dissection of the male germ cell lineage identifies putative spermatogonial stem cells in rhesus macaques. *Hum Reprod*. 2009;24:1704-1716.
24. Kirk AD, Burkly LC, Batty DS, et al. Treatment with humanized monoclonal antibody against CD154 prevents acute renal allograft rejection in nonhuman primates. *Nat Med*. 1999;5:686-693.
25. Byrne JA, Pedersen DA, Clepper LL, et al. Producing primate embryonic stem cells by somatic cell nuclear transfer. *Nature*. 2007;450:497-502.
26. Bishop CV, Reiter TE, Erikson DW, et al. Chronically elevated androgen and/or consumption of a Western-style diet impairs oocyte quality and granulosa cell function in the nonhuman primate periovulatory follicle. *J Assist Reprod Genet*. 2019;36:1497-1511.
27. Hewitson L, Dominko T, Takahashi D, et al. Unique checkpoints during the first cell cycle of fertilization after intracytoplasmic sperm injection in rhesus monkeys. *Nat Med*. 1999;5:431-433.
28. Mitalipov S, Kuo HC, Byrne J, et al. Isolation and characterization of novel rhesus monkey embryonic stem cell lines. *Stem Cells*. 2006;24:2177-2186.
29. Ramsey C, Hanna C. In vitro culture of rhesus macaque (Macaca mulatta) embryos. *Methods Mol Biol*. 2019;2006:341-353.
30. Chemes HE, Dym M, Raj HG. Hormonal regulation of sertoli cell differentiation. *Biol Reprod*. 1979;21:251-262.
31. Meistrich ML, Wilson G, Shuttlesworth G, Huhtaniemi I, Reissmann T. GnRH agonists and antagonists stimulate recovery of fertility in irradiated $LBNF_1$ rats. *J Androl*. 2001;22:809-817.
32. Gordon TP, Rose RM, Bernstein IS. Seasonal rhythm in plasma testosterone levels in the rhesus monkey (Macaca mulatta): a three year study. *Horm Behav*. 1976;7:229-243.
33. Wickings EJ, Nieschlag E. Seasonality in endocrine and exocrine testicular function of the adult rhesus monkey (Macaca mulatta) maintained in a controlled laboratory environment. *Int J Androl*. 1980;3:87-104.
34. Gubbels Bupp MR, Jorgensen TN. Androgen-Induced Immunosuppression. *Front Immunol*. 2018;9:1-16.
35. Trondle I, Westernstroer B, Wistuba J, Terwort N, Schlatt S, Neuhaus N. Irradiation affects germ and somatic cells in prepubertal monkey testis xenografts. *Mol Hum Reprod*. 2017;23:141-154.
36. Simorangkir DR, Ramaswamy S, Marshall GR, Roslund R, Plant TM. Sertoli cell differentiation in rhesus monkey (Macaca mulatta) is an early event in puberty and precedes attainment of the adult complement of undifferentiated spermatogonia. *Reproduction*. 2012;143:513-522.
37. Yokonishi T, McKey J, Ide S, Capel B. Sertoli cell ablation and replacement of the spermatogonial niche in mouse. *Nat Commun*. 2020;11:40.
38. Zhang Z, Shao S, Shetty G, Meistrich ML. Donor Sertoli cells transplanted into irradiated rat testes stimulate partial recovery of endogenous spermatogenesis. *Reproduction*. 2009;137:497-508.
39. Faes K, Lahoutte T, Hoorens A, Tournaye H, Goossens E. In search of an improved injection technique for the clinical application of spermatogonial stem cell transplantation. *Reprod Biomed Online*. 2017;34:291-297.
40. Gul M, Hildorf S, Dong L, et al. Review of injection techniques for spermatogonial stem cell transplantation. *Hum Reprod Update*. 2020;26:368-391.
41. Meistrich ML, van Beek MEAB. Radiation sensitivity of the human testis. *Adv Radiat Biol*. 1990;14:227-268.
42. Sanders JE, Buckner CD, Leonard JM, et al. Late effects on gonadal function of cyclophosphamide, total-body irradiation, and marrow transplantation. *Transplantation*. 1983;36:252-255.
43. Schlatt S, Foppiani L, Rolf C, Weinbauer GF, Nieschlag E. Germ cell transplantation into X-irradiated monkey testes. *Hum Reprod*. 2002;17:55-62.

SUPPORTING INFORMATION

Additional supporting information may be found online in the Supporting Information section.

How to cite this article: Shetty G, Mitchell JM, Lam TN, et al. Postpubertal spermatogonial stem cell transplantation restores functional sperm production in rhesus monkeys irradiated before and after puberty. *Andrology*. 2021;9 160331616. https://doi.org/10.1111/andr.13033

nature COMMUNICATIONS

ARTICLE

https://doi.org/10.1038/s41467-021-21517-5 OPEN

Triptonide is a reversible non-hormonal male contraceptive agent in mice and non-human primates

Zongliang Chang[1,7], Weibing Qin[2,3,7], Huili Zheng[1,7], Kathleen Schegg[1,7], Lu Han[2,3], Xiaohua Liu[2,3], Yue Wang[1], Zhuqing Wang[1], Hayden McSwiggin[1], Hongying Peng[1], Shuiqiao Yuan[1], Jiabao Wu[2,3], Yongxia Wang[2,3], Shenghui Zhu[2,3], Yanjia Jiang[2,3], Hua Nie[2,3], Yuan Tang[2,3], Yu Zhou[2,3], Michael J. M. Hitchcock[4], Yunge Tang[2,3]✉ & Wei Yan[1,5,6]✉

There are no non-hormonal male contraceptives currently on the market despite decades of efforts toward the development of "male pills". Here, we report that triptonide, a natural compound purified from the Chinese herb *Tripterygium Wilfordii Hook F* displays reversible male contraceptive effects in both mice and monkeys. Single daily oral doses of triptonide induces deformed sperm with minimal or no forward motility (close to 100% penetrance) and consequently male infertility in 3–4 and 5–6 weeks in mice and cynomolgus monkeys, respectively. Male fertility is regained in ~4–6 weeks after cessation of triptonide intake in both species. Either short- or long-term triptonide treatment causes no discernable systematic toxic side effects based on histological examination of vital organs in mice and hematological and serum biochemical analyses in monkeys. Triptonide appears to target junction plakoglobin and disrupts its interactions with SPEM1 during spermiogenesis. Our data further prove that targeting late spermiogenesis represents an effective strategy for developing non-hormonal male contraceptives.

[1] Department of Physiology and Cell Biology, University of Nevada, Reno School of Medicine, Reno, NV, USA. [2] NHC Key Laboratory of Male Reproduction and Genetics, Guangzhou, People's Republic of China. [3] Family Planning Research Institute of Guangdong Province, Guangzhou, People's Republic of China. [4] Department of Microbiology and Immunology, University of Nevada, Reno School of Medicine, Reno, NV, USA. [5] The Lundquist Institute for Biomedical Innovation at Harbor-UCLA Medical Center, Torrance, CA, USA. [6] Department of Medicine, David Geffen School of Medicine at UCLA, Los Angeles, CA, USA. [8] These authors contributed equally: Zongliang Chang, Weibing Qin, Huili Zheng, Kathleen Schegg. ✉email: tyg813@126.com; wei.yan@lundquist.org

Overpopulation and unintended pregnancy underscore a critical need for next-generation contraceptives that should be safe, convenient, effective, affordable, and acceptable to people of various cultural and religious backgrounds. Among all of the currently available contraceptives, "oral pills" remain the most popular method[1]. However, contraceptive pills are now only available for women. Despite five decades of efforts, there remain no nonhormonal male birth control pills on the horizon. Failure to develop nonhormonal male contraceptives stems, in part, from our incomplete understanding of spermatogenesis and sperm biology. For example, many believe that male pills should suppress sperm counts to very low or even zero to prevent pregnancy. However, a total blockage of sperm production requires the depletion of spermatogenic cells, which often causes testis shrinkage, an undesirable effect that may deter its usage. Moreover, germ cell depletion alters the cellular composition and microenvironment in the testis, which, in turn, tend to trigger the hypothalamus–pituitary–testis feedback system, leading to systematic side effects[2,3]. Therefore, it remains challenging to identify a compound which can eliminate all sperm without causing toxic side effects. We proposed a strategy for developing male contraceptives, i.e., disabling, instead of depleting, spermatogenic cells or sperm by causing sperm deformation and/or dysfunction[4]. This idea was inspired by several decades of studies on genes encoding proteins exclusively expressed in elongating and elongated spermatids, e.g., *Prm1, Tnp1, Spem1, Catsper1-4, Meig1*, etc., using gene knockout (KO) mouse models[4]. Although many of these KO males are completely infertile, their testis weight, sperm counts, and even testicular histology are largely normal, and infertility of these mice results from either sperm deformation (e.g., teratozoospermia in *Spem1*- or *Meig1-null* mice)[5], or lack of functional components (e.g., absence of an ion channel in *Catsper3*- or *Catsper4*-null sperm)[6,7]. Given that proteins encoded by these genes are exclusively expressed in late spermatids, these KO studies strongly suggest that late spermiogenesis appears to lack a stringent "checkpoint" for eliminating defective late spermatids[4]. Consequently, there are typically no histologically discernable disruptions in the seminiferous epithelium although defective sperm are made in these KO mice. The lack of such a "quality control" mechanism in late spermiogenesis is also supported by the fact that a significant proportion of spermatozoa collected from the mouse epididymis (~20–30%) or human ejaculates (30–40%) are immotile and/or morphologically abnormal[8,9]. Based on these observations, we proposed that gene products (e.g., proteins and RNAs) that are exclusively expressed in late spermatids and play an essential role in normal sperm production and male fertility represent ideal male contraceptive targets because a drug that acts on these targets would cause deformed and/or nonfunctional sperm that are incompetent for fertilization without causing significant decrease in either testis size or sperm counts[4].

With this idea in mind, we embarked on an extensive search for known drug candidates that have been documented to cause sperm deformation as a side effect. During this process, we identified triptonide, a compound purified from the extracts of a Chinese herb called *T. wilfordii Hook F* (Supplementary Fig. 1), as a promising nonhormonal male contraceptive agent. This herb has been used for more than two centuries in traditional Chinese medicine to treat a variety of autoimmune and inflammatory diseases, including rheumatoid arthritis[10,11]. However, it was first reported in 1983 that men taking this herbal mixture as medicine for an extended period (>3 months) displayed infertility due to deformed sperm and reduced sperm counts and motility[12]. Since then, researchers have been isolating and testing compounds purified from this herb, in the hope of identifying compounds that have "antisperm effects"[12–18]. To date, hundreds of individual compounds have been purified from this herb, including triptolide, tripdiolide, triptolidenol, tripchlorolide, 16-hydroxytriptolide, triptonide, and many more[19]. In particular, several initial studies on two of these compounds—triptolide and tripchlorolide—reported severe liver toxicity and limited reversibility of male fertility at doses that can effectively reduce sperm count and motility[20–24]. Reversibility of the contraceptive effect and minimal side effects are two essential properties for a good oral male contraceptive. Without these properties, candidate drugs cannot be developed. This limitation may partially explain why the remaining compounds, including triptonide, have not been further explored for their male contraceptive potential. Given the well-documented sperm deformation effects induced by this herb, we decided to examine ten other compounds, aiming to identify one that can induce sperm deformation and male infertility without deleterious side effects. Among the compounds tested, we found that triptonide displayed almost ideal contraceptive effects in male mice, including excellent bioavailability allowing for oral administration, initial male infertility achieved by 3–4 weeks of daily oral treatment, sustained infertility in male mice maintained on the same dose for months, and reversal from infertile to fertile states in ~3–4 weeks after cessation of the treatment. Importantly, we observed no discernable deleterious effects, such as organ toxicity. Therefore, we proceeded and conducted the comprehensive proof-of-concept (POC) efficacy testing using triptonide on both mice and cynomolgus monkeys (*Macaca fascicularis*), and also attempted to identify its specific target(s) and mechanism(s) of action. Here, we report our data on the discovery of triptonide as an efficient, reversible male contractive agent in both mice and nonhuman primates. Based on the initial efficacy and safety data reported here, triptonide has the potential to become a promising nonhormonal male contractive agent.

Results

Oral administration of triptonide causes male infertility due to deformed sperm and reduced motility in mice. As a pilot efficacy test, we first administered triptonide at five doses (0.1, 0.2, 0.4, 0.8, and 1.6 mg/kg BW) via oral gavage to adult male mice (C57BL/6J) at the age of 8–12 weeks. Mice from each dosing group were sacrificed weekly to examine both morphology and motility of epididymal sperm, as well as testicular histology for up to 6 weeks. We found the shortest time to achieve close to 100% sperm deformation characterized by head-bent-back and a complete lack of forward motility was between weeks 3 and 4 at the dose of 0.8 mg/kg BW or higher (Fig. 1a–e and Supplementary Movies 1 and 2). The pilot experiments were repeated two more times, and the same results were obtained. Thus, ~4 weeks of oral intake of triptonide at single daily doses of 0.8 mg/kg BW induce sperm deformation and loss of forward motility with close to 100% penetrance in adult male C57BL/6J mice. The "head-bent-back" phenotype in triptonide-treated sperm appeared to be homogenous and highly resembled the phenotype of *Spem1* KO sperm[5]. Transmission electron microscopic analyses confirmed that the sperm heads of triptonide-treated sperm were mostly bent at the connecting piece, and the bent head and neck were wrapped by residual cytoplasm (Fig. 1c). Moreover, scanning electron microscopic analyses revealed that testicular sperm already displayed the "head-bent-back" phenotype within the seminiferous epithelium, suggesting that the defects arise during spermatogenesis within the testis (Fig. 1c). In the official POC efficacy testing, after single oral daily doses of 0.8 mg/kg BW for 4 weeks, each of the treated male mice ($n = 12$) was mated with two fertility-proven female mice. While vaginal plugs were found in all of the females mated with the triptonide-treated male mice,

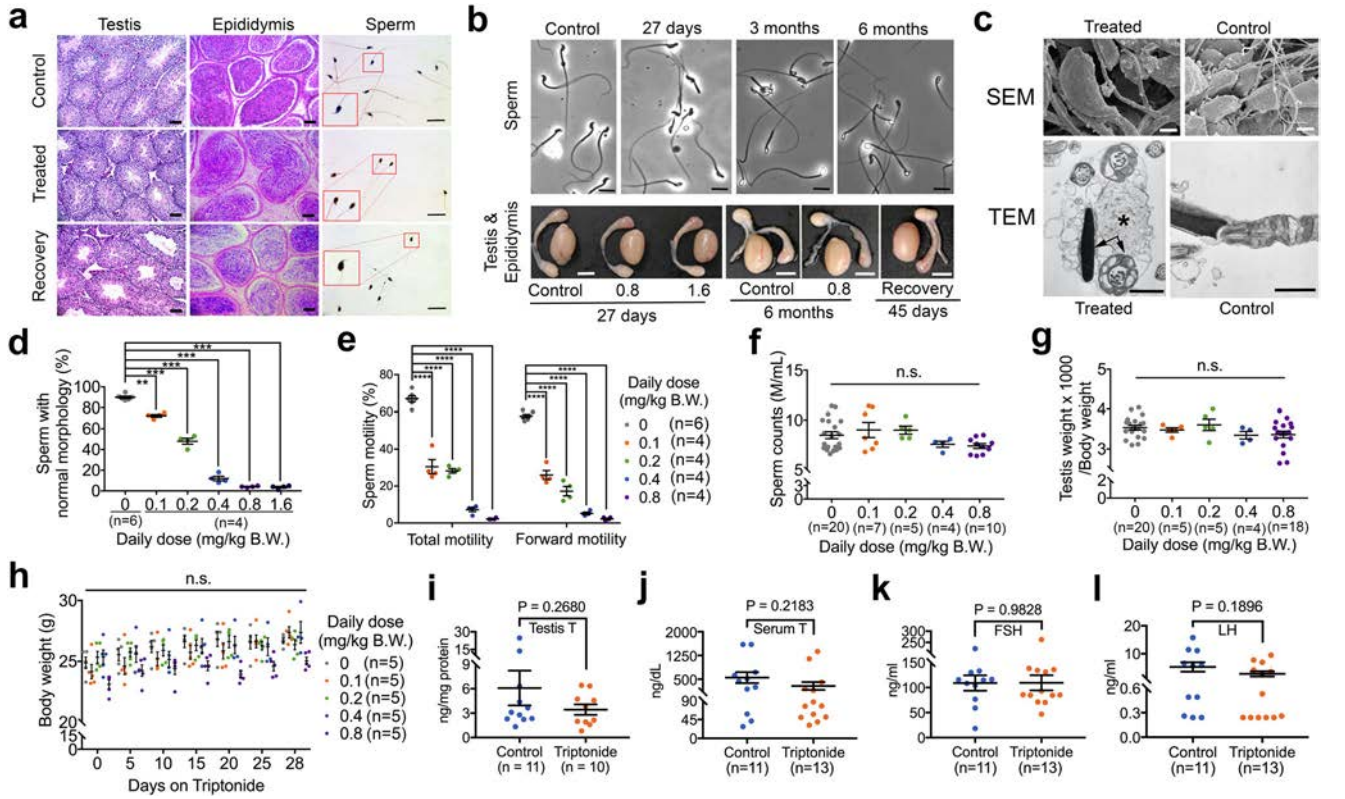

Fig. 1 Proof-of-concept efficacy testing of male contraceptive effects of triptonide in mice. a Representative histology of the testis, epididymis, and sperm from mice that received vehicle (control) and triptonide (treated) at single daily oral doses of 0.8 mg/kg BW for 4 weeks, and those recovered for 4 weeks after 4 weeks of triptonide treatment. Scale bars = 20 μm. Insets represent digitally enlarged framed areas. **b** Representative images of the gross morphology of sperm (upper panels, scale bars = 10 μm), testis, and epididymis (lower panels, scale bars = 20 mm) from mice that received short-term (27 days) and long-term (3 and 6 months) treatment with triptonide at single daily oral doses of 0.8 or 1.6 mg/kg BW, and those recovered for 45 days after 4 weeks of triptonide treatment. **c** Micrographs showing spermatozoa from triptonide-treated and control male mice. Bending of sperm heads occurs inside the seminiferous tubules of triptonide-treated male mice, as revealed by scanning electron microscopy (SEM; scale bar = 2 μm). Transmission electron microscopy (TEM) shows residual cytoplasmic contents (*) surrounding the bent sperm head and tail (arrows; scale bar = 1 μm). **d** Effects of different doses of triptonide (single daily oral gavage for 4 weeks) on sperm morphology in adult C57BL/6J male mice. Individual data points and mean (measure of center) ± SEM (error bars) are shown. $^{**}p < 0.01$; $^{***}p < 0.001$, as determined by one-way ANOVA with dosing groups ($n = 4$) compared to the vehicle control group ($n = 6$). **e** Effects of different doses of triptonide (single daily oral gavage for 4 weeks) on total and forward sperm motility in adult C57BL/6J male mice. Individual data points and mean (measure of center) ± SEM (error bars) are shown. $^{****}p < 0.0001$, as determined by one-way ANOVA with dosing groups ($n = 4$) compared to the vehicle control group ($n = 6$). **f**–**h** Effects of different doses of triptonide (single daily oral gavage for 4 weeks) on sperm counts (**f**), relative testis weight (testis weight × 1000/body weight) (**g**), and body weight (**h**) in adult C57BL/6J male mice. Individual data points and mean (measure of center) ± SEM (error bars) are shown. Sample sizes are marked in brackets. No statistical significance (n.s.) among the groups based on one-way ANOVA analyses. **i**–**l** Effects of triptonide (single daily oral dose of 0.8 mg/kg BW for 4 weeks) on intratesticular testosterone (**i**), serum testosterone (**j**), FSH (**k**), and LH (**l**) levels in adult C57BL/6J male mice. Individual data points and mean (measure of center) ± SEM (error bars) are shown. Sample sizes are marked in brackets. No statistical significance was detected between the control and treated groups based on one-way analyses of variance (ANOVA) with $p < 0.05$ considered statistically significant.

none of the plugged females became pregnant. In contrast, female mice mated with vehicle control male mice ($n = 12$) were all pregnant. This was not surprising given that sperm in the treated mice were all deformed and displayed minimal or no forward motility (Fig. 1d, e). During the 4-week long triptonide treatment, no significant changes in either sperm counts, or testicular weight (Fig. 1f, g) were observed. Moreover, triptonide treatment did not change the body weight at any of the doses tested (Fig. 1h). To exclude the possibility that the male contraceptive effects were strain-dependent, we also tested triptonide on CD-1 mice by administering a daily oral dose of 0.8 mg/kg BW for 4 weeks. A similar phenotype was observed in the CD-1 mice (Supplementary Fig. 2).

At the end of the 4-week long triptonide treatment, we analyzed hormonal profiles and found no significant changes in the levels of FSH, LH, or testosterone (both serum and intratesticular; Fig. 1i–l). Consistent with the normal hormonal profiles, no gross or histological abnormalities were observed in the testis or epididymis (Fig. 1a, b). Either at the end of or during the treatment, male mice displayed frequent mounting behavior and successfully mated with adult female mice primed with PMSG and hCG, suggesting no adverse effects on mating behavior or capability. Examination of histology of major organs, including heart, liver, spleen, lung, and kidney revealed no pathological changes (Supplementary Fig. 3). Moreover, no discernable physical and behavioral abnormalities were observed among the treated mice. Taken together, these results suggest that a short-term oral intake of triptonide at a dose of 0.8 mg/kg BW causes no systematic toxic effects in major somatic organs in adult C57BL/6J male mice.

We also conducted long-term triptonide treatment using single daily oral doses of 0.8 mg/kg BW for 3 and 6 months, respectively

(Supplementary Movies 3-4). All 16 male mice tested (8 in each group) became infertile after 4 weeks, and infertility persisted between week 4 and the third or sixth month of treatment, as evidenced by the fact that none of the 32 fertile adult females placed into the individually housed, treated male mice (2 females per male) became pregnant. Further examination revealed a similar phenotype between long- (3 or 6 months) and short-term (4 weeks) treatment with triptonide (Fig. 1b). Similarly, no discernable toxic effects were observed in the mice that had undergone the long-term treatment of triptonide.

The sperm from triptonide-treated male mice cannot fertilize eggs either naturally or through in vitro fertilization due to deformation and a lack of forward motility. To test the fertility competence of sperm from triptonide-treated male mice, we conducted intracytoplasmic sperm injection (ICSI) by injecting the deformed sperm heads from triptonide-treated male mice (single daily oral doses at 0.8 mg/kg BW for 4 weeks) into WT MII oocytes. Interestingly, while the triptonide-treated sperm could fertilize the MII oocytes, the developmental potential of early embryos derived from the triptonide-treated sperm was significantly reduced compared to controls (Supplementary Table 1). Moreover, no pups were born after the embryos of 2-pronucleus (2PN) stage were transferred to recipient females, whereas a significant proportion (~15%) of the control 2PN embryos developed to full term and live pups were born in controls (Supplementary Table 2). These data suggest that triptonide-treated sperm may not be competent to support full-term development in mice.

Oral administration of triptonide causes male infertility in cynomolgus monkeys. To test whether triptonide would exert the same male contraceptive effects in primates, we also conducted POC efficacy testing using adult male cynomolgus monkeys. To determine the minimal effective dose, we first conducted a pilot study by treating four adult male cynomolgus monkeys with single daily oral administration of triptonide at the following four doses: 0.05, 0.1, 0.2, or 0.8 mg/kg BW. Semen samples were collected weekly, and sperm counts, motility, and morphology were analyzed to monitor the effects. We observed that single daily oral doses at 0.1 mg/kg BW or above resulted in oligo-astheno-teratozoospermia (OAT; Supplementary Fig. 4), characterized by sperm deformation (headless/tailless sperm, sperm with large cytoplasmic droplets, sperm with heavily coiled tails, etc.), minimal or no forward motility, and gradually reduced sperm counts after 5 weeks of triptonide treatment (Supplementary Movies 5 and 6). After a period of 3 months for drug "washout", these monkeys were retested using the same protocol, and the same results were obtained, i.e., single daily oral intake of triptonide (0.1 mg/kg BW) for 5 weeks caused OAT in adult male cynomolgus monkeys. Hence, the dose of 0.1 mg/kg BW was used for subsequent testing of short- and long-term male contraceptive efficacy of triptonide, as well as fertility reversibility.

In the short-term (8 weeks) POC efficacy testing, while vehicle-treated control monkeys displayed normal sperm counts, morphology, and motility (Fig. 2a–d), all of the seven adult male monkeys treated with triptonide showed deformed sperm (>95% deformation rate; Fig. 2a, b) with severely compromised forward motility (Fig. 2c; Supplementary Movies 7 and 8), and progressively reduced sperm counts (Fig. 2d). It is noteworthy that although the sperm counts in triptonide-treated male monkeys appeared to be reduced with time, the differences between treated and control groups did not reach statistical significance, probably due to great variations among samples collected at different timepoints and the limited number of monkeys analyzed. Consistently, testicular biopsies revealed that elongating and elongated spermatids were largely absent, while other spermatogenic cells appeared to be normal in the seminiferous epithelium of treated monkey testes (Fig. 2e). As control, the testes from vehicle-treated monkeys showed robust spermatogenesis, with all types of spermatogenic cell present in the seminiferous epithelium (Fig. 2e). No significant decrease in testicular volume was observed between control and triptonide-treated groups (Supplementary Fig. 5). During the 8-week long treatment, weekly blood biochemical analyses revealed no major changes in hormonal (LH and testosterone) levels (Supplementary Fig. 6), blood chemistry (Supplementary Fig. 7), liver (Supplementary Fig. 8), or kidney (Supplementary Fig. 9) functions, suggesting that oral intake of triptonide at 0.1 mg/kg BW for 8 weeks causes male infertility without systemic side effects in adult male cynomolgus monkeys. We also continuously measured oxygen saturation for the first 7 weeks, and the readings ranged between 93–98%, and no differences were observed between treated and control groups (Supplementary Fig. 10).

In the long-term efficacy testing, four male monkeys were continuously treated with triptonide (at a daily oral dose of 0.1 mg/kg BW) for up to 126 weeks (~2.4 years), and no major health issues were observed except that all displayed OAT (Fig. 2f–h). On weeks 8 and 126, each of the control and treated males was paired with an adult female for 1 week to observe mating behavior, and the mating frequency appeared to be similar between the treated and vehicle-treated control groups (Fig. 2i and Supplementary Movie 9). To test fertility, two males from either control or treated group were paired with two fertility-proven females (one male with one female) between weeks 8 and 126. The two females paired with the two triptonide-treated males never became pregnant, whereas both of the females housed individually with the two control males did become pregnant. Of the two females impregnated by the two control males, one experienced a spontaneous miscarriage at ~3 months of gestation, and the other gave birth to a healthy male baby monkey at full term (~5.5 months) (Fig. 2j). These data suggest that the oral intake of triptonide at a daily dose of 0.1 mg/kg BW can cause male infertility due to OAT within 8 weeks, and that the effects can be potentially maintained indefinitely with oral administration of the same daily oral dose in adult male cynomolgus monkeys.

Male infertility induced by triptonide is fully reversible in both mice and cynomolgus monkeys. After 4 weeks of triptonide treatment with single daily oral doses of 0.8 mg/kg BW, all of the treated male mice displayed deformed sperm lacking forward motility with close to 100% penetrance. We then ceased triptonide treatment and added two to three adult fertility-proven female mice to each of four cages, where the treated male mice were individually housed (one treated male per cage). The first litter of pups were born within 40–45 days in each cage after cessation of triptonide treatment (Fig. 3a), suggesting that conception occurred between days 20 and 25 after cessation of triptonide treatment because the murine gestation length is ~20 days. Similarly, male fertility recovered within ~20–25 days following cessation of long-term (3 months) treatment of triptonide in male mice (Fig. 3a). Consistently, sperm morphology and motility returned to normal within 3 weeks after cessation of either short- (4 weeks) or long-term (3 months) triptonide treatment (Supplementary Movies 10 and 11). All pups sired by these fertility-recovered male mice were indistinguishable from those sired by control male mice, and both litter size and litter interval were comparable between control and treated males (Fig. 3b).

In POC efficacy testing using cynomolgus monkeys, four adult male monkeys that had received triptonide treatment for 10 weeks

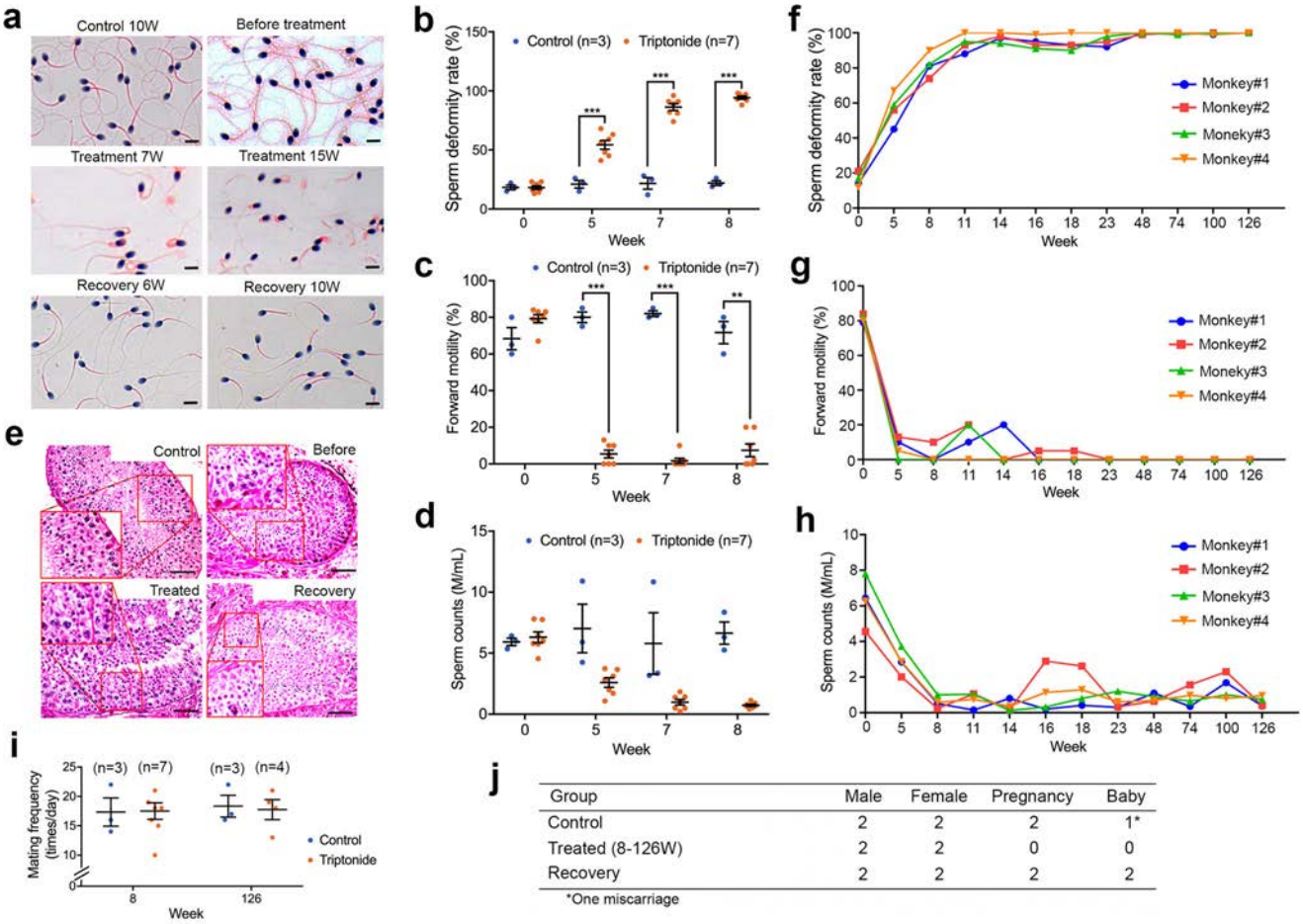

Fig. 2 Proof-of-concept efficacy testing of male contraceptive effects of triptonide using cynomolgus monkeys. a Representative images showing morphology of sperm from cynomolgus monkeys that received vehicle for 10 weeks (control), before and after triptonide treatment (single daily oral dose of 0.1 mg/kg BW for 7 and 15 weeks), or during recovery (6 and 10 weeks after 8 weeks of triptonide treatment). Scale bars = 5 μm. **b**–**d** Effects of short-term (8 weeks) triptonide treatment (single daily oral doses at 0.1 mg/kg BW) on the sperm morphology (**b**), sperm forward motility (**c**), and sperm counts (**d**) in adult male cynomolgus monkeys. Individual data points and mean (measure of center) ± SEM (error bars) are shown. $^{**}p < 0.01$; $^{***}p < 0.001$, as determined by two-way ANOVA with control ($n = 3$) compared to treated ($n = 7$) groups. **e** Representative testicular histology from monkeys that received vehicle (control), before and after triptonide treatment (single daily oral dose of 0.1 mg/kg BW for 8 weeks), or recovered from triptonide treatment (6 weeks after cessation of triptonide treatment). Insets represent digitally amplified, framed areas. Scale bars = 20 μm. **f**–**h** Effects of long-term (126 weeks) triptonide treatment (single daily oral doses at 0.1 mg/kg BW) on sperm morphology (**f**), sperm forward motility (**g**), and sperm counts (**h**) in 4 adult cynomolgus male monkeys. **i** Mating frequency of adult male monkeys that received either vehicle (control) or short-term (8 weeks) and long-term (126 weeks) triptonide treatment (single daily oral dose at 0.1 mg/kg BW). Individual data points and mean (measure of center) ± SEM (error bars) are shown. Sample sizes are marked in brackets. **j** Fertility performance of adult male monkeys that received vehicle (control) or triptonide (8–126 weeks), and those that recovered from 8 weeks of triptonide treatment (single daily oral dose at 0.1 mg/kg BW).

were transitioned to vehicle-only treatments between weeks 11 and 23, and their semen and blood samples were collected weekly to monitor the recovery process. Semen parameters among the recovery group reached control levels within 6 weeks after treatment cessation (Fig. 3c–e, and Supplementary Movies 12 and 13). Consistently, the monkeys recovered from triptonide treatment showed normal testicular histology (Fig. 2e) and testicular volume (Supplementary Fig. 5). During the 12-week long recovery period, weekly blood biochemical analyses revealed no pathological changes in hormonal (LH and testosterone) levels (Supplementary Fig. 6), blood cell counts (Supplementary Fig. 11), liver (Supplementary Fig. 12), or kidney (Supplementary Fig. 13) functions. The fertility-recovered males showed normal mating frequencies (Fig. 3f). Two of the four fertility-recovered male monkeys were individually paired with two fertility-proven adult females (one male with one female) for 6 months, and each of the female monkeys gave birth to a healthy full-term baby (Figs. 2j and 3g). These results suggest that triptonide-induced male infertility is effective and reversible in primates.

EC_{50} analyses suggest that triptonide is a potent and safe male contraceptive agent. To further evaluate the potency and safety of triptonide as a male contraceptive agent, we measured the 50% effective concentration (EC_{50}) of triptonide in inducing sperm motility loss and male infertility in adult C57BL/6J male mice. Based on the POC efficacy testing results (Fig. 1), adult C57BL/6J male mice of 8–12 weeks of age were treated with triptonide at 6 different doses (0, 0.1, 0.125, 0.2, 0.4, and 0.8 mg/kg BW, p.o. daily) for 4 weeks. At the end of week 4, sperm motility and morphology, as well as fertility were analyzed. By plotting sperm motility against each dose tested, values of the EC_{50} for inhibiting total and forward motility were determined to be 0.11 and 0.10 mg/kg BW, respectively (Fig. 4a). The most meaningful EC_{50}

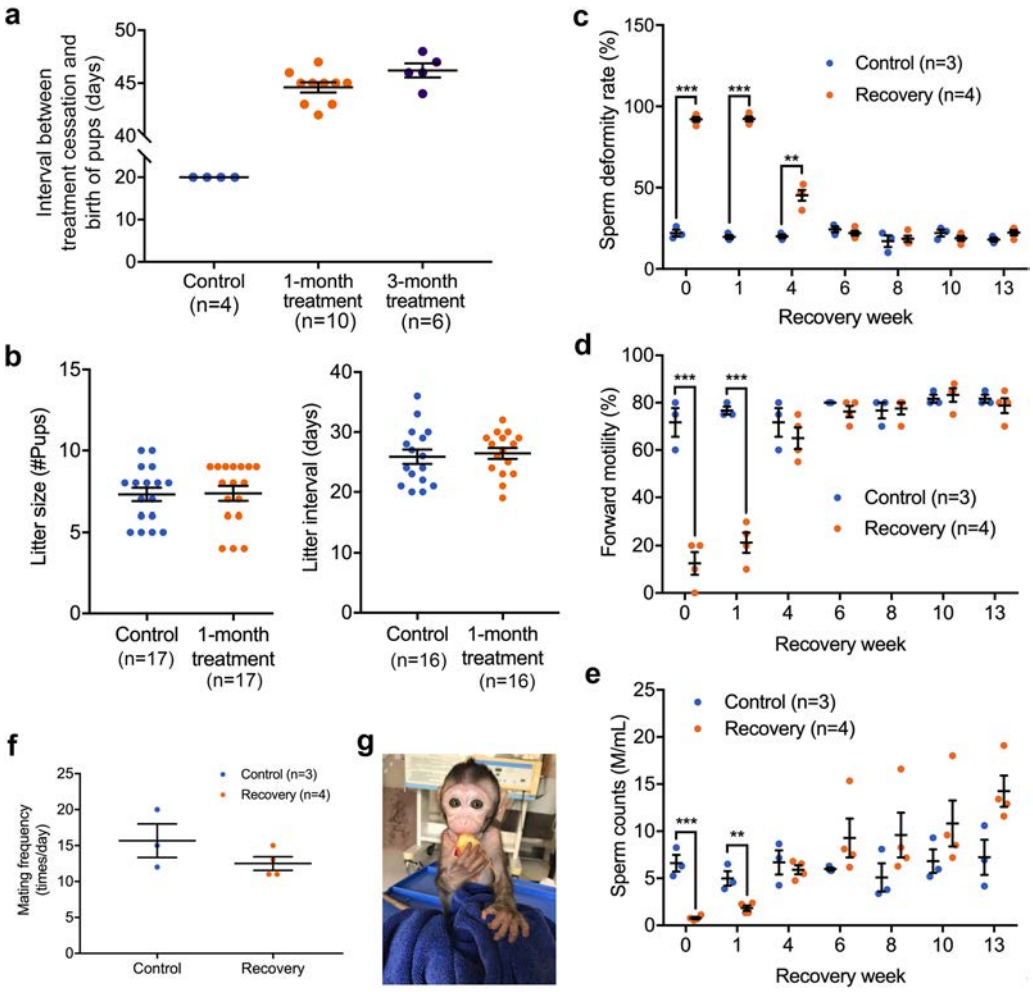

Fig. 3 Reversibility of triptonide-induced male infertility in adult mice and cynomolgus monkeys. a Male mice treated with triptonide (single daily oral doses at 0.8 mg/kg BW) for 4 weeks regained their fertility between days 20 and 25 after cessation of the treatment, as demonstrated by the birth of pups by females mated with previously treated males (single daily oral doses of 0.8 mg/kg BW for 4 weeks). Individual data points and mean (measure of center) ± SEM (error bars) are shown. Sample sizes are marked in brackets. **b** Litter size and interval of fertility-proven females mated with control male mice or those recovered from 1-month triptonide treatment (single daily oral dose at 0.8 mg/kg BW). Individual data points and mean (measure of center) ± SEM (error bars) are shown. Sample sizes are marked in brackets. No statistical significance between the control and treated groups based on the Kolmogorov–Smirnov *t* test. **c**–**e** Recovery of sperm morphology (**c**), sperm forward motility (**d**), and sperm counts (**e**) in adult male cynomolgus monkeys after 8 weeks of triptonide treatment (a single daily oral dose at 0.1 mg/kg BW). Individual data points and mean (measure of center) ± SEM (error bars) are shown. $^{**}p < 0.05$; $^{***}p < 0.01$, two-way ANOVA with the recovery group ($n = 4$) compared with the control group ($n = 3$). The exact *p* values can be found in the Source data file. **f** Mating frequency of adult male monkeys that recovered for 8 weeks from triptonide treatment (single daily oral dose at 0.1 mg/kg BW for 8 weeks). Individual data points and mean (measure of center) ± SEM (error bars) are shown. Sample sizes are marked in brackets. **g** A male baby monkey fathered by an adult male monkey recovered from 8 weeks of triptonide treatment (a single daily oral dose at 0.1 mg/kg BW).

value should be based on the male fertility. To this end, 14 adult C57BL/6J male mice of 8–12 weeks of age were treated with triptonide at five different doses (0, 0.1, 0.2, 0.4, and 0.8 mg/kg BW, p.o. daily) for 4 weeks. After 4 weeks of triptonide treatment, each male was mated with two to three adult fertility-proven female mice in three independent experiments, and pregnancy rates were calculated based on percentage of pregnancies among all of the plugged females (Supplementary Table 3). The EC_{50} of triptonide in causing male infertility was determined to be at 0.09 mg/kg BW (Fig. 4b). The LD_{50} of triptonide (p.o.) was previously shown to be 300 mg/kg BW in mice, 980 mg/kg BW in rats, and 3200 mg/kg BW in rabbits (Material Safety Data Sheet from the Clearsynth Labs Pvt. Ltd; Patent International Publication#: WO/2016/205539; International Application #: OCT/US2016/037900). Thus, the EC_{50} (~0.1 mg/kg BW) of triptonide is ~1/8 of the minimal effective dose, and ~1/3000 of the LD_{50} in mice, highlighting the excellent potency and safety of triptonide as an oral male contraceptive agent.

Triptonide does not cause DNA double-strand breaks. A previous report noted that triptonide may possess DNA alkylating activity due to its epoxide structure[25]. If triptonide alkylates DNA, it would cause DNA double-strand breaks (DSBs), which can be marked by γH2AX (the phosphorylation of the histone H2AX on serine 139)[26], a well-known indicator for DNA DSBs[27,28]. To this end, we performed immunohistochemistry and western blots to detect γH2AX levels in triptonide-treated mouse testes (Supplementary Fig. 14). To investigate whether triptonide causes DNA DSBs in somatic tissues, we also examined levels of γH2AX in the liver of triptonide-treated and control males (Supplementary Fig. 14). No significant changes in γH2AX levels were observed in either the testis or liver, suggesting that

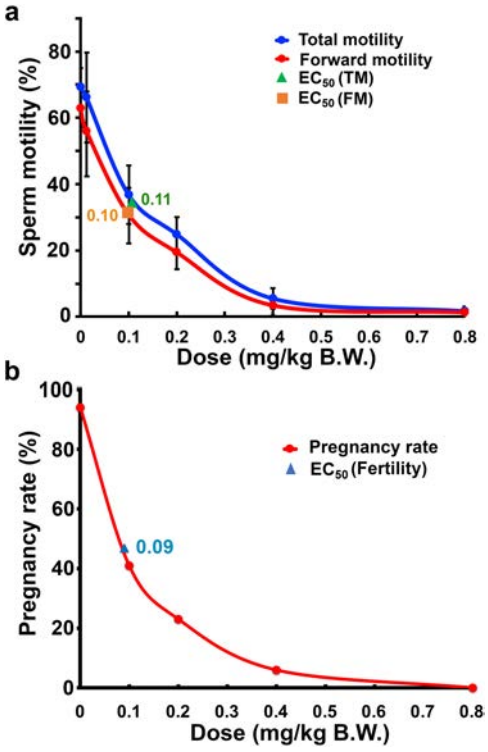

Fig. 4 The EC_{50} of triptonide in adult male C57BL/6J mice. a The EC_{50} of triptonide in inhibiting sperm total (TM) and forward (FM) motility in adult male mice. Data points represent mean ± SD; $n = 5$ for doses 0, 0.4, and 0.8 mg/kg BW, and $n = 9$ for doses 0.1, 0.125, and 0.2 mg/kg BW. **b** The EC_{50} of triptonide in inducing male infertility in adult mice. Data points represent pregnancy rate, which reflects percentage of pregnancy among all of the plugged females by the males treated with five doses of triptonide (0, 0.1, 0.2, 0.4, and 0.8 mg/kg BW) for 4 weeks. $n = 14$ for each of the five doses tested.

triptonide does not cause DNA DSBs. Failed repair of DNA DSBs is known to cause male germ cell depletion through apoptosis, and massive apoptosis would cause disrupted spermatogenesis characterized by multinucleated cells and sloughing of the damaged spermatogenic cells into the lumen of the seminiferous tubules[29–31]. None of these effects was observed in triptonide-treated testes, which are, in fact, largely indistinguishable from control testes (Fig. 1a). Similarly, no compromised liver functions were detected in the liver panel of blood tests (Supplementary Figs. 8 and 12). Moreover, these findings are also consistent with the fact that neither tumorigenesis nor any other deleterious side effects were observed in any of the triptonide-treated mice or monkeys that received long-term triptonide treatment (6 months for mice and >2.4 years for cynomolgus monkeys).

Identification of junction plakoglobin/gamma-catenin as the candidate target of triptonide. To identify the drug target that mediates the effect of triptonide treatment, we adopted the drug affinity responsive target stability (DARTS) assay, which represents an unbiased approach for the identification of drug targets[32,33]. DARTS is based upon the fact that when a compound binds specifically to its protein target, the presence of the molecule protects a part of the target protein from being hydrolyzed by proteases (Fig. 5a)[32,33]. We first performed in vitro DARTS experiments, where testis lysates were incubated with triptonide or vehicle (0.01% DMSO) followed by digestion, with either pronase or thermolysin at different concentrations for variable lengths of incubation. But we observed no protected protein bands after polyacrylamide gel electrophoresis (PAGE). We then investigated an in vivo variation of DARTS by extracting protein from testis lysates from mice treated with 0.8 mg/kg BW triptonide or vehicle (control) for 4 weeks. The precipitated protein was digested with trypsin for various lengths of time followed by PAGE. On the PAGE gels, one band of ~18 kDa was consistently seen in the treated, but not in the control, lysates in two independent experiments (Fig. 5b). Mass spectrometry (MS) of the band consistently identified four proteins, including keratin 5, junction plakoglobin (JUP; also called gamma-catenin), tubulin β-4B, and polyubiquitin C. Given that keratins are the most common contaminants in MS-based proteomic analyses, other proteins remained the more probable candidate targets.

We then attempted a GlycoLink resin microcolumn-based affinity purification method (Fig. 5c). The columns are intended for attachment of sugar molecules after the *cis* diols are oxidized to produce aldehydes, but they also react with ketones via a Schiff base reaction. The attachment reaction was achieved using an acidic buffer or an optional 0.2 M carbonate/bicarbonate basic (pH = 9.4) buffer. Acidic conditions could facilitate attachment of triptonide to the beads via the ketone or possibly the lactone, leaving unhindered epoxide groups, whereas basic conditions may promote binding via one of the epoxide groups. We, therefore, used both acidic and basic buffers to promote attachment of triptonide to the beads. A ~60 kDa band was detected in both triptonide and control conditions from both acid-conjugated and base-conjugated beads (Fig. 5d), but the bands were much lighter in controls than in triptonide-bound beads (Fig. 5d), suggesting that the binding might be specific. The bands were cut out and subjected to MS analyses which identified ~30 proteins, among which three proteins were also identified by the DARTS assays, including keratin 5, tubulin β-4B, and junction plakoglobin/gamma-catenin. To further validate these results, we attached triptonide to GlycoLink resin microcolumns using acidic buffer. Control resin was prepared with no attached triptonide. Total testicular proteins were then incubated with the triptonide-attached and control resin. After washing, the eluates were subjected to western blot analyses using anti-keratin 5 and anti-junction plakoglobin antibodies. Junction plakoglobin/gamma-catenin was detected (Fig. 5e), whereas keratin 5 appeared to be negative (Fig. 5f), suggesting that the binding between triptonide and junction plakoglobin/gamma-catenin is specific.

Given that triptonide-treated sperm phenocopy *Spem1*-null sperm[5], characterized by deformed sperm (head-bent-back) with no or minimal motility, we also adopted a candidate approach to explore whether SPEM1 interacts with any of the proteins identified to bind triptonide. Protein structural analyses predict that the N-terminus of SPEM1 acts as a domain for protein–protein interactions. Thus, the N-terminal portion of SPEM1 (~28 a.a.) was synthesized and purified. A biotin was added onto the C-terminus of this peptide. The biotin-labeled N-terminal 28 a.a. peptides of SPEM1 were attached to streptavidin beads, which were then used to probe testicular lysates prepared from an 8-week-old male mouse (Fig. 5g). Using this method, five proteins were identified to bind only to the N-terminus peptides, but not the control beads, including junction plakoglobin/gamma-catenin, heat shock-related 70 kDa protein 2 (HSP70-2), L-lactate dehydrogenase C chain (LCDHC), Y-box-binding protein 2, and retinal dehydrogenase 1. Interestingly, Y-box protein 2, LCDHC, and retinal dehydrogenase 1 were also identified to bind triptonide in the GlycoLink bead-based affinity purification assays (Fig. 5h). Taken together, these observations indicate that the SPEM1 N-terminus appears to interact with a number of proteins, including junction plakoglobin/gamma-catenin. Given that junction plakoglobin/gamma-catenin was

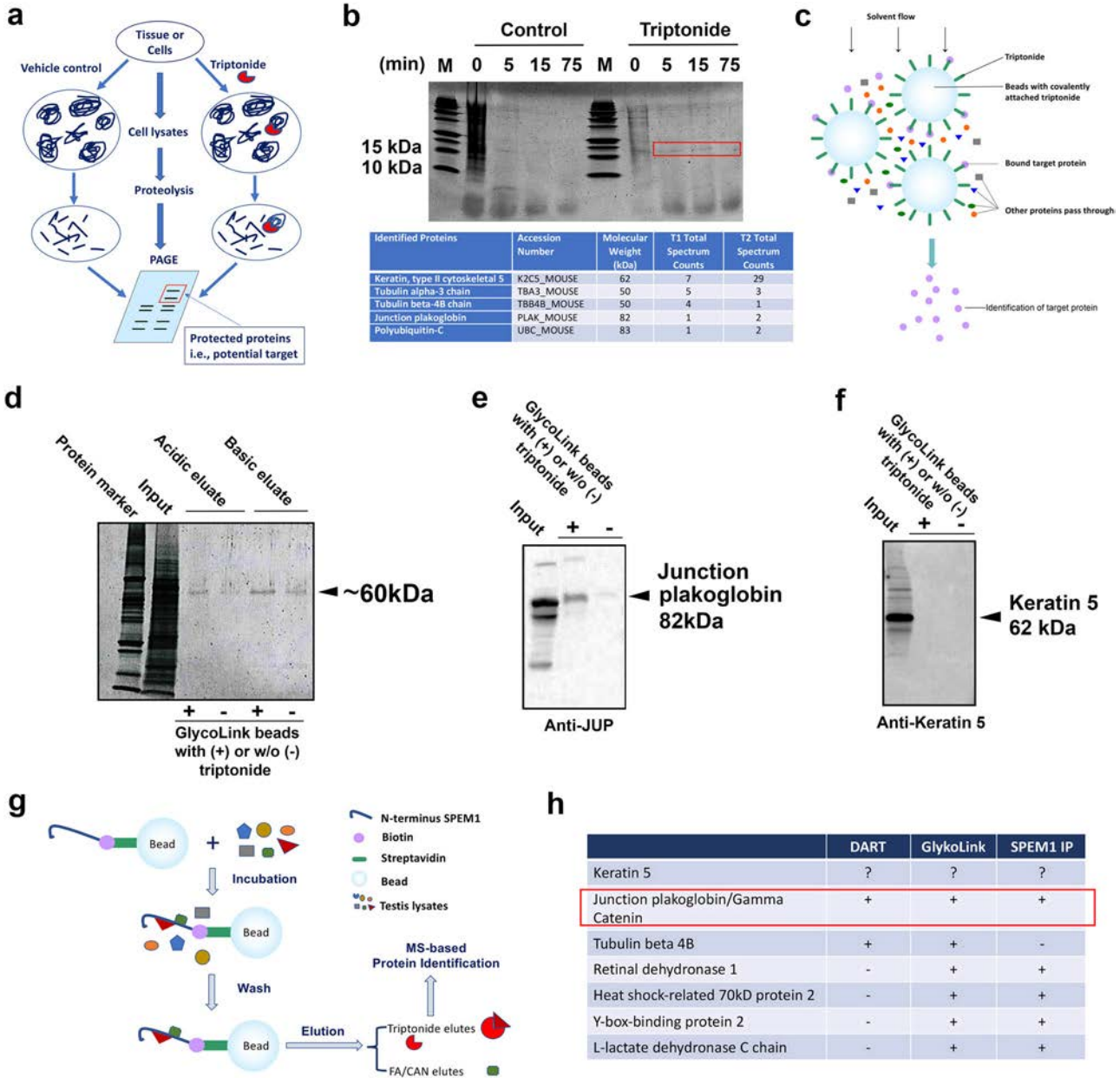

Identified Proteins	Accession Number	Molecular Weight (kDa)	T1 Total Spectrum Counts	T2 Total Spectrum Counts
Keratin, type II cytoskeletal 5	K2C5_MOUSE	62	7	29
Tubulin alpha-3 chain	TBA3_MOUSE	50	5	3
Tubulin beta-4B chain	TBB4B_MOUSE	50	4	1
Junction plakoglobin	PLAK_MOUSE	82	1	2
Polyubiquitin-C	UBC_MOUSE	83	1	2

	DART	GlykoLink	SPEM1 IP
Keratin 5	?	?	?
Junction plakoglobin/Gamma Catenin	+	+	+
Tubulin beta 4B	+	+	-
Retinal dehydronase 1	-	+	+
Heat shock-related 70kD protein 2	-	+	+
Y-box-binding protein 2	-	+	+
L-lactate dehydronase C chain	-	+	+

Fig. 5 Identification of potential target(s) of triptonide in murine testes. a Schematics showing a modified drug affinity responsive target stability (DARTS) assay used in this study to identify proteins interacting with triptonide. Protein lysates from total testes of adult male mice treated with triptonide (single daily oral dose at 0.8 mg/kg BW for 4 weeks) were subjected to digestion using different proteinases for various durations. **b** A representative gel image (upper panel) showing a specific band of ~18 kDa (red frame) unique to the triptonide-treated testes. The bands were cut out for mass spectrometry-based protein identification, and the top five hits were listed in the table (lower panel). **c** Schematics showing the GlycoLink beads-based affinity purification method used in this study. **d** A representative gel image showing a specific band of ~60 kDa eluted from triptonide-conjugated beads under acidic and basic conditions. The "input" lane shows the amount of testis lysates used in the assays. The bands were subjected to MS-based protein identification and some of the proteins identified are listed in **h**. **e** A representative western blot showing detection of junction plakoglobin/gamma-catenin in the eluates from beads conjugated with or without triptonide, as all we as the input of total testicular lysates used in the assays. **f** A representative western blot showing detection of keratin 5 in the eluates from beads conjugated with or without triptonide, as all we as the input of total testicular lysates used in the assays. **g** Schematics showing the immunoprecipitation-based identification of proteins interreacting with the N-terminus of SPEM1. The biotin–streptavidin system was utilized to bind the N-terminus of SPEM1 to magnetic beads. The major proteins identified using this method are listed in **h**. **h** A summary of major proteins identified by the three methods used in this study. Junction plakoglobin/gamma-catenin appears to be the most likely drug target (red frame).

also detected to bind triptonide in both DARTS and GlycoLink bead-based affinity purification assays, these data strongly suggest that junction plakoglobin/gamma-catenin is the most likely functional target of triptonide. Thus, triptonide binding of junction plakoglobin/gamma-catenin may interfere with its interactions with SPEM1 (Fig. 6), leading to defects in cytoplasmic removal and consequently bending of sperm heads, a phenotype resembling *Spem1*-null sperm[5].

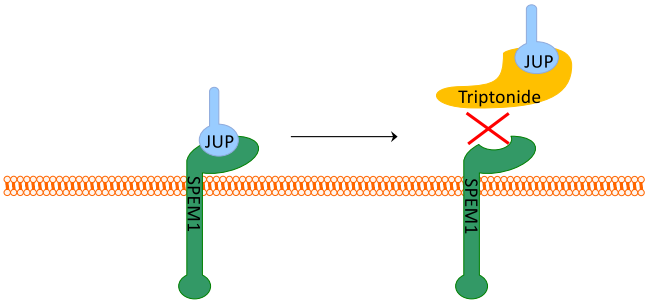

Fig. 6 The proposed action of triptonide in inducing sperm deformation and male infertility. Physiologically, SPEM1 interacts with junction plakoglobin through its N-terminus. However, triptonide binds junction plakoglobin with higher affinity, and this binding disrupts normal interactions between junction plakoglobin with SPEM1, causing a phenotype similar to that of *Spem1* knockout, i.e., sperm deformation and male infertility.

Discussion

The standard drug development process often starts with the identification of a drug target using either in vivo (e.g., genetic models) or in vitro (e.g., cell culture-based screening) assays, and proceeds with high-throughput screening of millions of compounds to identify those that interact with the targets, followed by animal testing for efficacy and safety. However, it must be emphasized that serendipity also plays a critical role in drug discovery[34–36]. For example, ~20% of the pharmaceuticals in clinical use today are chemical derivatives of drugs discovered serendipitously[34]. The so-called "antisperm" effects of the Chinese herb (*T. wilfordii Hook F*, commonly known as lei gong teng or thunder god vine) was serendipitously discovered because physicians noticed that some of the men who took this Chinese herbal medicine for an extended period (>3 months) displayed compromised fertility[12]. Although this observation triggered a wave of intensive research on the potential use of this herb or compounds isolated form this herb as male contraceptive agents, the enthusiasm soon dwindled because several initial studies found that either the crude herbal extracts or several of the most abundant compounds purified from this herb could indeed cause male infertility, but all exerted severe toxic side effects and infertility could hardly be reversed after the treatment was stopped[12–18,20–24].

Based on our genetic study on murine spermiogenesis using gene KO technologies, we put forward the idea for developing nonhormonal male contraceptives through disrupting the last several steps (i.e., post elongation) of spermiogenesis. The idea was based upon the fact that genetic disruptions of mid- or late spermiogenesis (from elongation onward) rarely cause apoptosis or massive germ cell depletion within the seminiferous epithelium, although sperm are consistently deformed and/or display no or very limited motility[4]. For example, *Spem1* encodes a protein exclusively expressed in elongating and elongated spermatids, and ablation of *Spem1* causes male infertility due to sperm deformation characterized by the head-bent-back by 180 degrees, and the bent head and neck surrounded by residual cytoplasm[5]. SPEM1 is mainly localized on the manchette, which is a microtubular apparatus unique to elongating and elongated spermatids, and is believed to function to facilitate nucleocytoplasmic transport[5]. In the absence of SPEM1, the coordinated nuclear and cytoplasmic elongation processes become unsynchronized with nuclear elongation continuing, while cytoplasmic elongation ceasing, leading to head bending followed by the tail wrapping around the bent head inside the residual cytoplasm[4]. In the absence of depletion of defective late spermatids within the seminiferous epithelium, testicular histology of *Spem1* KO mice is indistinguishable from that of wild-type controls except that all of the sperm are deformed and lack forward motility. Based on the phenotype of *Spem1* KO male mice, it is conceivable that if a compound directly or indirectly targets SPEM1, a phenotype similar to *Spem1* KO sperm would be expected. Indeed, our data suggest that triptonide appears to be such a compound. Triptonide displays excellent bioavailability allowing for oral administration. It induces total infertility in weeks (3–4 weeks in mice and 5–6 weeks in monkeys) and maintains the infertile state for months and years with the same dosage. Male fertility can be regained ~4–6 weeks after cessation of triptonide treatment. More importantly, no discernable deleterious side effects, e.g., organ toxicity, have ever been observed in our efficacy testing on either mice or monkeys. The discovery of triptonide as a promising male contraceptive agent serves as a testimony to the power of our strategy in developing male contraceptives.

Oral intake of triptonide requires 3–4 and 5–6 weeks to achieve full male infertility in mice and monkeys, respectively. The latent effect implies that triptonide acts on a specific step during spermiogenesis. Indeed, earlier studies have estimated that the duration of spermatogenic cycles is ~35 days in mice and ~42 days in cynomolgus monkeys[37,38]. Therefore, the one-week difference in the induction of full male infertility effects between mice and monkeys likely reflects the difference in the duration of spermatogenic cycle between these two species. It is noteworthy that the decrease in sperm counts induced by triptonide was more significant in cynomolgus monkeys than in mice, which may reflect differences in spermatogenesis between these two species. Indeed, the testicular histology is indistinguishable between triptonide-treated and control mice, whereas triptonide-treated monkey testes lacked elongating and elongated spermatids, suggesting that while triptonide may target the same protein within the testes in both species, the biological consequences may differ. Our drug target analyses strongly suggest that triptonide most likely binds junction plakoglobin/gamma-catenin and thus, disrupts its interactions with SPEM1, leading to a phenotype similar to that observed in *Spem1* KO testes. Phylogenetic analyses have shown that mouse and monkey SPEM1 proteins share ~69% amino acid sequence similarity[5], suggesting SPEM1 function has evolved from mice to monkeys, and this may explain the phenotypic differences observed between triptonide-treated mice and cynomolgus monkeys. Of interest, levels of major hormones, including FSH, LH, and testosterone, in treated mice or monkeys did not vary significantly from those of controls, suggesting that triptonide treatment does not adversely affect libido or other endocrine functions. More importantly, once triptonide treatment is stopped, infertile male mice and monkeys regain their fertility in ~3–4 and ~5–6 weeks, respectively. Thus, the recovery timeline is similar to that required to initially induce infertility, further supporting the notion that triptonide acts on one or more specific steps during spermiogenesis.

The biggest concern associated with the development of any contraceptives is the potential deleterious side effects. This was particularly true for our study because several of the major compounds isolated from *T. wilfordii* have been shown to exert significant toxic effects[12–18,20–24]. For treatment of life-threatening diseases, such as cancer, a certain level of deleterious side effects can be viewed as an acceptable consequence if unavoidable. However, for the development of a male contraceptive, even minor side effects may be sufficient to discourage its use by healthy men who are active both reproductively and sexually. Therefore, our finding that neither short- (4 weeks for mice and 8–24 weeks for monkeys) nor long- (3 or 6 months for mice and up to 2.4 years for monkeys) term oral intake of triptonide causes discernable toxic side effects in either species

represents a major asset in support of the potential advancement of this compound to the investigational new drug status and to the subsequent clinical trials.

A previous report suggested that triptonide may have DNA alkylating activity due to its epoxide structure[25]. However, for epoxides to alkylate DNA, an aromatic ring is required to intercalate between base pairs in the double helix so that the epoxide ring can react with a nitrogen atom in a DNA base[39]. Triptolide is structurally very similar to triptonide, and none of the multiple anticancer mechanisms of triptolide involves alkylation of DNA[40] given that triptonide is too large to intercalate between DNA base pairs[41]. The lack of alkylating activity of triptonide is further supported by the following facts: (1) this herbal medicine has been used by millions of people in China for many decades to treat a wide variety of dermatological conditions with no reports of increased tumorigenesis among long-term users. (2) None of the mice or monkeys that underwent long-term (3–6 months for mice and up to 2.4 years for monkeys) oral triptonide treatment in our POC efficacy tests developed cancer. (3) DNA alkylating activity tends to cause DNA DSBs, but no increase in gamma-H2AX levels was detected in triptonide-treated testes.

Another line of evidence supporting the safety of triptonide comes from the fact that its EC_{50} associated with induction of infertility and sperm motility loss is ~0.1 mg/kg BW, which is ~1/8 of the minimal effective dose (0.8 mg/kg) and ~1/3000 of LD_{50} (300 mg/kg BW) in mice. In other words, triptonide is very potent in suppressing male fertility because even 1/8 of the normal dose will generate maximum efficiacy in half of the mice treated. Thus, the effective dose of triptonide treatment required to achieve male contraception is far below the level that would induce any sort of deleterious side effects.

Given that triptolide is the most abundant compound in the Chinese herb *T. wilfordii*, triptonide purified from this herb can sometimes be contaminated with trace amounts of triptolide or other abundant compounds, which, unlike triptonide, have been shown to be highly toxic[42]. Therefore, trace contaminants would cause side effects, which are, in fact, not due to triptonide. Indeed, one of the batches of triptonide we purchased included a stated purity of 96%, but our testing on mice revealed multiple side effects similar to those seen in mice treated with triptolide. Therefore, it is critical to use highly pure triptonide for POC efficacy testing. We sent the two batches of purified triptonide and one batch of chemically synthesized triptonide used in this study to an independent commercial lab for purity tests, using both NMR and elemental analyses (Supplementary Fig. 15), and the results showed that all three were nearly 100% pure. Taking into consideration the stated margin of error of these testing systems (~0.4%), we determined that the purity of triptonide used in our study was at least 99.6%. We used the synthetic triptonide and performed POC efficacy testing on mice, and the same reversible male contraceptive effects were obtained (Supplementary Fig. 16). These data suggest that the male contraceptive effects of triptonide reported here are indeed caused by triptonide, rather than the potential trace contaminants in triptonide used.

It is noteworthy that the main focus of the present study was POC efficacy testing, and a lack of discernible side effects was based upon the observation of behavior (for both mice and monkeys), examination of gross morphology, and histology of vital organs (for mice only), as well as hematological and serum biochemical analyses (for monkeys only). While the data reported here suggest triptonide might be a promising contraceptive drug candidate for men, its safety needs to be further evaluated through comprehensive pharmacokinetics and toxicology studies in the future. An intriguing question is why triptonide only exerts effects on late spermiogenesis without affecting functions of other major organs? One explanation is that it may target a protein that is exclusively expressed in elongating and elongated spermatids. However, our drug target identification assays point to junction plakoglobin/gamma-catenin as its most likely target, which is known to be expressed ubiquitously[43,44]. However, SPEM1, which is an interacting partner of junction plakoglobin/gamma-catenin, is indeed exclusively expressed in elongating and elongated spermatids during spermiogenesis[5]. Therefore, it is highly likely that proper function of SPEM1 requires normal interactions with junction plakoglobin/gamma-catenin, and SEPM1 function is abolished once interactions between SPEM1 and junction plakoglobin/gamma-catenin are disrupted in the presence of triptonide. Although interactions between junction plakoglobin/gamma-catenin and SPEM1 may explain the testis-specific effect of triptonide, such a mechanism needs further validation using genetic models and in vitro assays in the future. Furthermore, it is critical to understand how triptonide is metabolized once it gets into the bloodstream and major organs, including the testis. To this end, a thorough pharmacokinetics study is warranted. To establish triptonide as an ultimate drug, scalable, efficient, and economic chemical synthesis of triptonide is also critical. If SPEM1 is proven to be the true target of triptonide, other small compounds that can specifically interact with SPEM1 may exert a similar male contraceptive effect to triptonide with even greater specificity and efficacy.

In summary, we report the discovery of triptonide as a potent and safe nonhormonal male contraceptive agent in mice and nonhuman primates. The success also validates a more general idea for developing male contraceptives. i.e., disabling, rather than "killing"/depleting, all sperm by targeting proteins or other gene products specific to the elongation steps during spermiogenesis. Finally, we note that serendipitous drug discovery should continue to be encouraged and supported as an integral part of the ongoing efforts to develop nonhormonal male contraceptives.

Methods

Animal use and care. Male and female adult (2–3 months) mice of C57BL/6J and CD-1 strains were used. Mice were housed in a specific pathogen-free and temperature- and humidity-controlled facility under a light–dark cycle (10 h light and 14 h dark) with food and water ad libitum at the University of Nevada, Reno. Animal use protocol was approved by Institutional Animal Care and Use Committee of the University of Nevada, Reno, and is in accordance with the "Guide for the Care and Use of Experimental Animals" established by National Institutes of Health (1996, revised 2011). All cynomolgus monkeys used were housed at the Blooming Spring Biological Technology Development Co. LTD, in Guangzhou, China, which is fully accredited by the Association for the Assessment and Accreditations of Laboratory Animal Care International. The animal use protocol was approved by the Research Ethics Committee of the Blooming Spring Biological Technology Development Co. LTD. A total of 12 healthy male adult (9–13 years of age with body weight ranging between 4.96 and 11.80 kg) and 6 fertility-proven adult females (9–13 years of age with body weight ranging between 3.89 and 4.00 kg) cynomolgus monkeys were used in this study. The general information of the monkeys used in this study is summarized in Supplementary Table 4.

Chemicals. Triptonide ($C_{20}H_{22}O_6$, MW: 356.39 g/mol) was purchased from the Chengdu Biopurity Phytochemicals (purity > 98%, Lot#: 15033012 and 14081502) and MCE (MedChem Express; purity > 98%, Cas#: 38647-11-9. Lot#:13216). DMSO was purchased from Sigma-Aldrich. In addition to HPLC data provided by the company, the purity of triptonide used was independently validated using NMR elemental analyses in NuMega Resonance Labs, Inc. (San Diego, CA; Supplementary Fig. 15).

Proof-of-concept efficacy testing in mice. For POC efficacy testing on mice, a stock solution of triptonide was prepared at 4 mg/ml in DMSO. Each vial was wrapped with aluminum foil to block light and stored at −20 °C. For gavage feeding, 125 µl of triptonide working solution (5 µl stock solution was added into 120 µl of PBS) containing 20 µg triptonide were administered to a mouse of 25 g (0.8 mg/kg B.W) using a gavage feeding needle (20 G 1–1/2 in., Cadence Science, Japan). Other doses (0.1, 0.2, 0.4, and 1.6 mg/kg BW) were prepared accordingly. Control mice received vehicle (4% DMSO in PBS). After oral administration of triptonide or vehicle, the mice were observed every hour for the first 3 h, followed by daily monitoring thereafter.

In the initial pilot study to identify minimal effective dose and duration, five doses (0.1, 0.2, 0.4, 0.8, and 1.6 mg/kg BW) were tested using 18 mice per dose group. Three mice from each dose group were sacrificed weekly to examine sperm parameters and testicular histology for up to 6 weeks. In the subsequent official POC efficacy testing, 6–20 mice in each test group were treated with triptonide at one of the four doses (0.1, 0.2, 0.4, and 0.8 mg/kg BW) via single daily oral gavage. At the end of the fourth week, all triptonide-treated and control mice were sacrificed and caudal epididymal sperm parameters were measured using a computer-assisted sperm analysis (CASA) system (Sperm Analyzer Mouse Traxx, Hamilton-Thorne). In addition, blood samples were collected and allowed to clot at room temperature for 1.5 h. After disrupting clot adhesion to the tube wall, the blood samples were centrifuged at 2000 × *g* for 10 min at room temperature. Serum was collected into a polypropylene microcentrifuge tube and stored at −20 °C for hormonal measurements. Hormonal levels were measured at the Ligand Assay and Analysis Core, Center for Research in Reproduction, University of Virginia School of Medicine, Charlottesville, Virginia. The Mouse Pituitary Magnetic Bead Panel Multiplex Kit (Cat.# MPTMAG-49K; Lot#3141797; Millipore Corporation, Billerica, MA) was used to determine the levels of FHS and LH following the manufacturer's instructions. The reportable range the FSH/LH assays was between 0.48 and 300 ng/ml, and the intra-assay CV was between 0.4 and 2.9% for FSH, and 3 and 7.8% for LH. To measure intratesticular testosterone levels, testicular homogenates were prepared by homogenizing the testis in cold (4 °C) PBS (without detergent or EDTA) on ice for 60 s followed by centrifugation (2000 × *g* for 10 min at 4 °C) to remove cell debris. The supernatants were then collected into 1.5 ml Eppendorf tubes and stored at −80 °C. Both serum and testicular testosterone levels were assayed using the Testosterone Mouse & Rat ELISA Kit (Cat. #IB79106; Kit Lot# 28K088-2; Immuno-Biological Laboratories, Inc., Minneapolis, MN) following the manufacturer's instructions. The assay is a solid phase enzyme-linked immunosorbent assay based on the principle of competitive binding. The microwells coated with a monoclonal antibody against a unique antigenic site of testosterone were first incubated with the samples so that testosterone in the samples competes with testosterone-conjugated horseradish peroxidase. After washing to remove the unbound molecules, the solid phase was then incubated with the substrate and the colorimetric reaction was used to quantify the levels of testosterone in the samples. A standard curve was first constructed by plotting OD values against concentrations of the standards, and the concentration of unknown samples were determined using this standard curve. The reportable range of this assay was between 8.3 and 1600 ng/dl, and intra-assay CV was between 0.8 and 3.7%.

Histology of all major organs including heart, liver, spleen, lung, lung, brain, colon, small intestine, testis, and male reproductive tracts (epididymis, seminal vesicle, and prostate) was analyzed in-house. Testes were fixed in Bouin's fixatives and other organs were fixed in 10% neutral buffered formalin followed by embedding into paraffin. Sections were cut followed stained using hematoxylin and eosin for microscopic evaluation.

To test fertility, after 3–4 weeks of oral administrations of triptonide and vehicle control, two or three females were added to individual cages containing single triptonide-treated or control male mice. The female mice were examined every morning for the presence/absence of vaginal plugs. Once plugs were identified, the female mice were removed and after 7 days, they were transferred to a new cage, and the pregnancies and pups were observed and recorded.

Electron microscopy of mouse seminiferous tubules and sperm. Both scanning and transmission electron microscopic analyses were conducted as described[5]. Scanning electron microscopy was conducted using stages VII and VIII seminiferous tubules dissected from control and triptonide-treated testes, whereas TEM was performed on sperm collected from the cauda epididymis of control and triptonide-treated male mice.

Intracytoplasmic sperm injection. Mouse ICSI was performed as described[5]. Cauda epididymal sperm were collected from control and triptonide-treated male mice. Only sperm heads were injected into MII oocytes from donor female mice. To study developmental potential of the preimplantation embryos, the injected oocytes were cultured in vitro. For evaluation of full-term development, the 2-pronuclear embryos were transferred into the recipient females.

Proof-of-concept efficacy testing in cynomolgus monkeys. To identify minimal effective dose and duration, four cynomolgus monkeys were treated with triptonide at four doses (0.05, 0.1, 0.2, 0.8, and 5 mg/kg BW) daily. Based on the weight of each monkey, the total amount of triptonide equivalent to 40 days of oral treatment of 0.1 mg/kg BW was calculated and weighted for making the stock solution in 2 ml DMSO. The working solution was prepared by diluting the stock solution with 18 ml PBS followed by aliquoting into 40 vials (0.5 ml each) for storage at −20 °C. One vial was thawed each day and the triptonide working solution (0.5 ml) was added into the food (steamed bun, bread, apple, banana, etc.) before feeding. The technician observed the feeding to make sure the triptonide-containing food was completely eaten. By the end of each week, semen and blood samples were collected for analyses of sperm parameters and blood chemistry. The pilot test was stopped at week 9 because almost all sperm became deformed with minimal or no forward motility and sperm counts had been drastically reduced. One monkey that received 5 mg/kg BW triptonide daily p.o. displayed signs of side effects starting at week 4 and became worse thereafter; thus, the experiment was stopped at the end of week 5 and that monkey was not used in subsequent POC efficacy testing.

Based on the pilot test, the minimal effective dose was determined to be 0.1 mg/kg (BW). In the official POC efficacy testing, seven male monkeys were treated with single daily doses of triptonide (0.1 mg/kg BW) and three control male monkeys received vehicle. Since we already knew that significant effects on sperm production started at week 4, semen and blood samples were collected weekly starting from week 5. By the end of week 8, triptonide treatment was stopped in three of the seven monkeys, and the other four continued with triptonide treatment until week 126 (~2.4 years). For the monkeys undergoing long-term treatment, semen and blood samples were collected at 11, 14, 16, 18, 23, 48, 74, 100, and 126 weeks for semen and blood chemistry analyses.

To test fertility, two out of the three monkeys with treatment stopped at week 8 were individually housed with two fertility-proven adult female monkeys (one male and one female per cage) for up to 1 year. Both female monkeys became pregnant after 3–4 months and each delivered a full-term baby. Two out of the four male monkeys undergoing long-term treatment were also housed with two fertility-proven adult female monkeys (one male and one female per cage) between weeks 8 and 126. None of the two females became pregnant during the entire treatment. Two of the three controls were housed with two fertility-proven adult female monkeys (one male and one female per cage) between weeks 8 and 100. Both female monkeys became pregnant after 3–4 months, but one ended up with abortion for unknown reasons, but the other delivered a full-term baby.

For semen collection, a rectal probe electrical stimulation method was conducted as previously described[45] with minor modifications. Monkeys were anesthetized with ketamine hydrochloride (Lianyungang International Trade Co., Ltd., Lianyungang City, China) at a dose of 10 mg/kg BW through intramuscular injection. The monkeys were then held in a supine position on an operating table and penis was cleaned using absorbent cotton soaked with warmed saline. A lubricated probe was inserted into rectum for ~8–10 cm and positioned with both electrodes oriented in mid-ventral direction. A stimulator with nine-step voltage control (Lane Manufacturing Inc., USA) was used, and each electrical stimulation consisted of pulses of 4–6 s duration with 2–3 s rest in between. Stimulation started at step 1 for five repeats. If no painful response was observed, stimulation was continued with the voltage raised to next step. The stimulation was repeated and gradually intensified until ejaculation occurred. The ejaculates were collected into a tube and incubated in 37 °C water bath for 30 min before analyses. Semen samples were diluted using a sperm culture medium (K-SISM-20/50/10020, Cook Medical) to an appropriate concentration, and an aliquot of 10 µl was added to a pre-warmed (37 °C) Makler counting chamber and sperm counts, total and forward motility were analyzed manually by an experienced evaluator. For motility evaluation, at least 300 sperm were analyzed. For sperm morphology analyses, sperm smear was prepared. After air dry, the slides were fixed in 95% ethanol for 15 min at room temperature, followed by staining using SpermBlue fixative and SpermBlue stain[45].

To analyze testicular histology, testicular biopsy was performed under anesthesia (ketamine hydrochloride at 10 mg/kg BW i.m.) and sterile conditions. A small piece of testis (~3 mm × 3 mm × 3 mm) was surgically removed, and immediately fixed in Bouin's fixative. After dehydration, the samples were embedded into paraffin and sections of 4 µm were then stained using hematoxylin-eosin followed by microscopic evaluation.

Blood oxygen saturation levels were measured using a pulse oximeter (Yuwell, YX303, Yunyue Medical Equipment, Ltd, Jiangsu, China) by clamping the oximeter to the tail of the monkey. Blood assays included counts of the red blood cells, lymphocytes, mean corpuscular volume, and levels of prothrombin, hemoglobin, and glucose. The liver panel contained the following: albumin-globulin, albumin, alkaline phosphatase, alanine aminotransferase, aspartate aminotransferase, carbon dioxide, gamma-glutamyl transferase, and total protein. The kidney panel consisted of creatinine, urine albumin, and urea. All the assays were conducted in the Central Clinical Laboratory of the Hospital affiliated to the Institute of Family Panning of Guangdong Province (Guangzhou, China) using the reagents, equipment, and methodologies for human blood lab work. In brief, blood cell types and biochemistry were analyzed using a hematology analyzer (Sysmex XN-1000, Japan). FSH, LH, and T levels were measured using fluorescent immunoassays on an immunology analyzer (Roche Cobas E602, Switzerland). Liver and kidney panels were analyzed using a clinical chemistry analyzer (Olympus, AU400, Japan). Assays were conducted using reagents and protocols provided by the manufactures of the equipment.

Determination of 50% of effective concentration. EC_{50} represents the dose at which a compound produces half of its maximal effect[46]. To determine the EC_{50} of triptonide, a series of dose–response data were collected using adult male mice treated with various doses of triptonide in three independent experiments. Sperm motility was evaluated using CASA (Hamilton Throne). To determine male fertility, two to three fertility-proven females were added to the cages containing a single triptonide-treated or control male mouse at the end of the fourth weeks of treatment. Vaginal plugs were examined early every morning to verify mating, and pregnancy became visible by day 10 after mating. Later, the number of pups borne

was documented (Supplemental Table S3). EC_{50} was calculated based on a basic rectilinear equation: $E = mx + E_0$, where E represents the triptonide effect, m stands for the slope ($\frac{E_0-E_{0.1}}{0-0.1}$), and x for triptonide concentration (C). Since $E = \frac{E_0-E_{0.1}}{0-0.1} C + E_0$, when $x = 0$, the E equals E_0 ($E = E_0$). Because $E = \frac{E_0-E_{0.1}}{0-0.1} C + E_0$, where E 0.1 equals E, when $C = 0.1$. When $E = \frac{E_0}{2}$, the $C = C_{0.5}$. Since $E = \left(\frac{E_0-E_{0.1}}{0-0.1}\right) \mathbf{C} + \mathbf{E_0}$; $\frac{E_0}{2} = \frac{E_0-E_{0.1}}{0-0.1} C_{0.5} + E_0$, and $\frac{E_0}{2} = M C_{0.5} + E_0$. Thus, $EC_{0.5} = \frac{\frac{E_0}{2}-E_0}{M} = \frac{-\frac{E_0}{2}}{M} = -\frac{E_0}{2M}$. Specifically, we utilized E_0 (sperm motility or male fertility of control male mice) through its slope $\left(\frac{E_0-E_{0.1}}{0-0.1}\right)$,and the equation ($C_{0.5} = -E_0/2m$), to acquire the EC_{50}.

Western blot analyses. Testes were lysed in Pierce IP lysis buffer (Thermo Scientific, no.87787, 25 mM Tris HCl, pH 7.4, 150 mM NaCl, 1% NP-40, 1 mM EDTA, and 5% glycerol) containing protease inhibitors (Roche, mini-complete, no EDTA) and homogenized. The lysates were vortexed and spun at 17,000 × *g*, 20 °C for 10 min, and the supernatants were collected. The protein concentrations were determined using Pierce BCA Protein Assay Kit (Thermo Scientific). The proteins from each sample were loaded onto one MiniProtean TGX 4–15% or 4–20% polyacrylamide gel (Bio-Rad) followed by electrophoresis at 200 V for 40 min. The gel was electroblotted onto nitrocellulose membrane at 100 V for 1 h in a cold room. After blocking with SuperBlock T20 (PBS) Blocking Buffer (Thermo Fisher Scientific) and the membrane was subjected to reactions with primary antibodies on a rocking platform in a cool room overnight. After washing, the membrane was incubated with goat anti-mouse IgG HRP or goat anti-rabbit IgG HRP for 1 h. The specific proteins were visualized using the Advanced Bright Enhanced Chemiluminescence kit. Imaging and qualification were performed using a ChemiDoc Imager Detector (Bio-Rad). The primary antibodies used included mouse monoclonal anti-γH2AX (phospS139, Abcam, Cat#: 2635), rabbit polyclonal anti-β-actin (Abcam, Cat#: 8227), rabbit polyclonal keratin 5 (K5; BioLegend, Cat#:905501), and mouse monoclonal anti-junction plakoglobin/gamma catenine (Life Technologies, Cat#:13-8500). Goat anti-rabbit (SouthernBiotech, Cat#: 4030-05) and goat anti-mouse IgG (H + L; SouthernBiotech, Cat#: 1036-05) HRP-conjugated secondary antibodies were purchased from SouthernBiotech. Original uncropped western blot scans or films can be found in the Source data file.

Drug affinity responsive target stability assay. Four testes were removed from adult male C57/BL/6J mice. Each testis was dissected into several pieces and put into a 1.5 ml tube containing 450 µl M-PER solution (Thermo Fisher Scientific) with protease inhibitors (Roche, complete mini, EDTA-free) and phosphatase inhibitors (Abcam, Phosphatase inhibitor cocktail I). The mixture was homogenized with 20 strokes of a plastic pestle and then homogenized with a Benchmark D1000 homogenizer at a setting of two for 15 s. All four testis samples sat on ice for a half hour and were then centrifuged at 17,200 × *g* for 10 min. The four supernatants were pooled in a 15 ml centrifuge tube. To the tube was added 200 µl 10× TNC (500 mM Tris HCl, 500 mM NaCl, 100 mM $CaCl_2$, pH 8.0). The homogenate was assayed for protein concentration with a BCA assay and was diluted to 5 mg/ml. Homogenate (297 µl) was aliquoted into two tubes. To the tubes were added either 3 µl 16 mg/ml triptonide in DMSO or DMSO alone. The tubes were mixed well and left at room temperature for 1 h. Meanwhile, a solution of 10 mg/ml Pronase was diluted as follows: 1:100, 1:300, 1:1000, 1:3000, and 1:10,000. When Thermolysin was used in place of Pronase, a 10 mg/ml solution of Thermolysin was diluted to 2, 0.4, 0.08, and 0.016 mg/ml. The triptonide-treated or control homogenate (50 µl) was incubated with each of trypsin dilution for 15 min. The reactions were then stopped by the addition of 5 µl 0.5 M EDTA. Each sample was then run on Bio-Rad mini-Protein TGX 4-20% polyacrylamide gels at 200 V. Gels were stained with Bio-Safe Coomassie (Bio-Rad).

An in vivo variation of the DARTS experiment was carried out using testis homogenates from mice treated with 0.8 mg/kg BW triptonide daily (p.o.) for 4 weeks. Protein was precipitated from these extracts with four volumes of ice-cold acetone. After overnight incubation at −20 °C, the samples were centrifuged at 16,000 × *g*, 4 °C, for 10 min. The pellet was washed three times with ice-cold acetone/water (4:1). The protein pellet was dried, dissolved, and digested for various lengths of time using the Flash Digest system from Perfinity Biosciences. The digest reaction was stopped after 0, 5, 15, and 75 min of incubation by removal of aliquots and addition into Laemmli buffer with β-mercaptoethanol. The aliquots were run on polyacrylamide gels followed by visualization of protein using staining. Bands of interest were cut out and submitted for MS analyses. Original gel images can be found in the source data file.

GlycoLink beads-based affinity purification. GlycoLink Micro Immobilization Kit was purchased from Thermo Fisher Scientific. GlycoLink beads contain a linker with a terminal hydrazide group which reacts with aldehydes and ketones. The coupling of triptonide to the beads was attempted in two ways. The GlycoLink kit comes with an acidic coupling buffer for coupling to aldehydes and ketones. An additional basic buffer was purchased which might couple via the epoxide groups of triptonide. Coupling was done by incubating beads with a saturated solution of triptonide in DMSO (40 mg/ml), or with DMSO alone for controls, in acidic and basic buffer. Triptonide was covalently attached to the beads with aniline according to the manufacturer's instructions. Testes from one sexually mature male mouse were homogenized in M-PER buffer (Thermo Fisher Scientific). The proteins in the homogenate were precipitated with four volumes of ice-cold acetone. After sitting for 3.5 h at −20 °C, the protein pellet was centrifuged at 16,000 × *g*, 4 °C, for 10 min. The pellet was washed three times with ice-cold 4:1 acetone/water. The final pellet was dried and dissolved in 2.5 ml Dulbecco's PBS. An aliquot (300 µl) was applied to each of the four types of beads and reacted with the beads as per instructions. After washing of the beads, proteins on the beads were eluted sequentially with the following solutions: a saturated solution of triptonide in DMSO in PBS, 0.1% formic acid/30% acetonitrile, and 0.2 M glycine, pH 2.6. The eluates were dried in a vacuum concentrator to ~60–70 µl. The eluates were then desalted with Zeba Spin Desalting Kit (Thermo Fisher Scientific, 7 K MWCO) and buffer exchanged into 0.1% formic acid/30% acetonitrile. The eluates were again dried to a volume of 35–40 µl. The eluates were then applied to a Bio-Rad mini-Protean TGX 4-20% polyacrylamide gels and run at 200 V. Gels were stained with Sypro Ruby. Bands of interest were cut out and submitted for MS analyses. Original gel images can be found in the Source data file.

Immunoprecipitation-based identification of proteins interreacting with the N-terminus of SPEM1. A peptide composed of the N-terminal 28 amino acids of murine SPEM1 was synthesized by BioLegend (San Diego, CA). A biotin was attached to the C-terminal amino acid of the peptide. Streptavidin magnetic beads were obtained from GenScript. Beads were incubated with either 0.3 mg of peptide in PBS or with PBS alone. The solutions were incubated with the beads for 1 h and then washed with PBS. A homogenate of testis from a sexually mature male mouse was prepared in PBS with protease inhibitors (Roche, complete mini, EDTA-free). The two types of beads were incubated with 120 µl of the testis homogenate (0.34 mg protein) for 1 h. After washing of the beads, proteins on the beads were eluted sequentially with a saturated solution of triptonide in DMSO in PBS, 0.1% formic acid/30% acetonitrile, and 0.2 M glycine, pH 2.6. The eluates were dried in a vacuum concentrator to ~60–70 µl. The eluates were then desalted with Zeba Spin Desalting Kit (Thermo Fisher Scientific, 7 K MWCO) and buffer exchanged into 0.1% formic acid/30% acetonitrile. The eluates were again dried to a volume of 35–40 µl. Half of each eluate was diluted with Laemmli buffer with β-mercaptoethanol and applied to a Bio-Rad mini-Protean TGX 4–20% polyacrylamide gels and run at 200 V. Gels were stained with Sypro Ruby. The remaining halves of the eluates were submitted for MS analysis.

Mass spectrophotometric identification of proteins. Proteins in the excised electrophoresis bands were reduced and alkylated using 10 mM dithiothreitol and 100 mM iodoacetamide. Proteins in solutions were denatured with acetonitrile, then reduced and alkylated with 6.7 mM DTT and 13.8 mM iodoacetamide. The proteins were then incubated with sequencing grade modified porcine trypsin (Promega, Fitchburg, WI) in 25 mM ammonium bicarbonate overnight at 37 °C.

Liquid chromatography. Peptide mixtures were separated using an UltiMate 3000 RSL Cnano system (Thermo Scientific, San Jose, CA) on a self-packed UChrom C18 column (100 µm × 35 cm). Elution was performed using a 90 min gradient of solvent B from 2–27% (solvent A 0.1% formic acid, and solvent B acetonitrile, 0.1% formic acid) at 50 °C using a digital Pico View nanospray source (New Objectives, Woburn, MA) that was modified with a custom-built column heater and an ABIRD background suppressor (ESI Source Solutions, Woburn, MA). Briefly, the self-packed column tapered tip was pulled with a laser micropipette puller P-2000 (Sutter Instrument Co, Novato, CA) to an approximate id of 10 µm. The column was packed with 1–2 cm of 5 µm Magic C18 followed by 35 cm of 1.8 µm UChrom C18 (120 A) at 9000 p.s.i., using a nano LC column packing kit (nanoLCMS, Golg River, CA).

Mass spectrometry. Mass spectral analysis was performed using an Orbitrap Fusion mass spectrometer (Thermo Scientific. San Jose, CA). Proteomic analysis was performed using a "Universal" data-dependent method (Eliuk et al. 2014 Thermo Application note). The MS1 precursor selection range was from 400 to 1500 m/z at a resolution of 120 K and intensity threshold of 4.0 × 105. Quadrupole isolation at 0.7T h for MS^2 analysis using CID fragmentation in the linear ion trap with a collision energy of 35%. The automatic gain control was set to 1.0 × 107 with a maximum injection time of 250 ms.The instrument was set in a top speed data-dependent mode with a most intense precursor priority. Dynamic exclusion was set to an exclusion duration of 60 s with a 10 ppm tolerance.

Database searching. Tandem mass spectra were extracted and charge state deconvoluted by Proteome Discover version 2.1. All MS/MS samples were analyzed using Sequest (Thermo Fisher Scientific, San Jose, CA, USA; version 2.0.0.802). Sequest was set up to search a custom C-term fasta, assuming the digestion enzyme trypsin and max number of missed cleavages get to 2. Sequest was searched with a fragment ion mass tolerance of 0.60 Da and a parent ion tolerance 10.0 PPM. Variable modifications included carbamidomethyl of cysteine, oxidation of methionine, deamidation, and acetylation of the N-terminus.

Criteria for protein identification. Scaffold (version Scaffold 4.8.2, Proteome Software Inc., Portland, OR) was used to validate MS/MS-based peptide and protein identification. Peptide identifications were accepted if they could be established at >80% probability by the Peptide Prophet algorithm[47] with Scaffold delta-mass correction. Protein identifications were accepted if they could be established at greater 99.0% probability and contained at least two identified peptides. Protein probabilities were assigned by the Peptide Prophet algorithm[48]. Proteins that contained similar peptides and could not be differentiated based on MS/MS analysis alone were grouped to satisfy the principles parsimony.

Statistics and reproducibility. Graph Pad Prism 7 software (La Jolla, CA, USA) was used for statistical analyses. Data are presented as mean ± SEM unless stated otherwise. Differences in measurements were compared by Kolmogorov–Smirnov *t* test or one-way analyses of variance (ANOVA) for two groups, and $p < 0.05$ was considered statistically significant. Two-way ANOVA with Bonferroni multiple comparison test were used to compare differences between groups and timepoints, and adjusted $p < 0.05$ was considered to be statistically significant.

Gross morphology and histology of both the testes and cauda epididymal sperm were routinely examined in both pilot and POC efficacy testing experiments using C57Bl/6J (approximately ten independent experiments expanding 7 years) and CD-1 (two independent experiments in two years) male mice, and results similar to the representative images shown in Figs. 1a, b and Supplementary Fig. 2 were obtained consistently. Both TEM and SEM were conducted once using three mice from three separate experiments, and the data similar to the representative images shown in Fig. 1c were obtained consistently. In the POC efficacy testing on monkeys, ejaculated sperm were collected from all monkeys once every 1–3 weeks, and testicular biopsy was conducted on six treated and three control monkeys at different timepoints. Both sperm morphology and testicular histology varied to some degree, but were generally consistent to the representative images shown in Fig. 2a, e, as well as Supplementary Fig. 4d–i. Pathology examinations at both gross and histological levels were conducted on six treated and three control male C57Bl/6J mice from three independent experiments, and no major pathology was detected and the histology of major vital organs of these mice was similar to the micrographs shown in Supplementary Fig. 3. DARTs were performed twice with similar results, and Fig. 5b is one the two gels obtained and subjected to MS-based protein identification. GlycoLink beads-based affinity purification was repeated four times using samples from four male C57Bl/6J male mice from two independent experiments, and results similar to Fig. 5d–f were obtained. Immunofluorescent and western blot analyses of gamma-H2Ax were carried out three times, using three control and six treated male mice from two independent experiments, and results similar to those shown in Supplementary Fig. 14 were obtained. Efficacy testing using chemically synthesized triptonide was performed twice, using four mice per group per timepoint, and both testicular histology and sperm morphology were similar to those shown in Supplementary Fig. 16.

Reporting summary. Further information on research design is available in the Nature Research Reporting Summary linked to this article.

Data availability

All data are available within the Article and Supplementary Files, or available from the corresponding author on reasonable request. Source data are provided with this paper.

Received: 30 September 2020; Accepted: 29 January 2021;
Published online: 23 February 2021

References

1. Mansour, D., Inki, P. & Gemzell-Danielsson, K. Efficacy of contraceptive methods: a review of the literature. *Eur. J. Contracept. Reprod. Health Care* **15** (Suppl 2), S19–S31 (2010).
2. Huhtaniemi, I. MECHANISMS IN ENDOCRINOLOGY: hormonal regulation of spermatogenesis: mutant mice challenging old paradigms. *Eur. J. Endocrinol.* **179**, R143–R150 (2018).
3. Rey, R. Regulation of spermatogenesis. *Endocr. Dev.* **5**, 38–55 (2003).
4. Yan, W. Male infertility caused by spermiogenic defects: lessons from gene knockouts. *Mol. Cell. Endocrinol.* **306**, 24–32 (2009).
5. Zheng, H. et al. Lack of Spem1 causes aberrant cytoplasm removal, sperm deformation, and male infertility. *Proc. Natl Acad. Sci. USA* **104**, 6852–6857 (2007).
6. Jin, J. et al. Catsper3 and Catsper4 are essential for sperm hyperactivated motility and male fertility in the mouse. *Biol. Reprod.* **77**, 37–44 (2007).
7. Qi, H. et al. All four CatSper ion channel proteins are required for male fertility and sperm cell hyperactivated motility. *Proc. Natl Acad. Sci. USA* **104**, 1219–1223 (2007).
8. De Jonge, C. Semen analysis: looking for an upgrade in class. *Fertil. Steril.* **97**, 260–266 (2012).
9. Chubb, C. Animal models of physiologic markers of male reproduction: genetically defined infertile mice. *Environ. Health Perspect.* **74**, 15–29 (1987).
10. Bao, J. & Dai, S. M. A Chinese herb *Tripterygium wilfordii Hook F* in the treatment of rheumatoid arthritis: mechanism, efficacy, and safety. *Rheumatol. Int.* **31**, 1123–1129 (2011).
11. Tao, X. & Lipsky, P. E. The Chinese anti-inflammatory and immunosuppressive herbal remedy *Tripterygium wilfordii Hook F. Rheum. Dis. Clin. North Am.* **26**, 29–50 (2000). viii.
12. Matlin, S. A. et al. Male antifertility compounds from *Tripterygium wilfordii Hook f. Contraception* **47**, 387–400 (1993).
13. Li, B. et al. A novel method to convert triptolide into tripchlorolide in *Tripterygium wilfordii. Phytochemical Anal.* **17**, 129–133 (2006).
14. Li, B. et al. Monitoring of the conversion from triptolide to tripchlorolide in *Triptergium wilfordii* by micellar electrokinetic caillary chromatography. *J. Chromatogr. A* **1097**, 199–202 (2005).
15. Wang, Z. P. et al. Effects of tripchlorolide on the epididymides and testes of rats. *Asian J. Androl.* **1**, 121–125 (1999).
16. Zuo, X. & Wang, N. [Study on antifertility mechanisms of tripchlorolide (T4)]. *Zhongguo Yi Xue Ke Xue Yuan Xue Bao* **17**, 387–389 (1995).
17. Zhen, Q. S., Ye, X. & Wei, Z. J. Recent progress in research on *Tripterygium*: a male antifertility plant. *Contraception* **51**, 121–129 (1995).
18. Ye, W., Den, Y., Huang, Y. & Xue, S. Antispermatogenic effect of *Tripterygium wilfordii* and tripchlorolide (T4) on rat gametogenesis and spermatozoa. *Chin. Med. Sci. J.* **9**, 110–113 (1994).
19. Wong, K. F., Yuan, Y. & Luk, J. M. Tripterygium wilfordii bioactive compounds as anticancer and anti-inflammatory agents. *Clin. Exp. Pharm. Physiol.* **39**, 311–320 (2012).
20. Ni, B. et al. Male reproductive toxicity and toxicokinetics of triptolide in rats. *Arzneim. Forsch.* **58**, 673–680 (2008).
21. Hikim, A. P. et al. Posttesticular antifertility action of triptolide in the male rat: evidence for severe impairment of cauda epididymal sperm ultrastructure. *J. Androl.* **21**, 431–437 (2000).
22. Lue, Y. et al. Triptolide: a potential male contraceptive. *J. Androl.* **19**, 479–486 (1998).
23. Dai, W., Liu, P. & Han, Y. [The effect of *Tripterygium wilfordii* monomers T4, T7,T15 and Triptolide on rat nuclear protein]. *Zhongguo Yi Xue Ke Xue Yuan Xue Bao* **16**, 20–23 (1994).
24. Chaudhury, R. R. The quest for a herbal contraceptive. *Natl Med. J. India* **6**, 199–201 (1993).
25. Kupchan, S. M. & Schubert, R. M. Selective alkylation: a biomimetic reaction of the antileukemic triptolides? *Science* **185**, 791–793 (1974).
26. Kuo, L. J. & Yang, L. X. Gamma-H2AX - a novel biomarker for DNA double-strand breaks. *Vivo* **22**, 305–309 (2008).
27. Dickey, J. S. et al. H2AX: functional roles and potential applications. *Chromosoma* **118**, 683–692 (2009).
28. Rybak, P. et al. Low level phosphorylation of histone H2AX on serine 139 (gammaH2AX) is not associated with DNA double-strand breaks. *Oncotarget* **7**, 49574–49587 (2016).
29. Anderson, M. B., Pedigo, N. G., Katz, R. P. & George, W. J. Histopathology of testes from mice chronically treated with cobalt. *Reprod. Toxicol.* **6**, 41–50 (1992).
30. Chung, S. et al. Infertility and testicular defects in hormone-sensitive lipase-deficient mice. *Endocrinology* **142**, 4272–4281 (2001).
31. Hansen, D. A., Esakky, P., Drury, A., Lamb, L. & Moley, K. H. The aryl hydrocarbon receptor is important for proper seminiferous tubule architecture and sperm development in mice. *Biol. Reprod.* **90**, 8 (2014).
32. Lomenick, B. et al. Target identification using drug affinity responsive target stability (DARTS). *Proc. Natl Acad. Sci. USA* **106**, 21984–21989 (2009).
33. Lomenick, B., Jung, G., Wohlschlegel, J. A. & Huang, J. Target identification using drug affinity responsive target stability (DARTS). *Curr. Protoc. Chem. Biol.* **3**, 163–180 (2011).
34. Ban, T. A. The role of serendipity in drug discovery. *Dialogues Clin. Neurosci.* **8**, 335–344 (2006).
35. Prasad, S., Gupta, S. C. & Aggarwal, B. B. Serendipity in cancer drug discovery: rational or coincidence? *Trends Pharm. Sci.* **37**, 435–450 (2016).
36. Schlueter, P. J. & Peterson, R. T. Systematizing serendipity for cardiovascular drug discovery. *Circulation* **120**, 255–263 (2009).
37. Dreef, H. C., Van Esch, E. & De Rijk, E. P. Spermatogenesis in the cynomolgus monkey (*Macaca fascicularis*): a practical guide for routine morphological staging. *Toxicol. Pathol.* **35**, 395–404 (2007).
38. Oakberg, E. F. Duration of spermatogenesis in the mouse and timing of stages of the cycle of the seminiferous epithelium. *Am. J. Anat.* **99**, 507–516 (1956).
39. Mountzouris, J. A. & Hurley, L. H. in *Bioorganic Chemistry: Nucleic Acids* (ed. Hecht, S. M.) (Oxford Univ. Press, 1996).
40. Xi, C., Peng, S., Wu, Z., Zhou, Q. & Zhou, J. Toxicity of triptolide and the molecular mechanisms involved. *Biomed. Pharmacother.* **90**, 531–541 (2017).

41. Sangwan, V. & Saluja, A. K. in *Nutraceuticals and Cancer* (ed. Sarkar F. H.) (Springer, 2012).
42. Xu, L. et al. Acute and subacute toxicity studies on triptolide and triptolide-loaded polymeric micelles following intravenous administration in rodents. *Food Chem. Toxicol.* **57**, 371–379 (2013).
43. Burdett, I. D. Aspects of the structure and assembly of desmosomes. *Micron* **29**, 309–328 (1998).
44. Stokes, D. L. Desmosomes from a structural perspective. *Curr. Opin. Cell Biol.* **19**, 565–571 (2007).
45. Weisbroth, S. & Young, F. A. The collection of primate semen by electro-ejaculation. *Fertil. Steril.* **16**, 229–235 (1965).
46. Noel, Z. A., Wang, J. & Chilvers, M. I. Significant influence of EC50 estimation by model choice and EC50 type. *Plant Dis.* **102**, 708–714 (2018).
47. Keller, A., Nesvizhskii, A. I., Kolker, E. & Aebersold, R. Empirical statistical model to estimate the accuracy of peptide identifications made by MS/MS and database search. *Anal. Chem.* **74**, 5383–5392 (2002).
48. Nesvizhskii, A. I., Keller, A., Kolker, E. & Aebersold, R. A statistical model for identifying proteins by tandem mass spectrometry. *Anal. Chem.* **75**, 4646–4658 (2003).

Acknowledgements

We are grateful to Dr. John R. McCarrey for critical reading of the manuscript. Drs. Thomas Bell and Ali Rameez are acknowledged for their help with triptonide purity analyses. This study was supported by grants from the XtraThordinary, LLC. and the Male Contraceptive Initiative (to W.Y.). The POC efficacy testing on cynomolgus monkeys was supported by grants from the National Natural Science Foundation of China (No. 81801523 to Y.Z.), the Natural Science Foundation of Guangdong Province (2015A030313884 to Y.T.; 2018A030313528 and 2019A1515011984 to W.Q.), Guangdong Province Medical Research Funding (No. A2018297 to W.Q., A2018075 to J. W., and A2018235 to X.L.), the Science and Technology Planning Foundation of Guangzhou City (201607010137 to S.D. and 201904010017 to Y.Z.), and the Family Planning Research Institute of Guangdong Province (S2014001 to Y.T., S2018004 to J.W., S2018012 to H.l., and S2018013 W.Q.). The University of Virginia Center for Research in Reproduction Ligand Assay and Analysis Core is supported by a National Centers for Translational Research In Reproduction and Infertility (NCTRI) grant from the NICHD (P50-HD28934).

Author contributions

W.Y. conceived and designed the overall study. W.Y. and H.Z. supervised all of the mouse studies conducted at the University of Nevada, Reno School of Medicine. W.Y., Y.T., and W.Q. supervised all of the testing on cynomolgus monkeys. Z.C., H.Z., K.S., Y.W., H.M., Z.W., H.P., and S.Y. conducted all of the experiments on mice, whereas W.Q., X.L., J.W., Y.W., S.Z., Y.J., H.N., Y.T., and Y.Z. performed all of the experiments on cynomolgus monkeys. M.J.M.H provided advices on the POC efficacy testing. L.H. performed all of the statistical analyses on data from monkeys. W.Y. wrote the manuscript. All authors reviewed and agreed on the contents of the manuscript.

Competing interests

The authors declare no competing interests.

Additional information

Supplementary information The online version contains supplementary material available at https://doi.org/10.1038/s41467-021-21517-5.

Correspondence and requests for materials should be addressed to Y.T. or W.Y.

Peer review information *Nature Communications* thanks Erwin Goldberg and the other, anonymous, reviewer(s) for their contribution to the peer review of this work. Peer reviewer reports are available.

Reprints and permission information is available at http://www.nature.com/reprints

Publisher's note Springer Nature remains neutral with regard to jurisdictional claims in published maps and institutional affiliations.